Geochemistry, Geophysics, Geosystems®

AGU
ADVANCING EARTH AND SPACE SCIENCES

Key Points:

- Lithospheric-scale transcurrent tectonics can promote low degrees of lithospheric mantle melting
- Different Low-Ti continental tholeiites can derive from an enriched lithospheric mantle, by variable assimilation of alkali crustal rocks
- Low-Ti continental tholeiites can behave as mafic precursors of magmas with calc-alkaline signature by crustal assimilation

Supporting Information:

Supporting Information may be found in the online version of this article.

Correspondence to:

F. Sarrionandia,
fernando.sarrionandia@ehu.eus

Low–Ti Continental Tholeiite Origin of Magmas With Calc-Alkaline Signature in Transcurrent Settings: The Mississippian Matachel Volcanic Field (SW Iberian Massif)

F. Sarrionandia[1] , **J. Errandonea-Martin[2]** , **E. Larrondo[3]** , **M. Carracedo-Sánchez[2]**, **B. Ábalos[2]**, and **J. I. Gil Ibarguchi[2]**

[1]Departamento de Geología, Facultad de Farmacia, Universidad del País Vasco UPV/EHU, Vitoria-Gasteiz, Spain, [2]Departamento de Geología, Facultad de Ciencia y Tecnología, Universidad del País Vasco UPV/EHU, Bilbao, Spain, [3]Team Ingeniería y Consultoría S.L., Parque Científico y Tecnológico de Bizkaia, Zamudio, Spain

Abstract In the Mississippian Matachel small volcanic field of the Ossa-Morena Zone (southern Iberian Massif) outpoured basic-intermediate lavas exhibit geochemical characteristics of Low-Ti continental tholeiites and calc-alkaline lavas. Low-Ti continental tholeiites integrate two contrasting groups of rocks: basalts (Mg#: 54 to 70; Ti/Zr: 61–79; La_N/Lu_N: 1.6–2.9; εNd_i: +4.0–+6.6; "Group #1"), and basalts and basaltic andesites (Mg#: 43 to 66; Ti/Zr: 36–58; La_N/Lu_N: 2.5–5.9; εNd_i: −0.2–+3.5; "Group #2"). Primitive Group #1 tholeiitic magmas were generated by partial melting of a garnet-free lherzolite from an enriched lithospheric mantle, near the lithosphere-asthenosphere thermal boundary layer (with a very limited asthenosphere melting input). Progressive interaction of these magmas with crustal alkali igneous rocks resulted in the formation of the petrological evolutionary trends observed, to a larger extent in the case of Group #2 Low-Ti tholeiites. Further assimilation of amphibole-rich calc-alkaline metaigneous rocks might have originated the basalts and basaltic andesites with calc-alkaline signature (Mg#: 33 to 56; Ti/Zr: 25–78; La_N/Lu_N: 2.0–5.6; εNd_i: +2.8–+4.8). These exhibit a "Cordilleran-type" evolutionary trend, though are unrelated to plate convergence. The magmas with calc-alkaline signature attest to a closed-system differentiation process controlled by the fractionation of plagioclase, clinopyroxene, magnetite and ilmenite. It is proposed that Mississippian lithospheric-scale intra-continental wrenching, unrelated to coeval mantle plume upwelling, reworked complexly docked mantle domains and triggered mantle melting. Enduring mid-upper crustal processes (magma storage in mid-crustal chambers and crustal assimilation) likely shaped the latest petrologic and geochemical aspects of the Matachel Low-Ti tholeiites and related rocks with calc-alkaline signature.

Plain Language Summary The Matachel area of the southern Iberian Massif was the scenario around 350 million years ago of intra-continental volcanism subsequent to a period of continental crust thickening (the Variscan Orogeny). The intra-plate volcanic products there are both acid and basic (bimodal) and outcrop at present along elongated basins directed NW-SE, bounded by strike-slip faults. In this study, we focused on the silica-poor basic units (basalts to basaltic andesites). The more basic units present characteristics of titanium-poor continental tholeiite magmas, that is, they are not related as usual to flood basalt emissions and formation of large igneous provinces. The less basic units correspond to magmas with calc-alkaline signature, richer in titanium and rare earth elements. Overall, the geochemical and mineralogical features of these two types of basic volcanic products within the same continental scenario attest to an evolution from purely mantle-derived magmas (tholeiite units) toward others that record contamination with an older crust (calc-alkaline units), either purely continental crust or, more likely, an Andean-type continental arc formed during the Lower Paleozoic Cadomian Orogeny.

1. Introduction

Continental tholeiites are usually associated to extraordinary flood basalt emissions and formation of large igneous provinces (Hawkesworth et al., 1999; Peate & Hawkesworth, 1996, and references therein). They represent the most widespread type of intra-plate basalts (Stepanova et al., 2014). Such large magma emissions generally developed in relation to either anorogenic (hot spot) or rift (plate divergence) geodynamic settings (Ingle et al., 2004; Keppie et al., 2008; Peate et al., 1992; Pouclet et al., 2017; Shellnutt et al., 2014; Stepanova et al., 2014; White & McKenzie, 1989), examples of their relationship with tectonic settings that do not associate deep mantle

Investigation: F. Sarrionandia, E. Larrondo, M. Carracedo-Sánchez
Methodology: E. Larrondo, M. Carracedo-Sánchez
Supervision: J. I. Gil Ibarguchi
Writing – original draft: F. Sarrionandia, B. Ábalos
Writing – review & editing: J. Errandonea-Martin, B. Ábalos, J. I. Gil Ibarguchi

upwelling (Hawkesworth et al., 1999; Shellnutt et al., 2014; White & McKenzie, 1989) or with lithospheric-scale shear zones (wrench and convergent; Dessureau et al., 2000) being scarce. Published petrotectonic models most often convey their generation directly or indirectly to mantle plumes (Dessureau et al., 2000; Hawkesworth et al., 1999; Ingle et al., 2004; Lassiter & DePaolo, 1997; Lightfoot et al., 1993; Neal et al., 2002; Peate & Hawkesworth, 1996; Peate et al., 1992; Sandeman et al., 2014; Stepanova et al., 2014; White & McKenzie, 1989). In large-scale tectono-magmatic settings such as the latter, the generation of crust-derived magmas is usually conspicuous (Keppie et al., 2008; Shellnutt et al., 2014), which also discloses an actual high extent of crustal reworking in relation with continental tholeiitic magmatism.

Continental tholeiites possess a prominent petrotectonic significance for the regions where they are found, the hypotheses that would explain their origin and the specific processes involved in their genesis being diverse (Dupuy & Dostal, 1984). Yet, continental tholeiite basalts have generally evolved rather than primitive geochemical/isotopic compositions that hinder the accurate recognition of their sources (Cox, 1980; Dessureau et al., 2000; Dostal & Dupuy, 1984; Dupuy & Dostal, 1984; Sandeman et al., 2014). Additionally, compositional variations observed in continental tholeiitic basalts may be conditioned by the interaction of magmas generated from different mantle and crustal sources (Ingle et al., 2004; Lightfoot et al., 1993; Pouclet et al., 2017; Sandeman et al., 2014) and by crustal contamination (Cox & Hawkesworth, 1985; Dupuy & Dostal, 1984; Hawkesworth et al., 1999; Ingle et al., 2004; Keppie et al., 2008; Sandeman et al., 2014; Shellnutt et al., 2014; Stepanova et al., 2014) all of which obscure their primary characteristics.

Extensive tholeiitic emissions have contributed significantly to crustal growth along Earth's history (Puchtel et al., 1998). Their lack of primary compositions constitutes a strong limitation for identification of the mantle source regions involved and, subsequently, for reconstruction of the tectono-magmatic evolution of the lithospheric domains where they occur. Presumed mantle source regions for tholeiitic magma extraction include (a) mantle plume asthenosphere/lithosphere systems (Dessureau et al., 2000; Ingle et al., 2004; Lassiter & DePaolo, 1997; Leat, 2008; Neal et al., 2002; Peate & Hawkesworth, 1996; Peate et al., 1992), (b) subcontinental mantle lithosphere (Hawkesworth et al., 1999; Lassiter & DePaolo, 1997; Peate & Hawkesworth, 1996; Pouclet et al., 2017; Shellnutt et al., 2014), and (c) depleted asthenosphere (Dostal & Dupuy, 1984; Dupuy & Dostal, 1984; Frey et al., 1996; Pouclet et al., 2017; Stepanova et al., 2014). The apparently concomitant occurrence of High-Ti and Low-Ti continental tholeiites, or emission of associated alkali basalts, has been used as supporting evidence to unravel joint contributions of different mantle sources (Ingle et al., 2004; Lightfoot et al., 1993; Neal et al., 2002; Peate, 1997; Peate et al., 1992; Pouclet et al., 2017). Alternative petrogenetic models suggest that both High-Ti and Low-Ti continental tholeiites can be generated by different degrees of partial melting of a spinel–peridotite lithospheric mantle (i.e., EMII-like), followed by variable amounts of crustal assimilation (Shellnutt et al., 2014). Hence, comprehension of the mantle sources implied in the generation of primitive tholeiitic magmas is still puzzling.

This article deals with Tournaisian–Lower Viséan (Mississippian) Low-Ti continental tholeiites recently identified in volcanic outpourings from the Ossa-Morena Zone of the southwestern Iberian Massif. These include principally pillow-lava flows that constructed a several km in areal extension (but volumetrically limited) lava field within an ephemeral Carboniferous continental marine basin regionally known as the Matachel basin. Its current tectonic context relates to a major lithospheric-scale shear zone active during the Variscan orogeny (Burg et al., 1981) that reworked an older suture (Ábalos et al., 2023; Eguíluz et al., 2000). Continental tholeiitic volcanism also involved the coeval emission of calc-alkaline basalts and basaltic andesites. As far as we know, few examples have been reported of outpourings of continental tholeiites and associated basalts with calc-alkaline signature (Benek et al., 1996; Mitjavila et al., 1997; Pouclet et al., 2017). Based on the petrologic data presented (Sarrionandia et al., 2023) and discussed here, a genetic relationship between those geochemical assemblages is disclosed and a new petrotectonic model is proposed. Identification of the geochemical association reported, coupled to the relatively small emission volumes, provides an opportunity to further improve the knowledge of lithospheric processes that operated during the Variscan evolution of the Late Paleozoic northern Gondwana edge.

2. Regional Setting

2.1. The Ossa-Morena Zone

The Iberian Massif represents the most extensive and complete segment exposed of the European Variscan Belt (Lotze, 1945; Figure 1a) This orogen resulted from a largely diachronous oblique collision between Laurussia
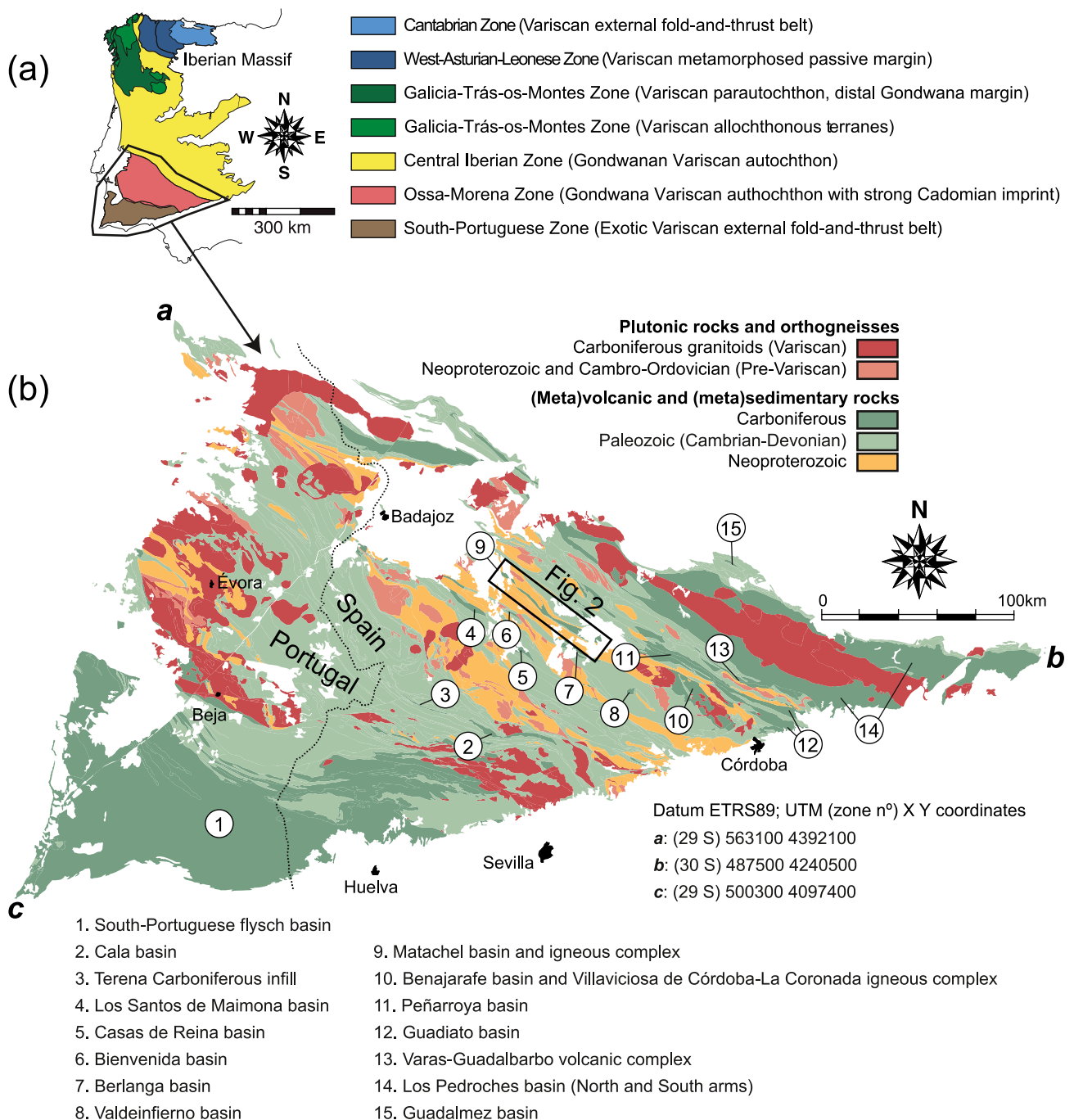
Figure 1. (a) Geological sketch map of the Iberian Massif. (b) Expanded Geological sketch map of the southern Iberian Massif, which displays the Carboniferous basins and the relative location of the Matachel Basin.

and Gondwana, and the consumption of the Rheic ocean (Braid et al., 2018; Díez-Fernández et al., 2016; Gutiérrez-Alonso et al., 2011; Matte & Ribeiro, 1975; Pereira, Chichorro, Johnston, et al., 2012; Pereira et al., 2017). The Iberian Massif was subdivided into major tectono-stratigraphic domains (Julivert et al., 1972; Lotze, 1945) bounded by tectonic contacts that sometimes correspond to complex crustal-scale suture zones (Díez-Fernández et al., 2016; Quesada, 1991; Schulmann et al., 2022, and references therein). Among these areas, the Ossa-Morena Zone (hereafter OMZ) of the SW Iberian Massif (Figure 1b) encloses the remnants of a Cadomian arc ascribable to Andean-type plate convergence and subduction (Bandrés et al., 2002, 2004; Eguíluz et al., 2000; López-Guijarro et al., 2008; Pin et al., 2002; Sánchez-Lorda et al., 2014). The active margin involved

Gondwana hyper-extended crust and was active between ca. 645 Ma and ca. 534 Ma (Sarrionandia et al., 2020). The Cadomian arc constitutes the basement onto which the sedimentary and volcanic sequences of the Variscan cycle were unconformably overlain in the OMZ.

The Variscan cycle was initiated in the mid- to late Cambrian with the development of an intra-continental rift (Chichorro et al., 2008; Sánchez-García et al., 2010, 2014; Sarrionandia et al., 2012) that evolved into a passive margin with Ordovician-Silurian platform siliciclastic sequences (Robardet & Gutiérrez-Marco, 2004). Middle Devonian–Carboniferous syn-orogenic ensembles were later deposited unconformably onto the rift-to-drift ensemble (Oliveira & Quesada, 2019), tracking the complex and protracted closure of a re-entrant of the Rheic ocean (Braid et al., 2018). So far, it is widely accepted that Variscan orogenic development was diachronous and incorporated outstanding orogen-parallel (transcurrent) tectonic displacements (Kroner & Romer, 2013; Pereira et al., 2010; Stampfli et al., 2013). At the Variscan orogen scale, this transcurrent stage has been ascribed as well to escape tectonics (e.g., Arthaud & Matte, 1977; Brun & Burg, 1982; Shelley & Bossière, 2000). All this enabled the formation and closure of intra-orogenic strike-slip basins bounded by crustal-scale faults (Ábalos & Eguíluz, 1991). As occurs in similar tectonic settings worldwide, these basins usually associate an outstanding magmatism (Dessureau et al., 2000, and references therein). Variscan wrenching was bracketed between 360 and 320 Ma by some authors (Ábalos et al., 1991; Pereira, Chichorro, Johnston, et al., 2012; Pereira, Chichorro, Silva, et al., 2012; Pereira et al., 2009), whereas others hypothesize Tournaisian extension stages (ca. 360–345 Ma) were followed by Viséan (345–330 Ma) transpression (Simancas et al., 2006). Whatever the case, the continental-scale strike-slip faults bounded ephemeral marine basins infilled with interbedded syn-orogenic detrital sediments and volcanic deposits that were later deformed in a sinistral transpressional context until the late Carboniferous (Ábalos & Eguíluz, 1991; Díez Fernández et al., 2021; Silva & Pereira, 2004; Simancas et al., 2006).

2.2. The Early Carboniferous Magmatism and Its Origin

Early Carboniferous magmatism in SW Iberia (including plutonic and volcanic rocks) was voluminous (Castro, 2019; Sánchez-Carretero et al., 1990; Figure 1b). In the case of intrusive plutonic rocks, this magmatism is represented by meta-aluminous and peraluminous calc-alkaline granitoids s.l., with rare alkali terms (Errandonea-Martin et al., 2019; García Casquero, 1991; Lima et al., 2012; Moita et al., 2009, 2015; Pereira et al., 2009; Pin et al., 2008; Pons, 1982; Santos et al., 1990; Sarrionandia et al., 2013). The volcanic counterparts include meta-aluminous high-K calc-alkaline, peraluminous, N-MORB-like, and alkali rocks (Armendáriz et al., 2008; Munhá, 1983; Oliveira et al., 2013; Rosa et al., 2008; Sánchez Carretero et al., 1989; Tornos et al., 2005).

Excluding N-MORB-like and crustal-derived peraluminous magmatic rocks, the mantle source of the early Carboniferous calc-alkaline/alkaline magmatism remains unexplained. Two principal tectono-magmatic hypotheses have been proposed that envisage different regions of the mantle for magma extraction: an active or immediately demised subduction setting and a mantle plume. On one hand, the subduction context considers melt extraction from an enriched lithospheric mantle and/or upwelling asthenospheric mantle underneath (Castro et al., 1996; Díaz Azpíroz et al., 2006; Jesus et al., 2007; Moita et al., 2009, 2015; Pereira et al., 2009, 2017; Pin et al., 2008; Santos et al., 1990; Sarrionandia, 2006; Tornos et al., 2005). On the other hand, the mantle plume hypothesis involves plume activity at ca. 350–340 Ma in order to explain extraction of mantle-derived alkali magmas (Cambeses et al., 2015). Apart from these two models, the possibility also exists that the suggested subduction context actually corresponds to a frozen, earlier subduction-related edifice (late Neoproterozoic-Early Cambrian) that underwent Cambrian rifting and Variscan strike-slip reactivation. This might be supported by a correlation of surface alignments of Variscan granitoid plutons, batholiths and volcanic complexes with the thermal effects of coeval lithospheric shear zones separating mantle pieces with distinct pre-Variscan fabrics (Ábalos & Díaz, 1995; Díaz et al., 1996; Sarrionandia et al., 2012, and references therein).

2.3. The Synorogenic Carboniferous Basins

During the late Devonian–early Carboniferous, two main shallow marine basins developed in the SW Iberian Massif, separated by an emerged area that roughly corresponds with the central OMZ. These are the Los Pedroches basin to the North (Armendáriz et al., 2019), and the South-Portuguese Zone (Colmenero et al., 2002; Gabaldón et al., 1985) to the South (Figure 1b), which are characterized by turbiditic successions and by a significant

volcanic input (Armendáriz et al., 2008; Oliveira & Quesada, 2019; Pereira, Chichorro, Silva, et al., 2012). Gabaldón et al. (1985) and Oliveira and Quesada (2019) suggested that, excluding the South-Portuguese Zone, the disconnected Mississippian outcrops bounded by regional-scale faults in the OMZ (localities from 2 to 15 in Figure 1b) would conform a single marine basin referred to as the North Marine Basin or the Los Pedroches Basin. Sánchez Carretero et al. (1989, 1990) considered that their volcanic deposits were genetically related to the so-called Villaviciosa de Córdoba–La Coronada magmatic alignment that hosts a complex of bimodal igneous rocks. To the North of this volcanic alignment a shallow marine, storm-dominated, mixed (siliciclastic-carbonate) platform exists (Armendáriz et al., 2008; Colmenero et al., 2002; Gabaldón et al., 1985). Distal platform marine sequences include pillow MORB-type and alkali basalts interbedded with rhyolitic volcaniclastic deposits and slates (Armendáriz et al., 2008; Larrondo, 2014; Pérez-Lorente, 1979). The Tournaisian–Viséan (350–335 Ma) volcanic record in the South-Portuguese Zone (the South Marine Basin) and neighbor domains was concomitant with sedimentation in a similar shallow-mixed marine platform, and it has been related to a geochemically complex bimodal magmatism too (Chichorro, 2006; Pereira et al., 2009, Oliveira & Quesada, 2019, and references therein). It consists of basic-intermediate arc-tholeiites and moderately alkaline lavas, basic to acid I-type, low-K to high-K calc-alkaline rocks (Chichorro, 2006; Pereira et al., 2009; Ribeiro, 1983), and acid igneous rocks of crustal derivation (Munhá, 1983). The world-class massive sulphide deposits of the Iberian Pyrite Belt (Oliveira et al., 2013; Quesada, 1998; Tornos et al., 2005) are genetically related with the acid magmatic rocks.

3. The Basic Volcanism of the Matachel Basin

The Matachel basin currently forms a ~55 km long and >2 km wide, NW-SE trending, tight, vertical and symmetric syncline. It is bounded by two regional-scale strike-slip faults converging down-dip, subsidiary with the Hornachos fault to the Northeast (Ábalos & Eguíluz, 1991; Larrondo, 2014). These faults separate the Carboniferous record of this syncline from Late Ediacaran and earliest Cambrian units of the Badajoz-Córdoba (or Coimbra-Córdoba; e.g., Burg et al., 1981) ductile shear belt (Figure 2). The shear belt represents a reworked suture zone with a complex and protracted polyphase tectonothermal evolution (Ábalos et al., 1991, 2023). Geological maps of the Matachel basin (Apalategui et al., 1983; Arriola et al., 1983; Sánchez Cela et al., 1977) disclose a ~2 km thick Mississippian volcano-sedimentary succession made of conglomerates, slates, greywackes and limestones with interbedded volcanic rocks. Three distinct volcanic episodes can be recognized that, according to their stratigraphic position from base to top, are as follows: an older "acid volcanism I," a "basic volcanism", and a younger "acid volcanism II" (Apalategui et al., 1983; Larrondo, 2014). Sánchez Carretero et al. (1989) merged the igneous record of the Matachel basin with that of the Benajarafe basin, located at its SE prolongation within the regional-scale Villaviciosa de Córdoba–La Coronada magmatic alignment. Two main lithostratigraphic groups resulted from this correlation: the Campana (consisting of andesites, dacites and basalts) and Erillas (made of dacites and rhyolites) volcanic complexes. The Tournaisian–Lower Viséan Erillas group encloses the "basic volcanism" episode reported above.

Ábalos and Eguíluz (1991) identified the left-lateral strike-slip character of the Matachel basin NW-SE bounding faults and reconstructed its traverse geometry as an inverted flower structure. According to these authors, the stair-stepped, dextral NNW–SSE faults that offset NW-SE linear basin and fault segments allowed accommodation of N–S stretching components that first drove basin subsidence and then structural inversion into a tight syncline (Apalategui et al., 1983). Localized sinistral transpression was recorded both by the basin infilling and by neighbor major faults (Ábalos, 1992; Díez Fernández et al., 2021). Transpression gave rise in the volcano-sedimentary basin infilling to the development of a pervasive N130-140E foliation bearing gently dipping intersection and stretching lineations and to the generation of transected folds (Ábalos, 1992). A syn-deformational very low-grade metamorphic overprint (chlorite zone) accompanied structural development.

The "basic volcanism" of the Matachel basin can be petrologically characterized and geologically mapped (e.g., in the synthesis after the 1:25.000 survey conducted by Larrondo (2014); Figure 2). According to the field relationships, it is represented mostly by pillow-lava flows (~75% in volume) and to a lower extent by pahoe-hoe-like sheet lava flows, agglomerates, lapilli-tuffs, and tuffs (Figure 3). The volcanic package also contains minor slate, greywacke, and micro-conglomerate beds. Gabbro and diorite syn-volcanic shallow intrusions were emplaced in the volcano-sedimentary package, too. These intrusives usually conform isolated or interconnected small-sized sills (<50 m thick and <1.5 km long), though occasionally form larger (400 m thick and 3.5 km long) irregular-shaped intrusions (Figure 2). Field relationships also reveal that the volcanic centers were unevenly
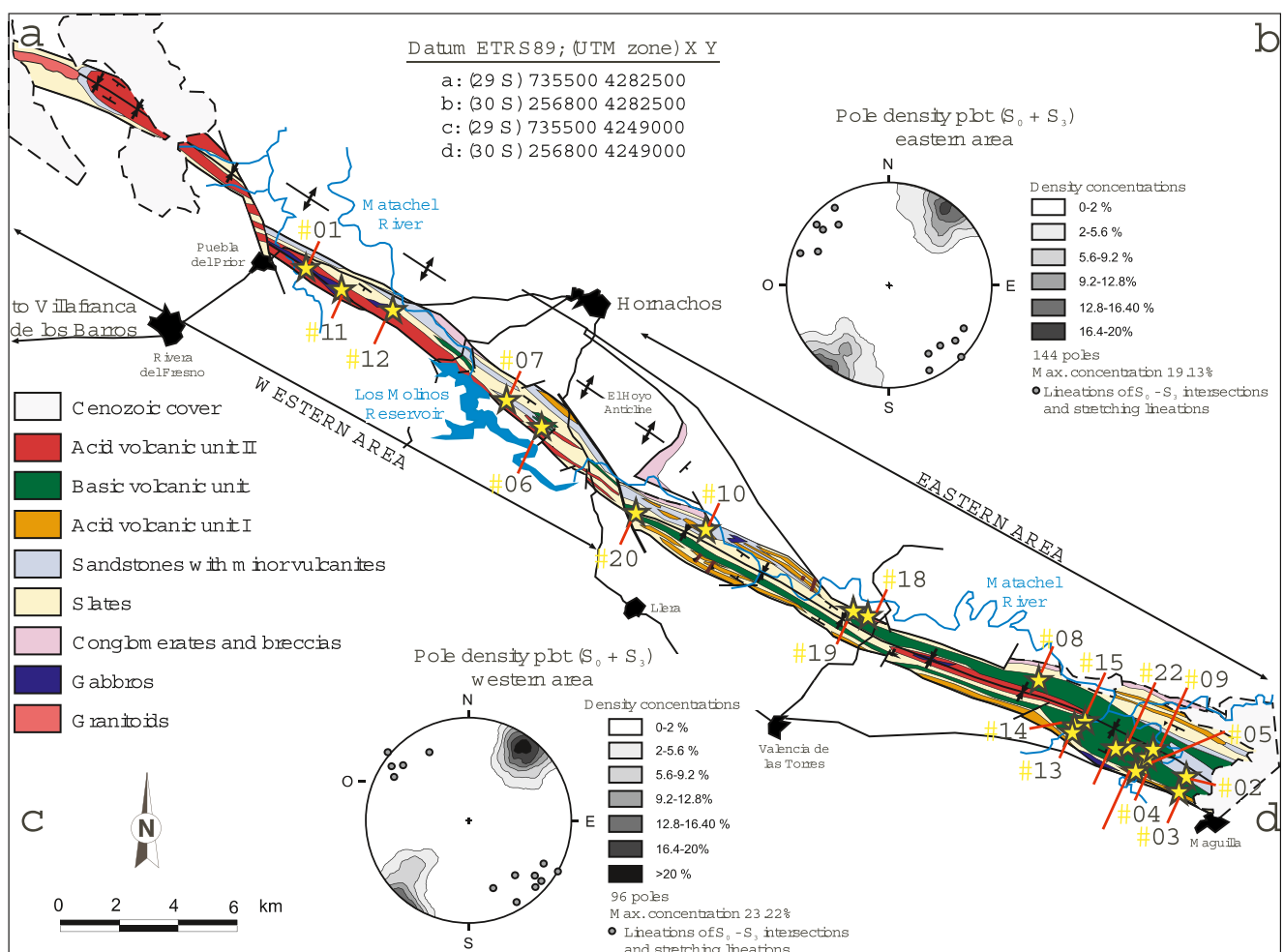
Figure 2. Geological sketch map of the Tournaisian–Lower Viséan Matachel Basin. Pole diagrams refer to the volcano-sedimentary sequence bedding of the west and east areas of the basin. These diagrams also include stretching lineations and lineations of bedding and foliation intersections. See Table S1 in Supporting Information S1 for the location UTM coordinates of the studied samples (#1 to #23).

distributed, being more common in the central and eastern areas of the Matachel basin (Figure 2). In this regard, only three lava flows (20–45 m thick) have been recognized in the central area of the Matachel basin. By contrast, in the southern limb of the far-east area 30 lava flows (some of them up to 55 m thick) were identified by Larrondo (2014).

At the outcrops, the basic volcanic rocks studied appear as massive, apparently isotropic and dark colored. A general aphyric and poorly vesicular character of the lava flows is outstanding, whereas aphanitic textures prevail in the intrusives. Only in a few cases plagioclase phenocrysts (up to 4 mm in size) are discernible to the naked eye in the lava flows. Pyroxene oikocrysts (up to 15 mm in size) and plagioclase phenocrysts (up to 12 mm in size) can be observed in the intrusives.

4. Methods

A collection of 23 samples from different Matachel basic lava flows (10 samples) and intrusive bodies (13 samples) was selected for this study (see sample location in Table S1 in Supporting Information S1). Analytical studies included a detailed petrographic characterization of each sample, as well as mineral chemistry and whole-rock elemental and Sr, Sm-Nd isotopic determinations presented herein or available in Sarrionandia et al. (2023).

Geological mapping was improved with Light Detection And Ranging (LIDAR) images at 5 m resolution and with ortophotographs of the Spanish National Plan of Aerial Ortophotography (PNOA, 2009, 2011, and 2013).
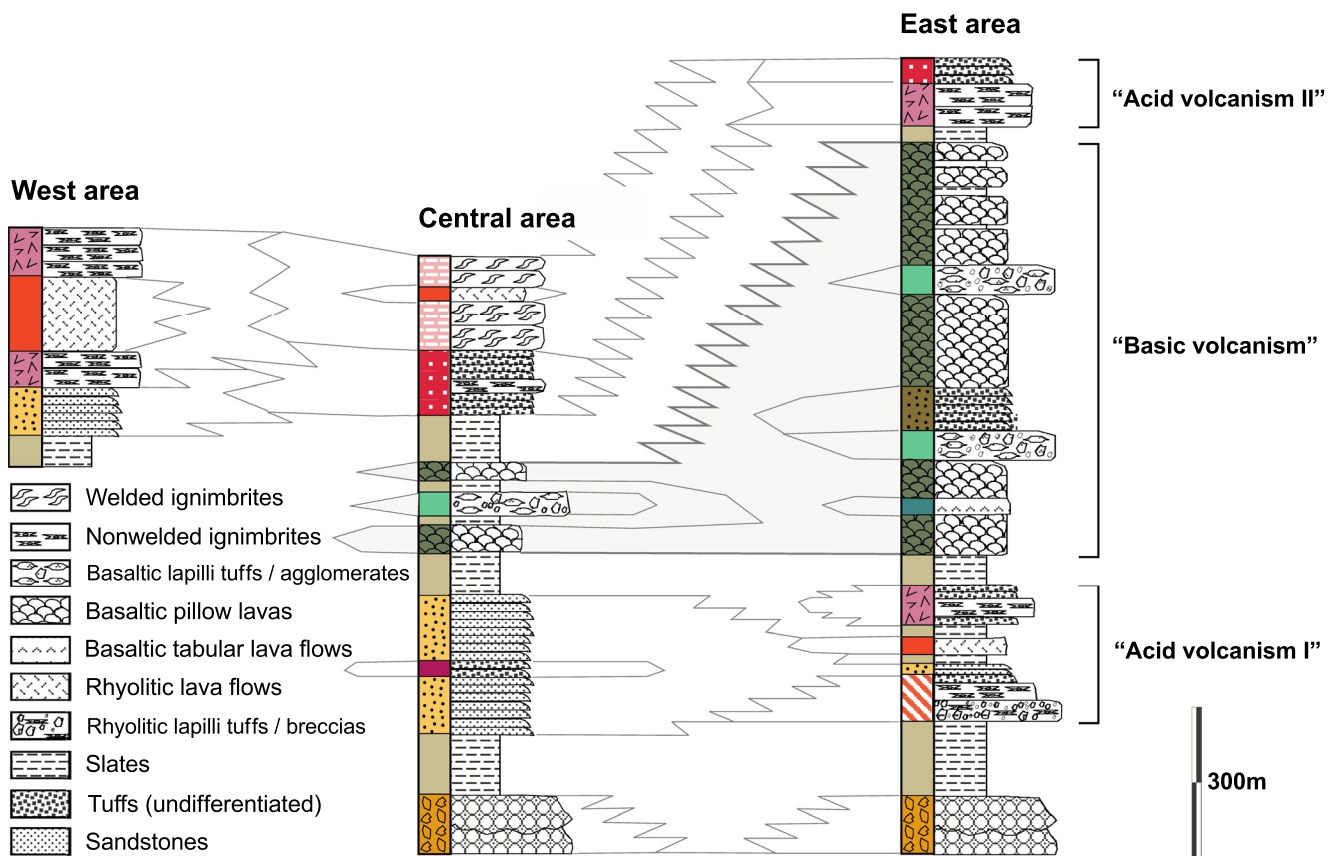
Figure 3. Synthetic stratigraphic logs of the West and East areas of the Matachel Basin, outstanding the main Tournaisian–Lower Viséan volcanic events defined by Apalategui et al. (1983). For correlation purposes it has been also included a synthetic stratigraphic log of a central sector of this basin.

Subsequent image analysis allowed planning of field itineraries and improved delineation of the main contacts in the field at the scale 1:18.000. Detailed outcrop descriptions in terms of rock structure and texture followed the procedure of McPhie et al. (1993). The preliminary map design was made at the 1:25.000 scale (Larrondo, 2014) on the basis of the Villafranca de los Barros (0829-II and 0829-IV), Hornachos (0830-I, 0830-III, and 0830-IV), Usagre (0855-I, 0855-II, and 0855-IV) and Maguilla (0856-III) sheets of the Spanish Topographic Map (MTN).

For the petrographic characterization, rock thin sections (48 mm × 28 mm in size, 30 μm thick) were prepared by the Technical Service of the University of the Basque Country (UPV/EHU). Various thin sections were stained following the method of Marsaglia and Tazaki (1992) and exposed to concentrated hydrofluoric acid before immersion in a supersaturated solution of sodium cobaltinitrite and, subsequently, in a supersaturated solution of barium chloride. Microscopic surveys were performed using a Leica DM LP device fitted with a CCD camera for microphotographic image acquisition. Modal determinations of rock-forming constituents were obtained by the point-count method (1,500 points/sample; Tables S2 and S3 in Supporting Information S1).

Mineral element concentrations were determined by Electron Microprobe using a Cameca SX 100 instrument at the University of Oviedo. Operating conditions of the microprobe were as follows: 10 s counting time (peak), ~10 nA beam current and 15 kV accelerating voltage. Calibration was done against French Geological Survey (BRGM) standard minerals and matrix correction factors (PAP) were used. Fe^{3+}/Fe^{2+} was estimated by charge balance criteria (Droop, 1987) and mineral formulae were normalized to 6 O for pyroxene, 23 O for amphibole, 8 O for plagioclase and alkali feldspar, and 4 O for titanomagnetite and ilmenite (Sarrionandia et al., 2023).

Before the whole rock major, trace and isotope geochemical characterization at the Geochronology and Isotope Geochemistry–SGIker Facility of the University of the Basque Country (UPV/EHU), rock samples were crushed and 2–4 cm in size pieces free of exotic components (e.g., hydrothermal infills, enclaves, weathered edges, etc.) were picked. These were reduced to small fragments (<0.8 mm) with a tungsten jaw crusher and quartered,

then milled in a tungsten ring mill to a homogenized powder. Major, trace and rare earth element concentrations were obtained by ICP–MS using the same mass spectrometer after sample fusion at ~1100°C with LiBO2 and dissolution in diluted HNO3:HF acid mixture. Precision of all analyses was in general <2% (always <4%; cf. García de Madinabeitia et al., 2008, for additional details).

Whole-rock Sr and Sm–Nd isotopic composition determinations involved purification of Sr, Sm and Nd following the procedures of Pin et al. (1994) and Pin and Santos Zalduegui (1997). Analyses were conducted on a multicollector ICP–MS (Neptune, Thermo Fisher Scientific). Mass fractionation was corrected following Balcaen et al. (2005) for Sr, Hofmann (1971) for Sm, and considering exponential laws of instrumental fractionation and specific algorithms for Nd. Elemental Sm and Nd concentrations were determined by isotope dilution using a mixed $^{149}Sm/^{150}Nd$ tracer.

5. Petrography and Mineral Chemistry

The "basic volcanism" episode generated rocks made of variable amounts of plagioclase, clinopyroxene and accessory magnetite and ilmenite. Some of the associated intrusives include also amphibole and accessory alkali feldspar, apatite and zircon (Tables S2 and S3 in Supporting Information S1). In general, these rocks appear variably altered to a secondary mineral assemblage including chlorite, opaque minerals, titanite, epidote, calcite, quartz, biotite, muscovite, actinolite-tremolite and alkali feldspar. This secondary assemblage is prevalent in the walls or infillings of rock micro-cracks and vesicles (amygdales). Its origin might be related to a mild regional metamorphic and/or to hydrothermal overprint.

Petrography of the basic lava flows studied reveals a broad textural spectrum, particularly in the case of pillow-lavas. In them, undercooling textural evidence are widespread. Although secondary alteration puts limits to a detailed petrographic characterization of the primary mesostasis, the microtextures observed can be grouped into the following four holocrystalline textural types: microlithic with a cryptocrystalline groundmass, (micro)-porphyritic with an intergranular groundmass, intergranular, and subophitic. Textures of the associated intrusive rocks vary from diabasic (interstitial) to subophitic, with only the coarsest-grained terms showing panidiomorphic seriated microtextures.

5.1. Plagioclase

In the basic lava flows, plagioclase generally appears as euhedral microliths. Plagioclase (micro)-phenocrysts and microliths exhibit undercooling textures such as skeletal, swallowtail, belt-buckle and bow-tie. Radiating microliths of plagioclase are also observed forming varioles in some textural varieties. In the intrusive basic rocks, plagioclase appears as euhedral crystals up to 5 mm long with negligible compositional zoning between cores and rims (An_{60-52}; Sarrionandia et al., 2023). By contrast, plagioclase in lava flows and in certain gabbros depicts extensive zoning (An_{58-01} and An_{66-01}, respectively). Such strong compositional variations might be related to the secondary processes that affected these rocks. Compositional variations are markedly narrower in plagioclases from dioritic intrusives (ranging from An_{22-39} at cores to An_{20-35} at rims).

5.2. Clinopyroxene

Clinopyroxene crystals exhibit a variety of undercooling morphologies (skeletal, dendritic, fibrous, radial) and, occasionally, constitute glomero-porphyritic or cumulophyric aggregates in the groundmass of the basic volcanic rocks. In subophitic textural varieties, they can form oikocrysts up to 8 mm in size. In the diorites, clinopyroxene appears transformed to ferropargasitic amphibole. Compositional zoning has not been observed (Sarrionandia et al., 2023). Clinopyroxene structural formulae correspond to the Ca–Mg–Fe type of Morimoto (1988), with similar augite compositions in the gabbros ($Wo_{37-41}En_{36-46}Fs_{8-15}$) and in the lava-flows ($Wo_{31-39}En_{32-49}Fs_{7-22}$; Figure 4a). The analyzed augites possess relatively high Mg# values (0.61–0.88 in lava-flows, 0.71–0.85 in gabbros) and exhibit wide variations in TiO_2 (0.47–3.54 wt.%) and Cr_2O_3 (0–0.72 wt.%) contents (Sarrionandia et al., 2023).

5.3. Amphibole

Amphibole variably replaces the clinopyroxene in the intrusives (fully in the diorites), where it forms coronitic textures. It appears as up to 0.02 mm long, hypidiomorphic crystals with short prismatic shapes. Occasionally, it may also form isolated, up to 2 mm long twinned xenomorphic to hypidiomorphic crystals with patchy zoning.
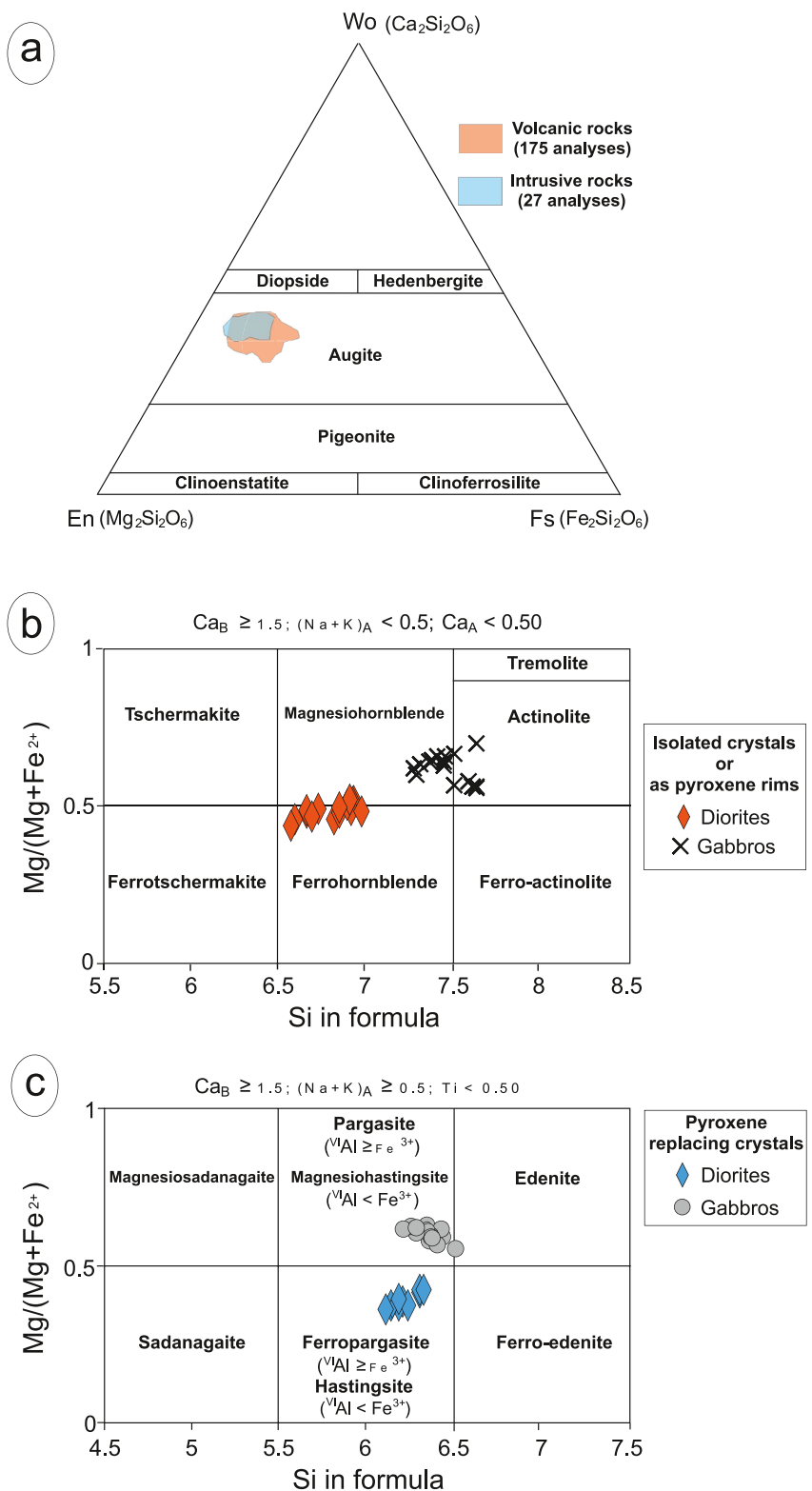
Figure 4. (a) Projection of analyzed pyroxenes in the Ca–Mg–Fe clinopyroxenes classification diagram of Morimoto (1988). (b, c) Projection of analyzed amphiboles in the classification diagram for calcic amphiboles of Leake et al. (1997).

Amphiboles replacing clinopyroxene in the gabbros are titanian magnesiohastingsite in the classification of Leake et al. (1997), whereas isolated single crystals correspond to actinolite and magnesiohornblende (Figures 4b and 4c). Cation site occupancies in titanian magnesiohastingsites are relatively homogeneous for $(Na + K)^A$ (0.63–0.74 atoms per formula unit, a.p.f.u.) and Al^{IV} (1.48–1.78 a.p.f.u.). They also exhibit homogeneous $Mg/(Mg + Fe^{2+})$ ratios (0.60–0.69) and relatively high Ti contents (0.32–0.40 a.p.f.u.). By contrast, actinolite and magnesiohornblende are characterized by wider ranges of cation site occupancy, with $(Na + K)^A = 0.07$–0.32 a.p.f.u., $Al^{IV} = 0.35$–0.71 a.p.f.u., low Ti contents (0.03–0.13 a.p.f.u.) and $Mg/(Mg + Fe^{2+})$ ratios (0.58–0.73) close to those of titanian magnesiohastingsites (Sarrionandia et al., 2023). In general, amphiboles from the studied gabbros are poor in Cr (<0.03 a.p.f.u.) and lack core-rim compositional variations.

Isolated amphibole crystals in diorites are magnesiohornblende and ferrohornblende and show minor compositional variations from core to rim. They exhibit slightly higher contents of $(Na + K)^A$ (0.21–0.46 a.p.f.u.), Al^{IV} (1.01–1.42 a.p.f.u.) and Ti (0.08–0.26 a.p.f.u.), and lower $Mg/(Mg + Fe^{2+})$ ratios (0.48–0.60) than amphiboles from gabbros. Amphiboles replacing clinopyroxene in diorites are ferropargasite (Figure 4c). Compared to the texturally equivalent titanian magnesiohastingsite of gabbros, these are unzoned and depict a wider range of $(Na + K)^A$ (0.50–0.64 a.p.f.u.) and Al^{IV} (1.67–1.89 a.p.f.u.), distinctly lower Ti (0.04–0.09 a.p.f.u.) and Cr contents (<0.01 a.p.f.u.), and $Mg/(Mg + Fe^{2+})$ ratios of 0.41–0.48.

5.4. Opaque and Accessory Minerals

Opaque minerals are mostly titanomagnetite and ilmenite, usually appearing as isolated crystals with undercooling microtextures (e.g., acicular, skeletal, and dendritic). Occasionally they exhibit radial arrangements. Rare alkali feldspar (orthoclase, Or_{93-97}; Deer et al., 1963) has been observed as micro-phenocrysts (an interstitial phase from the mesostasis) only in one basic lava-flow (intermediate composition pillow-lava sample VFB-9) with a ~28% modal proportion (Sarrionandia et al., 2023). In intrusive gabbro and diorite rocks, it is an accessory phase restricted to the groundmass.

6. Whole-Rock Geochemistry

6.1. Major and Trace Element Geochemistry

The hydrothermal and/or low-grade metamorphic alteration described in the previous section is likely responsible for the relatively high values of lost on ignition material (LOI > 2.5 wt.% at 1,100°C) observed in 13 samples (Table 1). Nevertheless, this alteration seems not pervasive since part of the LOI in a number of studied samples could be related to the presence of primary amphibole (and not exclusively associated with clay minerals, among others, product of alteration). In fact, calculation of the chemical index of alteration (CIA; Nesbitt & Young, 1982) of the studied samples provides CIA values of 38–43, comparable to those of unaltered basalts (CIA = 30–45; Nesbitt & Young, 1982). Only three samples with SiO_2 < 52 wt% show CIA values ≥45. Nevertheless, the geochemical characterization that follows is based mainly upon elements that behave as relatively immobile during secondary hydrothermal or metamorphic overprints (up to P and T conditions of the amphibolite facies). Those elements are Al, V, Sc, Cr, Ni, high field strength elements (Th, Zr, Hf, Ti, Nb, Ta), and the rare earth elements (REE) excluding Ce and Eu (Pin & Waldhausrová, 2007).

The rock samples analyzed are basic to intermediate (SiO_2: 47.11–56.46 wt.%) sub-alkali basalts and basaltic andesites in the Nb/Y-Zr/Ti diagram (Pearce, 1996; Figure 5a). According to displayed FeO^{Tot}/MgO ratios, TiO_2, Nb, Th, Y, and REE contents (Figures 5b–5d), and, in the less evolved samples, the normative mineralogy, three rock groups can be defined for description and discussion purposes, hereafter labeled Group #1, #2, and #3. Moreover, the geochemical characteristics of the samples ascribed to Group #3 depart markedly from those of Groups #1 and #2 characteristics, suggesting the existence of different magmatic associations.

Basalts of the Group #1 and basalts and basaltic andesites of the Group #2 are relatively richer in Al_2O_3 (~15–22 wt.%) than the Group #3 sub-alkali basalts and basaltic andesites (~15 wt.%; Table 1). Mg# values (100*MgO/ $[FeO^t + MgO]$, expressed in molecular percent; mol%) are markedly higher in the Groups #1 (54–70), and #2 (43–66) than in Group #3 rocks (33–56; Table 1). Fe_2O_3, TiO_2, P_2O_5, V and, particularly, Zr, Y and total REE (ΣREE) contents, are lower in Group #1 and #2 rocks than in Group #3, whereas the converse occurs with Cr and Ni contents (Figure 6). In spite of their overall geochemical similarity, basalts of Group #1 differ from Group #2 rocks by their slightly lower contents in P_2O_5, Zr, Nb, Th and ΣREE (Figure 6; Table 1).

Table 1
Whole-Rock Geochemical Data of the Lava-Flows and Intrusives Integrated in the "Basic Volcanism" of the Matachel Basin

Sample	MGA-1	MTC-84B	MTC-83	MTC-42	HNC-3	VFB-12	MTC-48	MGA-20	MGA-22	MGA-12	VFB-11	MDL
Geochemical group	#1	#1	#1	#1	#1	#1	#2	#2	#2	#2	#2	ppm
SiO_2	47.11	47.24	47.92	48.05	48.82	52.12	49.80	49.90	50.13	50.72	50.95	0.801
TiO_2	1.24	1.25	1.94	0.81	1.32	1.60	1.53	1.12	1.17	1.42	1.52	0.001
Al_2O_3	16.83	20.13	16.70	16.81	17.51	15.69	16.03	17.20	16.60	15.19	16.51	0.002
Fe_2O_3	8.40	7.50	10.08	7.75	8.81	9.10	9.35	8.15	7.90	10.00	8.13	0.005
MnO	0.14	0.16	0.17	0.15	0.15	0.15	0.14	0.12	0.13	0.14	0.17	2.003
MgO	8.60	6.21	7.09	9.02	6.02	5.42	7.26	8.00	7.70	3.80	6.86	0.002
CaO	10.53	11.00	9.61	10.82	10.60	7.84	8.83	9.07	8.80	8.44	8.76	0.991
Na_2O	3.00	3.10	3.49	2.75	3.80	4.19	3.21	2.81	2.82	3.84	3.21	0.001
K_2O	0.58	0.51	0.52	0.95	0.40	1.89	0.69	0.65	1.88	3.39	0.97	0.026
P_2O_5	0.14	0.23	0.29	0.10	0.16	0.14	0.19	0.12	0.21	0.19	0.30	0.011
LOI	3.37	2.67	2.17	2.75	2.29	1.88	2.93	2.94	2.59	2.72	2.54	
TOTAL	99.94	100.00	99.98	99.96	99.88	100.02	99.96	100.08	99.93	99.85	99.92	
Ba	114	151	229	229	145	315	175	160	360	277	371	0.794
Co	53.5	41.6	48.4	50.4	51.0	46.0	45.7	48.2	44.9	50.6	49.3	0.302
Cr	201	117	190	392	95.3	26.3	126	264	359	111	254	0.756
Cu	61.1	34.5	54.5	79.1	59.3	58.7	45.6	38.9	18.4	10.2	36.9	0.021
Nb	5.10	8.20	9.80	3.90	4.10	5.40	6.50	5.50	8.10	6.20	11.8	0.179
Ni	135	84.0	63.8	115	47.0	12.0	83.5	67.3	67.3	42.4	136	3.746
Pb	4.80	9.90	4.60	8.20	5.60	4.50	6.30	4.50	7.60	5.20	6.90	0.022
Rb	28.6	14.0	11.5	59.5	18.7	53.4	15.6	17.2	67.4	174	32.7	0.138
Sr	266	380	207	292	297	270	223	194	515	234	406	0.092
Th	1.50	2.10	2.10	2.10	2.30	3.30	4.00	4.00	4.50	4.70	5.70	0.004
U	0.10	0.20	0.70	0.50	0.30	0.20	1.30	1.30	0.50	<0.01	3.00	0.004
V	153	139	205	143	207	210	180	163	184	182	169	0.151
Y	22.5	19.9	34.4	18.9	25.3	33.1	34.0	26.6	22.5	35.8	27.9	0.012
Zn	61.2	81.5	79.8	74.3	65.4	62.4	73.3	54.2	67.2	72.5	67.1	2.747
Zr	101	103	163	79.8	100	143	175	136	121	185	189	0.177
La	4.75	8.08	10.7	3.99	5.73	8.28	11.9	10.0	16.3	12.7	18.6	0.013
Ce	12.9	19.7	26.9	11.0	15.5	21.7	29.7	24.5	36.5	30.9	42.5	0.016
Pr	1.98	2.49	3.74	1.62	2.25	2.88	3.71	3.12	4.39	3.91	5	0.003
Nd	9.66	12.6	18.5	8.28	11.7	14.9	18.6	14.1	19.1	19.4	23.1	0.025
Sm	2.70	2.98	4.81	2.37	3.24	4.02	4.48	3.65	4.15	4.60	4.81	0.021
Eu	1.04	1.18	1.63	0.94	1.28	1.46	1.41	1.13	1.28	1.45	1.50	0.003
Gd	3.22	2.96	5.19	2.48	3.43	4.31	4.11	3.93	4.05	4.47	4.25	0.006

Table 1
Continued

Sample	MGA-1	MTC-84B	MTC-83	MTC-42	HNC-3	VFB-12	MTC-48	MGA-20	MGA-22	MGA-12	VFB-11	MDL
Geochemical group	#1	#1	#1	#1	#1	#1	#2	#2	#2	#2	#2	ppm
Tb	0.560	0.610	0.930	0.540	0.720	0.950	0.910	0.690	0.660	1.00	0.850	0.001
Dy	3.53	3.49	5.60	3.21	4.26	5.56	5.48	4.29	3.91	6.04	4.76	0.004
Ho	0.610	0.730	1.00	0.690	0.910	1.22	1.20	0.800	0.690	1.31	1.02	0.001
Er	1.89	1.98	2.90	1.85	2.43	3.29	3.24	2.34	1.99	3.56	2.71	0.003
Tm	0.360	0.310	0.460	0.320	0.410	0.520	0.510	0.360	0.300	0.540	0.390	0.002
Yb	2.00	1.90	2.84	1.76	2.34	3.22	3.16	2.33	1.96	3.46	2.57	0.003
Lu	0.270	0.300	0.460	0.270	0.360	0.510	0.500	0.360	0.310	0.520	0.380	0.000
ΣREE	45.5	59.3	85.6	39.3	54.5	72.8	88.8	71.7	95.6	93.7	112	
$(La/Lu)_N$	1.89	2.89	2.49	1.58	1.71	1.74	2.54	2.99	5.65	2.61	5.24	
$(La/Sm)_N$	1.14	1.75	1.43	1.09	1.14	1.33	1.71	1.78	2.54	1.78	2.49	
$(Gd/Lu)_N$	1.47	1.22	1.39	1.14	1.18	1.04	1.02	1.35	1.61	1.06	1.38	
Ti/Y	330	377	338	257	313	290	270	252	312	238	327	
Ti/Zr	74	73	72	61	79	67	52	49	58	46	48	
#Mg	66.98	62.13	58.22	69.75	57.52	54.13	60.61	66.04	65.88	42.95	62.57	

Sample	MGA-19	MTC-17	USG-14	MTC-275	MGA-2	MTC274B	MTC-75	MTC-76	MTC-77	VFB-9	MGA-25	MGA-13	MDL
Geochemical group	#2	#2	#2	#3	#3	#3	#3	#3	#3	#3	#3	#3	ppm
SiO_2	51.19	52.31	54.51	47.38	49.10	50.25	50.45	51.36	52.55	54.04	54.75	56.46	0.801
TiO_2	1.03	1.13	1.05	3.19	2.34	2.48	2.30	2.26	2.37	1.73	2.12	1.08	0.001
Al_2O_3	21.97	15.76	15.02	15.21	14.82	16.63	14.75	14.69	14.90	13.32	14.29	15.32	0.002
Fe_2O_3	5.18	9.37	7.20	13.34	11.29	12.00	11.75	11.52	10.45	10.69	9.80	7.43	0.005
MnO	0.12	0.10	0.15	0.21	0.23	0.20	0.15	0.16	0.15	0.17	0.14	0.10	2.003
MgO	3.57	5.22	4.01	4.47	2.75	4.16	5.10	4.84	4.55	3.99	4.20	4.71	0.002
CaO	7.42	4.02	8.55	7.36	8.17	7.28	8.85	8.64	5.90	5.63	7.68	5.29	0.991
Na_2O	3.96	4.10	4.70	3.39	5.24	3.94	3.34	3.37	5.70	6.87	3.73	6.66	0.001
K_2O	2.37	3.40	1.59	0.66	1.03	0.94	0.91	0.80	0.95	2.03	0.89	0.37	0.026
P_2O_5	0.13	0.57	0.19	0.42	0.59	0.35	0.32	0.34	0.34	0.23	0.33	0.48	0.011
LOI	2.74	3.15	3.01	4.04	4.07	1.54	2.00	1.69	2.10	1.31	1.68	2.10	
TOTAL	99.68	99.13	99.98	99.67	99.63	99.77	99.92	99.67	99.96	100.01	99.61	100.00	
Ba	324	1,020	473	258	600	297	306	265	370	438	358	265	0.794
Co	35.4	41.1	45.2	48.4	35.5	52.5	51.8	48.0	53.2	57.7	62.1	48.2	0.302
Cr	42.3	19.9	94.0	99.5	9.20	27.5	19.5	18.1	19.8	52.0	19.6	51.1	0.756
Cu	21.2	13.8	18.2	25.2	18.5	21.1	36.0	25.1	21.1	24.2	37.1	0.70	0.021
Nb	5.50	8.80	8.10	8.90	16.2	9.40	8.90	9.50	9.70	7.00	9.30	10.5	0.179

Table 1
Continued

| Sample	MGA-19	MTC-17	USG-14	MTC-275	MGA-2	MTC274B	MTC-75	MTC-76	MTC-77	VFB-9	MGA-25	MGA-13	MDL
Geochemical group	#2	#2	#2	#3	#3	#3	#3	#3	#3	#3	#3	#3	ppm
Ni	21.0	5.30	17.5	19.7	3.75	1.70	12.2	11.7	11.4	20.2	14.4	21.8	3.746
Pb	5.70	6.90	6.60	18.6	9.60	18.6	6.70	6.60	5.70	6.50	6.90	5.30	0.022
Rb	63.5	128	51.9	20.2	20.3	25.9	15.7	15.1	13.0	318	18.5	5.60	0.138
Sr	351	366	387	234	309	270	237	226	152	226	218	145	0.092
Th	4.50	5.70	7.30	4.30	8.70	2.90	4.90	4.90	5.70	5.60	5.40	12.5	0.004
U	<0.01	0.60	1.00	0.10	4.40	0.80	1.50	2.00	2.20	<0.01	0.80	2.30	0.004
V	126	218	149	346	227	334	261	258	285	201	249	158	0.151
Y	25.0	26.1	25.3	58.7	52.4	50.0	46.3	47.3	49.4	45.2	42.4	34.4	0.012
Zn	39.0	47.2	56.6	124	114	131	101	95.6	99.8	84.6	83.9	49.7	2.747
Zr	141	148	174	283	294	192	245	254	268	240	250	255	0.177
La	10.4	17.8	18.1	18.5	29.2	21.1	18.6	18.8	19.8	17.0	17.9	23.8	0.013
Ce	25.3	40.0	40.3	45.1	70.3	49.2	44.7	46.0	49.4	40.6	43.1	55.7	0.016
Pr	3.21	4.67	4.65	7	8.35	7.27	5.54	5.71	6.17	5.05	5.52	6.51	0.003
Nd	14.6	21.9	19.4	31.8	39.8	31.8	27.2	27.9	29.9	24.7	26.0	29.5	0.025
Sm	3.79	4.60	4.18	8.54	8.68	7.96	6.41	6.67	7.04	6.12	6.38	6.24	0.021
Eu	1.09	1.42	1.08	2.37	2.22	2.14	2.16	2.15	1.99	1.78	2.05	1.77	0.003
Gd	3.93	4.03	4.03	8.82	8.39	7.89	6.47	6.59	6.50	6.22	6.65	5.21	0.006
Tb	0.700	0.790	0.670	1.60	1.63	1.44	1.36	1.37	1.40	1.33	1.20	1.00	0.001
Dy	4.25	4.54	3.93	10.6	9.27	9.59	7.83	8.08	8.25	7.89	7.09	5.65	0.004
Ho	0.770	0.930	0.680	2.18	1.97	1.97	1.68	1.74	1.77	1.70	1.28	1.19	0.001
Er	2.29	2.52	2.00	5.80	5.25	5.20	4.55	4.64	4.82	4.62	3.70	3.16	0.003
Tm	0.370	0.370	0.330	0.980	0.830	0.870	0.740	0.760	0.740	0.760	0.600	0.480	0.002
Yb	2.30	2.41	2.00	5.89	5.00	5.18	4.39	4.50	4.66	4.56	3.72	3.06	0.003
Lu	0.370	0.360	0.330	1.010	0.790	0.890	0.690	0.700	0.700	0.720	0.590	0.460	0.000
ΣREE	73.3	106	102	150	192	152	132	136	143	123	126	144	
$(La/Lu)_N$	3.00	5.30	5.86	1.97	3.95	2.54	2.89	2.88	3.03	2.53	3.25	5.55	
$(La/Sm)_N$	1.76	2.50	2.79	1.40	2.17	1.71	1.88	1.82	1.81	1.79	1.81	2.46	
$(Gd/Lu)_N$	1.31	1.38	1.51	1.08	1.31	1.10	1.16	1.16	1.15	1.07	1.39	1.40	
Ti/Y	247	260	249	326	268	297	298	286	288	229	300	188	
Ti/Zr	44	46	36	68	48	78	56	53	53	43	51	25	
#Mg	57.73	52.47	52.46	39.90	32.55	40.72	46.24	45.43	46.31	42.51	45.92	55.67	

Note. Major elements in wt.% and trace elements in ppm. There have been also included Mg# values ($100*MgO/[FeO^t + MgO]$ expressed in mol.%), total contents of Rare Earth Elements (ΣREE), and Chondrite (Sun & McDonough, 1989) normalized La/Lu; La/Sm; and Gd/Lu ratios. MDL: method detection limit.
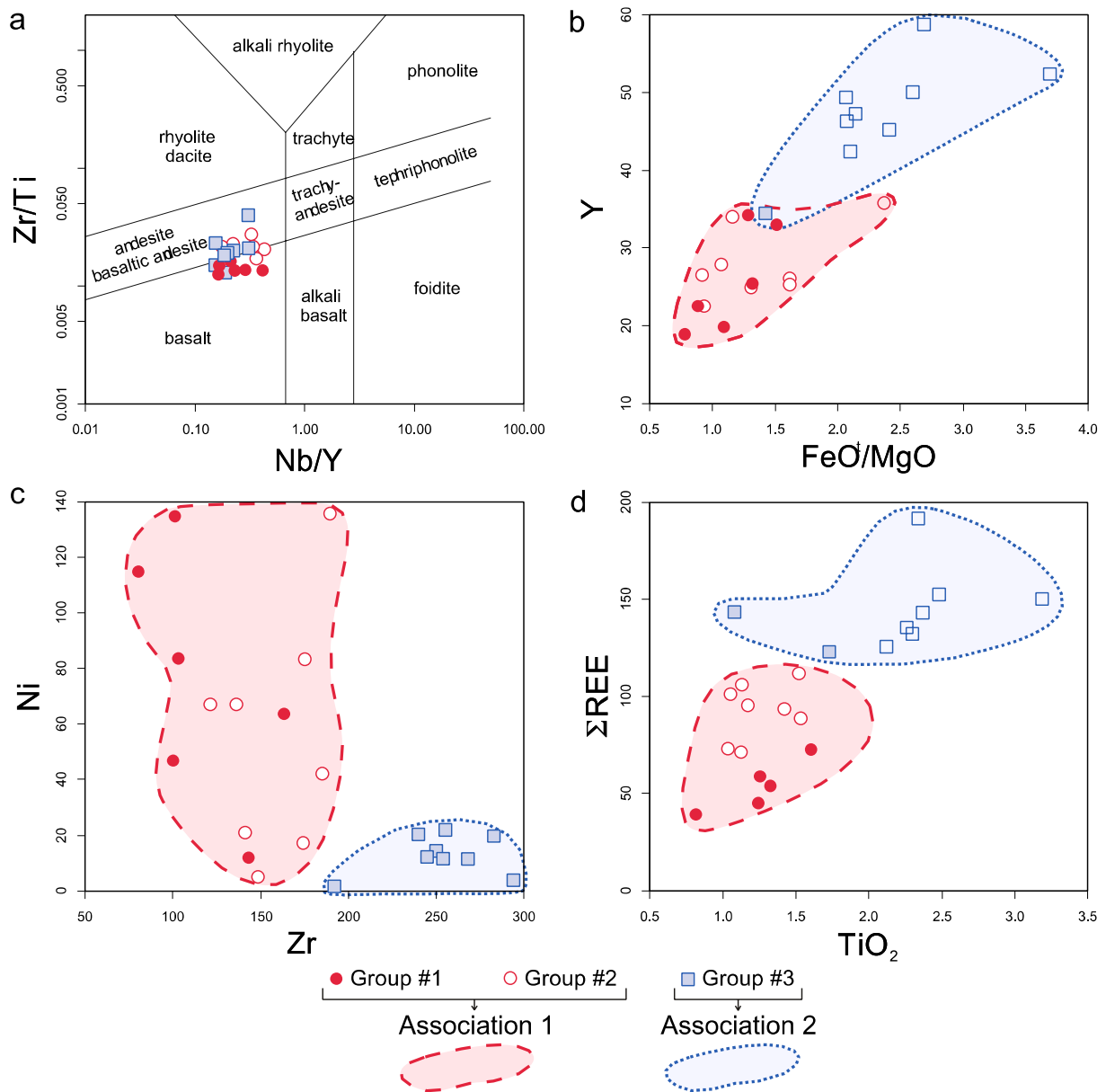
Figure 5. (a) Projection of the analyzed samples in the Zr/Ti–Nb/Y diagram for altered and/or metamorphosed volcanic rocks (Pearce, 1996). Projection of the identified associations and geochemical groups of the Matachel Basin "basic volcanism" in the (b) Y–FeO^t/MgO diagram, (c) Ni–Zr diagram, and (d) ΣREE–TiO$_2$ diagram.

Major and trace element variation diagrams depict rough linear correlations within each group (Figure 6). This might point to a single magmatic differentiation array, notably in the case of Groups #1 and #3, since a greater dispersion is shown by Group #2 samples. As regards the whole rock geochemical trends, the main difference among the three rock groups relates to the variations of MgO, Fe$_2$O$_3$, and TiO$_2$ with respect to the silica contents (Figure 6). Progressive enrichment of residual liquids in Fe and Ti in Groups #1 and #2 concurs with a Fenner differentiation trend (Fenner, 1929) whereas in Group #3 Fe and Ti enrichment is more consistent with a calc-alkaline trend (Figure 6).

Alteration effects in most samples preclude conventional interpretations after AFM diagram projections (Tilley, 1960). The same stands for the definition of clear trends in the TiO$_2$ versus FeO*/MgO diagram (Miyashiro, 1974), but in the FeOt/MgO versus SiO$_2$ diagram (Figure 7; Miyashiro, 1974) both contrasting trends are discernible. Notwithstanding, the tholeiitic character of Groups #1 and #2 samples (in part overlapping)
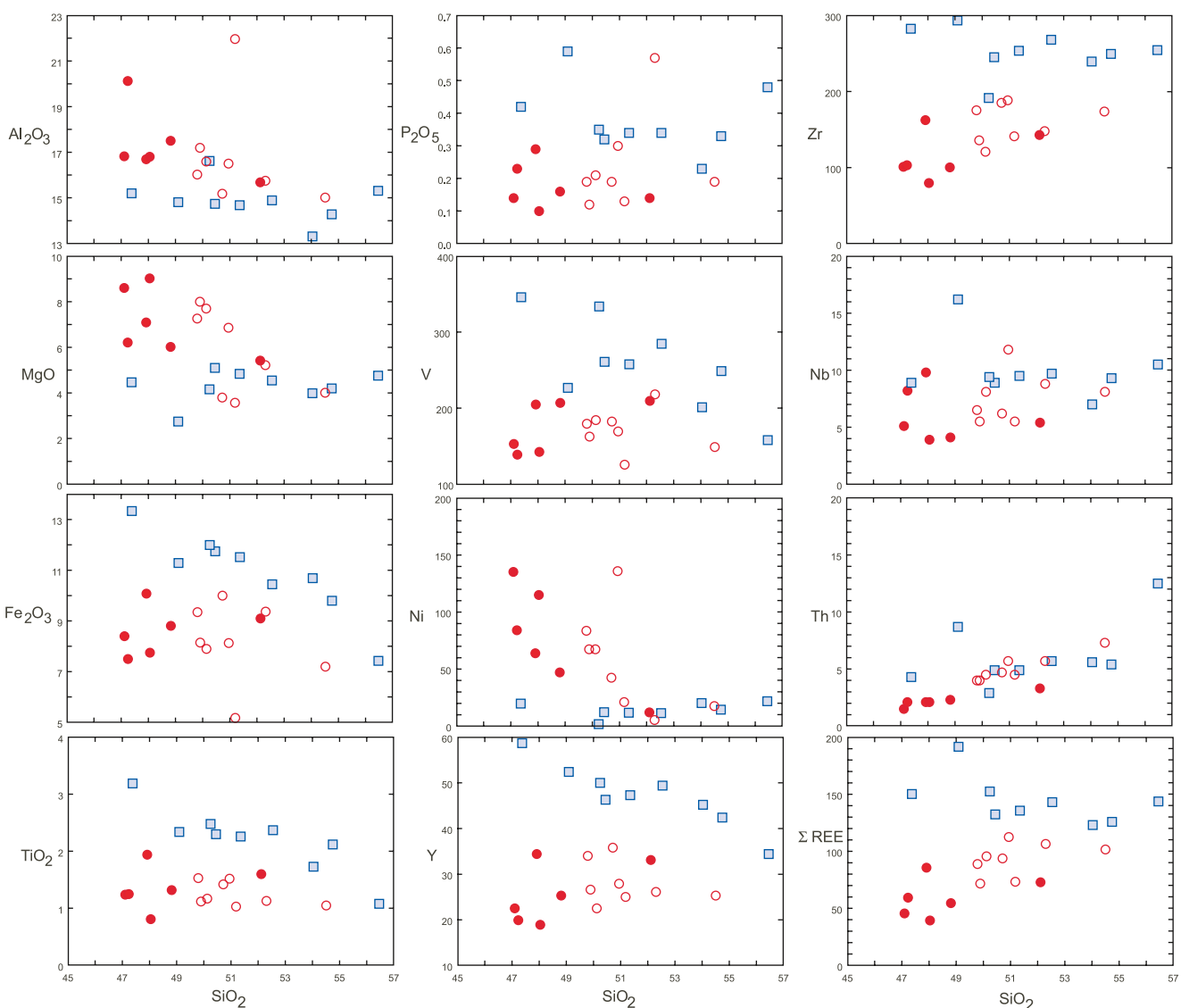
Figure 6. Variation diagrams of immobile major and trace elements of the geochemical groups identified in the "basic volcanism" of the Matachel Basin. Employed symbols correspond to those of Figure 5.

can be inferred from the broadly positive slopes of their plotted data fields. Group #3 samples appear slightly displaced in the TiO_2 versus FeO^*/MgO diagram and lack a clear trend, but in the $FeOt/MgO$ versus SiO_2 diagram they define a marked negative trend (Figure 7). The Al_2O_3 contents observed in the basalts of Groups #1 and #2 (15.19–21.97 wt.%) are consistent in general with a tholeiitic character (Bertrand et al., 1982; Dessureau et al., 2000; Dostal & Dupuy, 1984; Peate & Hawkesworth, 1996; Stepanova et al., 2014), though some samples are particularly enriched ($Al_2O_3 > 16$ wt.%). By contrast, seemingly calc-alkaline basalts of the Group #3 bear smaller Al_2O_3 (14.69–16.63 wt.%) contents that are not uncommon in tholeiitic basalts. Chemical differences among the less altered basalts (LOI < 2.5 wt.%) are also reflected in their normative mineralogy. Following Yoder and Tilley (1962), basic samples of Group #1 rocks would classify as olivine basalts and as alkali basalts, whereas those of the Groups #2 and #3 would be saturated and oversaturated tholeiites, respectively.

A distinctive geochemical characteristic of the Group #3 rocks is the progressive decrease in total REE with the increase in SiO_2, contrary to the trends observed in Groups #1 and #2 (Figure 6). Chondrite-normalized REE diagrams (Sun & McDonough, 1989) are similar for the three groups but differ in their enrichment with respect to the chondrite values. In this respect, it is outstanding in Group #3 rocks a ca. two orders of magnitude LREE enrichment with respect to the chondrite (Figure 8). This enrichment is also observable in the ΣREE versus SiO_2
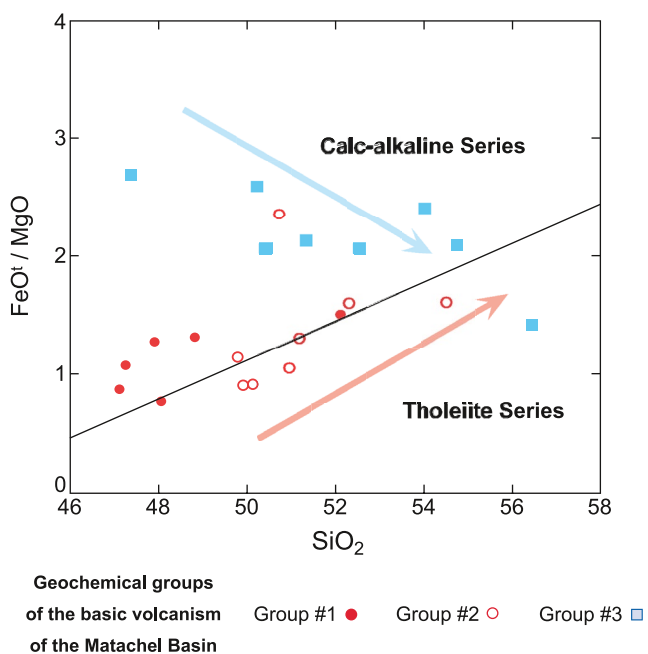
Figure 7. FeOt/MgO–SiO$_2$ diagram for the discrimination of tholeiitic and calc-alkaline series evolution (adapted from Miyashiro, 1974).

diagram (Figure 6). Normalized patterns are in general almost flat-shaped and less fractionated in the case of Group #1 (La$_N$/Lu$_N$: 1.6–2.9) than in Groups #3 (La$_N$/Lu$_N$: 2.0–5.6) and #2 (La$_N$/Lu$_N$: 2.5–5.9). From this viewpoint, fractionation in the Group #1 is similar for LREE (La$_N$/Sm$_N$: 1.1–1.8) and HREE (Gd$_N$/Lu$_N$: 1.0–1.5), whereas in the Groups #2 and #3 the fractionation of LREE is more pronounced, as reflected by their slightly segmented normalization profiles (La$_N$/Sm$_N$: 1.7–2.8; Gd$_N$/Lu$_N$: 1.0–1.6 and La$_N$/Sm$_N$: 1.4–2.5; Gd$_N$/Lu$_N$: 1.1–1.4, respectively; Figure 8).

N-MORB–normalized multi-element diagrams (Sun & McDonough, 1989) show in general similar segmented patterns for the three geochemical groups, with marked enrichments in Th, particularly in Groups #2 and #3 (Figure 8). These diagrams show an overall slight enrichment in LREE for the three groups, clearly less pronounced in Group #1, with roughly similar HREE contents respect to N-MORB and a slight depletion in P that is not always observable in Groups #2 and #3 (Figure 8). E-MORB–normalized multi-element diagrams show near horizontal profiles with marked enrichments in Th. In detail, the Group #1 profiles fit overall to the E-MORB (albeit with marked depletions in Nb and, to a lesser extent, in P) whereas Group #2 and, particularly, Group #3 profiles display more enriched patterns (Figure 8). Moreover, depletion in Nb and P respect to E-MORB are not always present in the Group #2 and are practically absent in Group #3 samples (Figure 8).

6.2. Isotope Geochemistry

Hydrothermal alteration and/or low-grade metamorphism can affect the Rb and Sr elemental contents (Pin & Waldhausrová, 2007, and references therein) and, therefore, the Rb–Sr isotope systematics. In the rocks studied, this is reflected by the wide ranges of ^{87}Rb/^{86}Sr and 87Sr/86Sr isotopic ratios in each geochemical group (Table 2). Those ratios appear uncorrelated with SiO$_2$ contents and, thus, prevent the consideration of this isotopic system for further petrogenetic considerations. By contrast, the linear correlation observed in the elemental Sm–Nd diagram (Figure 9a) reflects the stability of Sm and Nd during secondary alteration (DePaolo, 1988). In Figure 9a a rough clustering of the samples analyzed into the three geochemical groups already identified is outstanding. The Group #3 rocks appear as the most enriched in Nd (24.5–38.4 ppm) and Sm (6.35–9.04 ppm), the less enriched being the Group #1 basalts (Nd: 10.1–18.8 ppm; Sm: 2.92–5.18 ppm). Basalts and basaltic andesites of Group #2 (Nd: 15.2–20.3 ppm; Sm: 4.02–5.06 ppm) overlap the field of the most enriched samples of Group #1 (Figure 9a; Table 2).

Geochemical differences among the three compositional groups identified are also reflected in their ^{147}Sm/^{144}Nd and ^{143}Nd/^{144}Nd ratios (Figure 9b; Table 2), that also enable us to discern a rough positive general trend in the ^{143}Nd/^{144}Nd–^{147}Sm/^{144}Nd diagram (Figure 9b). In general, Group #1 basalts are the most radiogenic and exhibit the highest isotopic ratios, whereas some Group #2 rocks exhibit the least radiogenic ratios. Sub-alkali basalts and basaltic andesites of the Group #3 lie in between both groups, though partially overlapping the projection area of Group #2 rocks (Figure 9b; Table 2). It may be noted in this diagram the nearly vertical trends defined by the Group #1 and, to a lesser extent, the Group #3 samples, while those of Group #2 show a marked positive correlation (Figure 9b; Table 2).

As regards the εNd$_{335Ma}$ values (Table 2), these also support the geochemical group distinction. The Group #1 basalts include the most radiogenic samples, which exhibit moderately positive εNd$_{335Ma}$ values comprised in a relatively narrow range (+4.0–+6.6). The Group #2 rocks include the less radiogenic samples, with εNd$_{335Ma}$ values mainly positive but encompassing a wider range (−0.2–+3.5). Finally, the Group #3 rocks (with the exception of the particularly unradiogenic sample MTC274B, with εNd$_{335Ma}$ = +0.9) present and the narrowest εNd$_{335Ma}$ range (+2.8–+4.8) and positive values comprised between those of the Groups #1 and #2.

The projection of the whole set of εNd$_{335Ma}$ values versus SiO$_2$ and Th contents shows two general evolutionary trends (Figures 9c and 9d). Samples of the Groups #1 and #2 can be integrated in a single array showing a rough negative correlation (Figures 9c and 9d). Samples of the Group #3 (excluding the deviating sample MTC274B)
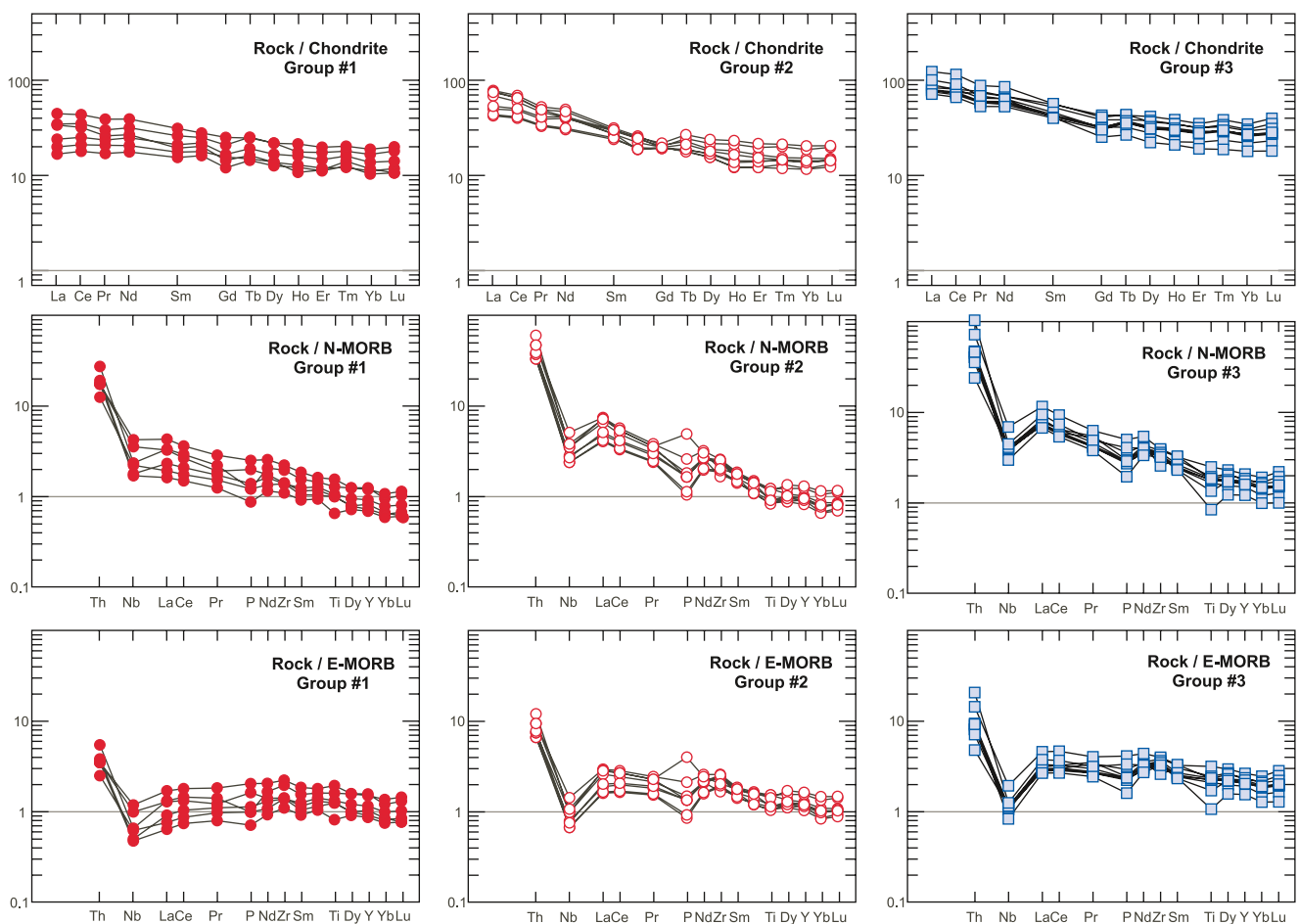
Figure 8. Normalized multi-element diagrams of the geochemical groups identified in the "basic volcanism" of the Matachel Basin. Normalization values correspond to Chondrite (Sun & McDonough, 1989), N–MORB (Sun & McDonough, 1989), and E–MORB (Sun & McDonough, 1989).

define a nearly horizontal array that intercepts the general trend integrated by Groups #1 and #2. Interestingly, the paths' intersection coincides with the transition from Group #1 to Group #2 samples (Figures 9c and 9d). Finally, it may be noted that Sm–Nd depleted mantle model ages (TDM; DePaolo, 1988) are similar for the three geochemical groups (Table 2; Figure 9e). In detail, however, the calculated TDM values for Group #1 basalts (following Liew & Hofmann, 1988) are slightly younger (0.77–1.22 Ga) than those of the Group #2 (1.03–1.36 Ga) and Group #3 rocks (0.84–1.34 Ga).

7. Discussion

In the following sections, we discuss the geochemical nature and linkage of the three magmatic associations identified in the Mississippian Matachel mid "basic volcanism" (and cogenetic subvolcanic intrusions) of its up to 1.000 m thick volcanic basin infill. We bring to a focus their mantle sources, differentiation processes and petrotectonic significance in the regional geologic context of SW Iberia.

### 7.1. Geochemical Nature of the Magmatic Associations

Whole-rock geochemical characteristics of basalts and basaltic andesites indicate that the "basic volcanism" of the Matachel Basin was nurtured by tholeiitic (Groups #1 and #2) and seemingly calc-alkaline (Group #3) magmas. Occurrence in the southern Iberian Massif of a Mississippian MORB-type tholeiitic magmatism was documented either in the distal areas of the Los Pedroches (North Marine) basin (Armendáriz et al., 2008) or in the South-Portuguese (South Marine) basin (Munhá, 1983). In the latter domain Mitjavila et al. (1997) also

Table 2
Whole-Rock Isotope Data (Rb–Sr and Sm–Nd Systematics) of the Lava-Flows and Intrusives Integrated in the "Basic Volcanism" of the Matachel Basin (Measured and Age Corrected to 335 Ma)

Sample	Group	SiO$_2$ (wt.%)	Rb (ppm)	Sr (ppm)	^{87}Rb/^{86}Sr	^{87}Sr/^{86}Sr	2σ error (abs)	^{87}Sr/^{86}Sr$_{335}$	Sm (ppm)	Nd (ppm)	^{147}Sm/^{144}Nd	^{143}Nd/^{144}Nd	2σ error (abs)	^{143}Nd/^{144}Nd$_{335}$	εNd$_{335}$	T$_{DM}$ (Ga)	T$_{DM}$ 2stg (Ga)
MGA-1	#1	47.11	28.6	266	0.311	0.705792	0.000007	0.7043	12.2	3.72	0.1852	0.512949	0.000006	0.512543	6.6	0.91	0.53
MTC-84B	#1	47.24	14.0	380	0.107	0.704568	0.000006	0.7041	12.7	3.33	0.1578	0.512844	0.000005	0.512498	5.7	0.77	0.60
MTC-83	#1	47.92	11.5	207	0.161	0.704455	0.000007	0.7037	18.8	5.18	0.1664	0.512841	0.000006	0.512476	5.3	0.90	0.64
MTC-42	#1	48.05	59.5	292	0.590	0.708690	0.000005	0.7059	10.1	2.92	0.1757	0.512853	0.000007	0.512468	5.1	1.05	0.65
HNC-3	#1	48.82	18.7	297	0.182	0.706050	0.000007	0.7052	12.6	3.63	0.1742	0.512793	0.000007	0.512411	4.0	1.22	0.74
VFB-12	#1	52.12	53.4	270	0.573	0.707910	0.000006	0.7052	14.9	4.24	0.1718	0.512847	0.000004	0.512470	5.1	0.98	0.64
MTC-48	#2	49.80	15.6	223	0.202	0.705146	0.000005	0.7042	18.4	4.82	0.1586	0.512725	0.000008	0.512377	3.3	1.08	0.79
MGA-20	#2	49.90	17.2	194	0.257	0.706400	0.000006	0.7052	15.2	4.02	0.1595	0.512620	0.000007	0.512270	1.2	1.36	0.95
MGA-22	#2	50.13	67.4	515	0.379	0.708335	0.000007	0.7065	18.7	4.26	0.1373	0.512600	0.000006	0.512299	1.8	1.03	0.91
MGA-12	#2	50.72	174	234	2.149	0.715514	0.000005	0.7053	19.1	5.06	0.1599	0.512737	0.000005	0.512386	3.5	1.07	0.77
USG-14	#2	54.51	51.9	387	0.388	0.706429	0.000007	0.7046	20.3	4.51	0.1345	0.512493	0.000005	0.512198	−0.2	1.19	1.06
MTC-275	#3	47.38	20.2	234	0.249	0.706489	0.000006	0.7053	31.3	8.49	0.1643	0.512728	0.000004	0.512368	3.1	1.18	0.80
MGA-2	#3	49.10	20.3	309	0.190	0.706278	0.000007	0.7054	38.4	9.04	0.1422	0.512661	0.000008	0.512349	2.8	0.97	0.83
MTC274B	#3	50.25	25.9	270	0.278	0.706968	0.000008	0.7056	30.6	7.85	0.1552	0.512591	0.000006	0.512251	0.9	1.34	0.98
MTC-75	#3	50.45	15.7	237	0.192	0.704510	0.000007	0.7036	27.3	6.86	0.1519	0.512765	0.000007	0.512432	4.4	0.88	0.70
MTC-76	#3	51.36	15.1	226	0.193	0.704455	0.000006	0.7035	29.2	7.34	0.1520	0.512783	0.000007	0.512450	4.8	0.84	0.68
VFB-9	#3	54.04	318	226	4.072	0.724440	0.000005	0.7050	24.5	6.35	0.1567	0.512751	0.000004	0.512407	3.9	0.98	0.74
MGA-25	#3	54.75	18.5	218	0.245	0.705034	0.000007	0.7039	25.9	6.61	0.1546	0.512753	0.000007	0.512414	4.1	0.94	0.73
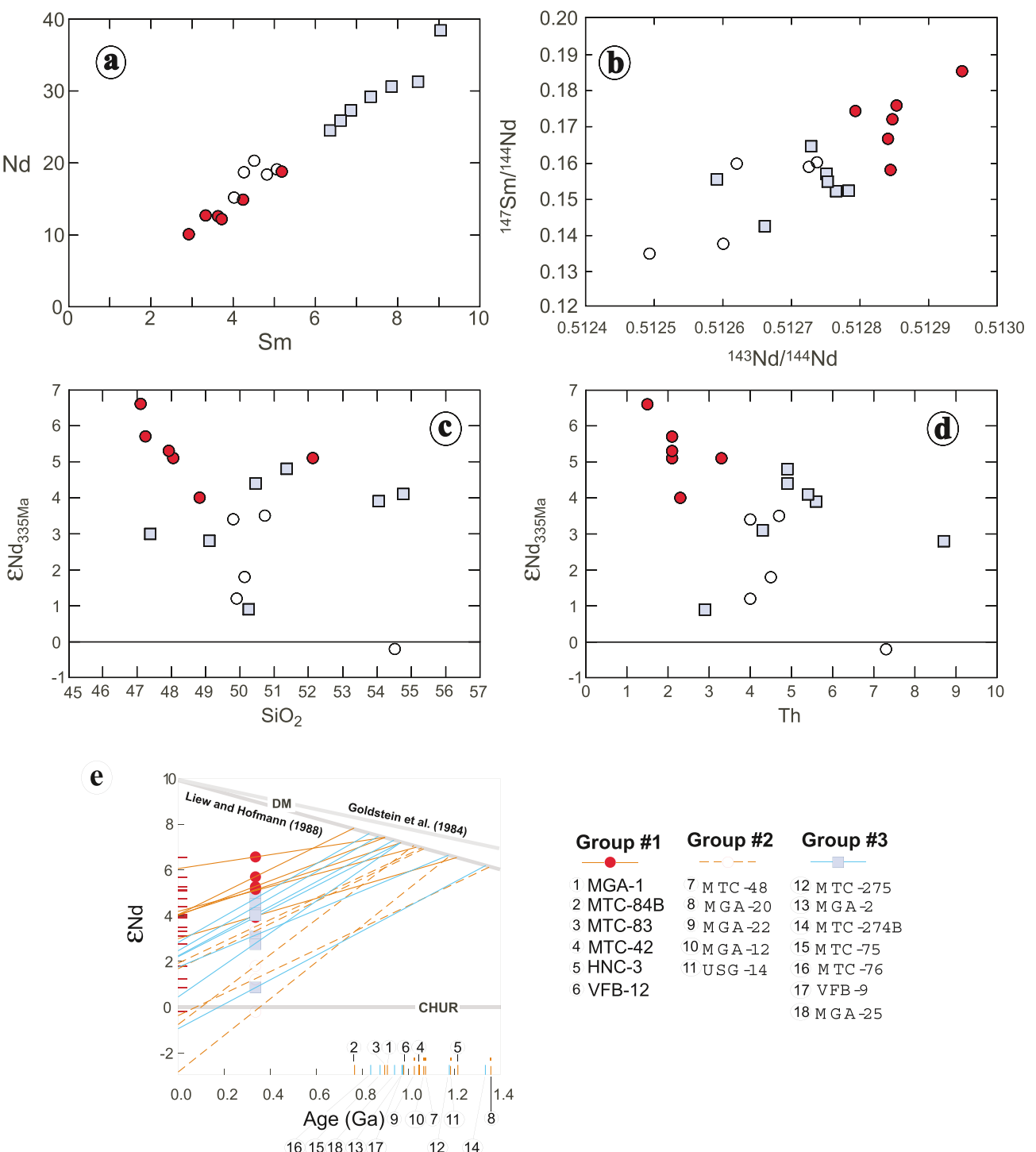
Figure 9. Isotopic and elemental relations relative to the Sm–Nd systematics (whole-rock) of the "basic volcanism" of the Matachel Basin. (a) Nd versus Sm elemental variation diagram. (b) $^{147}Sm/^{144}Nd$ versus $^{143}Nd/^{144}Nd$ isotopic ratios. (c) εNd_i versus silica contents. (d) εNd_i versus thorium contents. (e) Model ages of the analyzed samples determined from depleted mantle evolution following Liew and Hofmann (1988). The evolution of the depleted mantle of Goldstein et al. (1984) has also been projected.
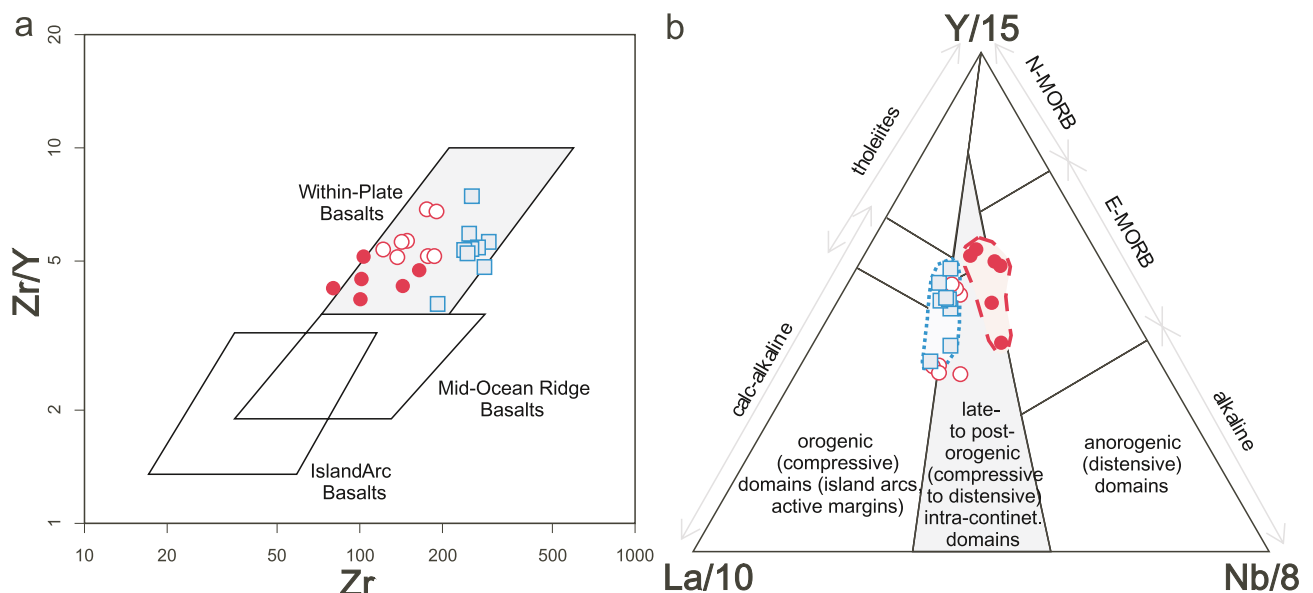
Figure 10. Projection of the geochemical groups identified in the "basic volcanism" of the Matachel Basin in tectono-magmatic discrimination diagrams: (a) Zr/Y–Zr diagram (Pearce & Norry, 1979), and (b) La/10–Y/15–Nb/8 diagram (Cabanis & Lecolle, 1989). Employed symbols are those of Figure 5.

identified continental tholeiites associated with alkali basalts and calc-alkaline dacites and rhyolites, although their genetic linkage remains loosely ascribed in terms of compositional criteria.

The moderate radiogenic character ($\varepsilon Nd_i = -0.2–+6.6$) of the Matachel Groups #1 and #2 tholeiites and the shapes of their multi-element normalization patterns are similar to those of enriched-MORB type basalts (Figure 8). This points to a lithospheric contribution of source components that would also be supported by the characteristics of trace element systematics (Figure 8; Table 1). This is the case in particular of immobile incompatible elements sensitive to crustal contamination processes (e.g., Th and LREE), given that continental crust, particularly the upper crust, is enriched in La and Th relative to the primitive mantle (Puchtel et al., 1997; Rudnick & Fountain, 1995; Rudnick & Gao, 2003; Taylor & McLennan, 1985).

A crustal contribution to the tholeiitic magmas can be unraveled after various lines of geochemical evidence. Relative abundances in Th_{PM} of the studied tholeiites (Group #1: 17.6–38.8; Group #2: 47.1–85.9) are an order of magnitude higher than those of the average N-MORB (Sun & McDonough, 1989), whereas La_{PM} values (Group #1: 5.81–15.1; Group #2: 14.6–27.0) are only slightly higher. Conversely, Nb/Th_{PM} values (Group #1: 0.195–0.556; Group #2: 0.132–0.247) are markedly low relative to those calculated for the average N-MORB, whereas Nb/La_{PM} values (Group #1: 0.628–1.03; Group #2: 0.432–0.610) are fairly similar. The differences between La and Th enrichments are more pronounced in the Group #2 tholeiites, which would initially point to a higher upper crustal contribution in them. The prominent Nb negative anomaly in the primitive mantle-normalized diagram is also consistent with a generalized crustal contribution (Barth et al., 2000; Puchtel et al., 1997; Rudnick & Gao, 2003; Weaver, 1991). Its extent is reflected by the Nb/Nb* ratio, defined as $Nb_{PM}/(Th_{PM} \times La_{PM})^{1/2}$ (Puchtel et al., 1997; Stepanova et al., 2014). Observed similar ranges of this parameter in the Groups #1 (0.35–0.70) and #2 (0.24–0.39) suggest significant albeit variable degrees of crustal contamination within each group, which is also consistent with the observed variability of Nb/Th_{PM} and, to a lesser extent, Nb/La_{PM} values. The lower Nb/Nb* ratio of Group #2 reflects again a higher crustal contribution in these tholeiites than in those of the Group #1. This effect of variable crustal contribution is also reflected in several tectono-magmatic diagrams. In the Zr/Y–Zr diagram of Pearce and Norry (1979), studied samples appear projected in the "within-plate basalts' field (Figure 10a). Nevertheless, most of the Group #1 samples project clustered in the "MORB+within-plate basalts' field, slightly apart from the Groups #2 and #3 samples. Similarly occurs in the La/10–Y/15–Nb/8 diagram of Cabanis and Lecolle (1989; Figure 10b). Though most samples appear projected in the "late to post-orogenic intra-continental" domain, the crustal input in Groups #2 and #3 rocks leads to their displaced projection from the Group #1 samples. It can, thus, be concluded that the "basic volcanism" of the Matachel Basin actually includes ordinary continental tholeiites among its different magmatic rock associations.

The wide geochemical diversity of continental tholeiites worldwide led to a preliminary subdivision into the Low–Ti (<2 wt.% TiO_2) and High–Ti (>2 wt.% TiO_2) tholeiite types (Bellieni et al., 1984; Mantovani et al., 1985). Peate et al. (1992) proposed a more comprehensive classification scheme based on high-field strength element contents such as Ti, Zr, Y and compiled Sr-, Nd-, and Pb-isotope data of the Paraná Gondwanan continental tholeiites. According to these authors, High–Ti tholeiites exhibit higher ratios in Ti/Y (>350), Zr/Y (>4.0) and Sr/Y (>4.5) than those of Low–Ti tholeiites (Ti/Y < 330; Zr/Y < 7.0; Sr/Y < 13). In the Matachel tholeiitic basalts and basaltic andesites, the observed TiO_2 contents (<1.94 wt.% TiO_2) and Ti/Y (238–338) and Zr/Y (3.96–6.87) ratios compare to those of Low–Ti continental tholeiites. Only one sample (MTC-84B) departs of this ascription, due to a relatively high Ti/Y ratio (Ti/Y: 377).

Peate and Hawkesworth (1996) revisited the classification of Low–Ti tholeiites, and conducted a more detailed geochemical and isotopic characterization. They proposed distinction between two end-members with contrasting Ti/Zr ratios and Nd-, Sr-, and Pb-isotope characteristics, termed "Esmeralda-type" and "Gramado-type." "Esmeralda-type" tholeiites have lower $^{87}Sr/^{86}Sr_i$ (0.7045–0.7080) and higher Ti/Zr (>60) and εNd_i (−4 to +3) than "Gramado-type" rocks ($^{87}Sr/^{86}Sr_i$: 0.7070–0.7150; Ti/Zr < 60; εNd_i: −8 to −3). Regardless of their higher radiogenic character, the composition of the Matachel Low–Ti continental tholeiites unravels the presence of both types. The composition of Group #1 basalts (Ti/Zr: 61–79; εNd_i: +4.0 to +6.6) concurs with the "Esmeralda-type", whilst Group #2 basalts and basaltic andesites (Ti/Zr: 36–58; εNd_i: −0.2 to +3.5) are closer to the "Gramado-type" (Figure S1 in Supporting Information S1). Nevertheless, considering that emitted lava volumes in the Matachel Basin are extremely far from those of Paraná continental flood basalts, the coined "Esmeralda" and "Gramado" terms to differentiate both Low-Ti sub-types have been loosely applied in the studied case.

Apart from the Low-Ti tholeiites, a calc-alkaline association has also been identified in the Matachel basic volcanic rocks. The Group #3 sub-alkali basalts and basaltic andesites integrate it. Notwithstanding, basalts of this association display low CaO/Al_2O_3 ratios (0.4–0.6), comparable to those exhibited by "high-Mg" calc-alkaline series rocks such as boninites (0.5–0.6; Pearce & Reagan, 2019, and references therein), adakites (0.3–0.5; Martin et al., 2005) and sanukitoids (~0.3; Martin et al., 2009). Specifically, they are slightly enriched in TiO_2 (2.26–3.19 wt.%), Zr (192–294 ppm) and Y (46.3–58.7 ppm) with respect to common values in boninites (TiO_2 < 0.5 wt.%; Zr < 58 ppm; Y < 19 ppm; Pearce & Reagan, 2019, and references therein) and adakites (TiO_2 < 1.49 wt.%; Zr < 188 ppm; Y < 13 ppm; Martin et al., 2005). On their part, basaltic andesites of this association are also slightly enriched in TiO_2 (1.08–2.37 wt.%), Zr (240–268 ppm) and Y (34.4–49.4 ppm) with respect to common values in sanukitoids (TiO_2 < 1.21 wt.%; Zr < 316 ppm; Yb < 35.0 ppm). The markedly low MgO (2.8–5.1 wt.%), Ni (<22 ppm) and Cr (<100 ppm) contents of the Group #3 rocks in comparison with those exhibited by boninites (MgO > 8 wt.%; Ni > 59 ppm; Cr > 300 ppm; Pearce & Reagan, 2019), adakites (MgO ~ 5.0 wt.%; Ni: 103 ppm; Cr: 157 ppm; Martin et al., 2005) and sanukitoids (MgO: ~4.0 wt.%; Ni > 36 ppm; Cr > 58 ppm; Martin et al., 2009) elsewhere, and the near flat-shaped REE normalization-patterns (La/Yb_{PM} = 2.63–6.48), altogether lead us to discard their consideration as genuine "high-Mg" calc-alkaline series rocks. This conclusion would be reinforced by the exhibited relatively low K_2O contents of analyzed samples with respect to their SiO_2 contents (Table 1).

The Matachel Group #3 ("calc-alkaline") association could be considered tentatively as made of basalts and basaltic andesites as those of "normal" arc settings. If the plate convergence setting were correct, their Nb (up to 16.2 wt.%), P_2O_5 (0.23–0.59 wt.%), La (up to 29.2 wt.%), Nd (up to 39.8 wt.%) and Th contents (up to 12.5 wt.%) would be closer to those of calc-alkaline andesites of active continental margins than to those of intra-oceanic and island arcs (Kelemen et al., 2007). Nevertheless, their relatively low Mg# values (33–56; Table 1) and $^{143}Nd/^{144}Nd$ ratios (0.512591–0.512783; Table 2), and their markedly high TiO_2 (1.08–3.19 wt.%; Table 1) and Fe_2O_3 (7.43–13.34 wt.%; Table 1) are at variance with those of average subduction-related magmatic rock equivalents (Kelemen et al., 2007). It is outstanding that Al_2O_3 contents of the Group #3 basalts are akin to those of tholeiitic basalts. Additionally, the normative mineralogy of the less altered basalts (LOI < 2.5 wt.%) corresponds to oversaturated tholeiites (Yoder & Tilley, 1962) and the same can be concluded after their εNd_i values (+2.8–+4.8; excluding sample MTC274B). All the above permits us to conclude that, despite the Group #3 rocks exhibit in appearance a calc-alkaline evolutionary trend, a considerable uncertainty remains regarding the actual nature of this geochemical association. Consequently, the inference of a plate-convergence tectonic setting on geochemical grounds can be seriously challenged based upon the detailed geochemical data presented here.

7.2. Inferences on the Magma Sources

On the basis of isotope and element abundances/ratios, two distinct Low-Ti continental tholeiite types and a (not necessarily so) "Cordilleran-type" calc-alkaline association may be distinguished in the Matachel Mississippian volcanic sequences. A close temporal and spatial occurrence of High- and Low-Ti tholeiitic basalts, commonly associated also with alkali basalts and/or peraluminous rhyolites, is a well-documented phenomenon world-wide (Dessureau et al., 2000; LaFléche et al., 1998; Lightfoot et al., 1993; Neal et al., 2002; Peate et al., 1992; Pouclet et al., 2017; Shellnutt & Jahn, 2011). Nevertheless, as far as we know, few examples have been reported of outpourings of continental tholeiites with associated calc-alkaline basalts and basaltic andesites (Benek et al., 1996; Mitjavila et al., 1997; Pouclet et al., 2017) unrelated to plate-convergence geodynamic scenarios.

In a first approximation, the existence of tholeiitic and "calc-alkaline" basaltic lava flows in the Matachel basic magmatic association might point to a possible derivation from separate mantle sources. Indeed, compositional variations in continental tholeiites of other igneous provinces have sometimes been related to simultaneous, or temporally close, magma contributions from distinct mantle sources (Ingle et al., 2004; Lightfoot et al., 1993; Neal et al., 2002; Peate, 1997; Peate et al., 1992; Pouclet et al., 2017). The whole-rock geochemistry of the three Matachel geochemical groups distinguished puts constraints to a straightforward interpretation of primary compositional magmas and their source (e.g., $MgO \geq 13$ wt.%; $Ni = 300\text{--}500$ ppm; e.g., Green et al., 2001; Sato, 1977). Conservative incompatible elemental contents and ratios of Nb/Th_{PM}, Th/Yb_{PM}, and Nb/La_{PM} reveal as well a variable crustal contribution. Notwithstanding, coupling Nd isotopic compositions with indicators of crustal contamination (such as the $\varepsilon Nd_i\text{--}Th/Zr_{PM}$ and $\varepsilon Nd_i\text{--}La/Nb_{PM}$ graphs) unravels a rough single negative array that integrates the tholeiitic (Groups #1 and #2) and calc-alkaline (Group #3) associations that had been originally clustered according to their whole-rock geochemistry (Figures 11a and 11b). This transition cannot be explained simply in terms of an increasing "en route" crustal contamination of mantle-derived melts. Instead, it appears that those associations already evolved before traversing the crust.

Primary magma source identification for the Matachel magmatic rocks can be traced from the relations of the usually conservative elements during crystal fractionation (Nb/Yb, Th/Yb, La/Sc, Zr/Y, Ti/Y, Ti/V, and La/Yb). Their variations might also reflect changes in the nature of the source, its depth and/or melting rates (Condie, 2005; Fitton et al., 1997; Pearce, 2008). Projection in the Th/Nb–Nb/Yb diagram (Pearce, 2008) of the data available shows a departure from the "MORB–OIB array" and unravels the interaction of mantle-derived magmas with crustal components (Figure 11c). Some elemental ratios (e.g., Th/Yb and La/Y) of the source mantle material could have been thus modified by crustal assimilation. Metabasic crustal rocks are the best candidates as sources of crustal contamination, since a significant contribution of sediments or ancient continental crust would not be supported by the εNd_i values determined herein (DePaolo, 1988).

Identification of the samples with a smaller "crustal" input, and therefore a presumed stronger mantle source signature, might be guided by consideration of only those bearing Nb/La ratios >0.85 times the chondritic value (Lassiter & DePaolo, 1997). Surprisingly, among the Matachel magmatic rocks, the less evolved tholeiitic samples exhibit Nb/La ratios higher than 0.85 (Group #1: 0.92–1.07), being the samples of the association with calc-alkaline signature those displaying sub-chondritic and markedly low Nb/La ratios (<0.56). Therefore, the less evolved Matachel tholeiitic samples (considering alternative criteria) could be the geochemically closer candidates to track the "primitive" tholeiitic magmas. Those specific samples plot clustered in the domain for enriched-MORB sources in the Th/Nb–Nb/Yb diagram (Pearce, 2008; Figure 11c). This is in accordance with the E-MORB character inferred from their multi-element normalization-patterns (Figure 8) and with their trace element systematics departure from OIB parameters (Sun & McDonough, 1989). All this permits us to discard a deep mantle-source for the tholeiitic magmas.

In order to constrain further the depth of the mantle source of the studied Low-Ti continental tholeiites, a discussion on the presence or absence of stable garnet in the magma source mantle rocks is required (Green & Ringwood, 1970; Lassiter & DePaolo, 1997). In this regard, it can be highlighted that the La/Yb_{PM}, La/Y_{PM}, Sm/Yb_{PM}, Nb/Y_{PM}, and Zr/Y_{PM} ratios are directly related to the degree and depth of partial melting, since in the presence of stable garnet, HREE are preferentially retained by this mineral over the light and middle REE during melting (Class et al., 1998; Lassiter & DePaolo, 1997; Shaw et al., 2003). In the case studied here, normalization with respect to primitive-mantle compositions (Taylor & McLennan, 1985) results in relatively low $Dy/Yb_{(N)}$ (1.15–1.28) and $La/Yb_{(N)}$ (1.53–2.87) values in the presumed "primitive" samples of Group #1 rocks. This (together with low values of the Sm/Yb_{PM} or La/Yb_{PM}) might have resulted from partial melting of a garnet-free mantle source (Shaw et al., 2003). Specifically, the aforementioned low ratios, together with the relatively flat
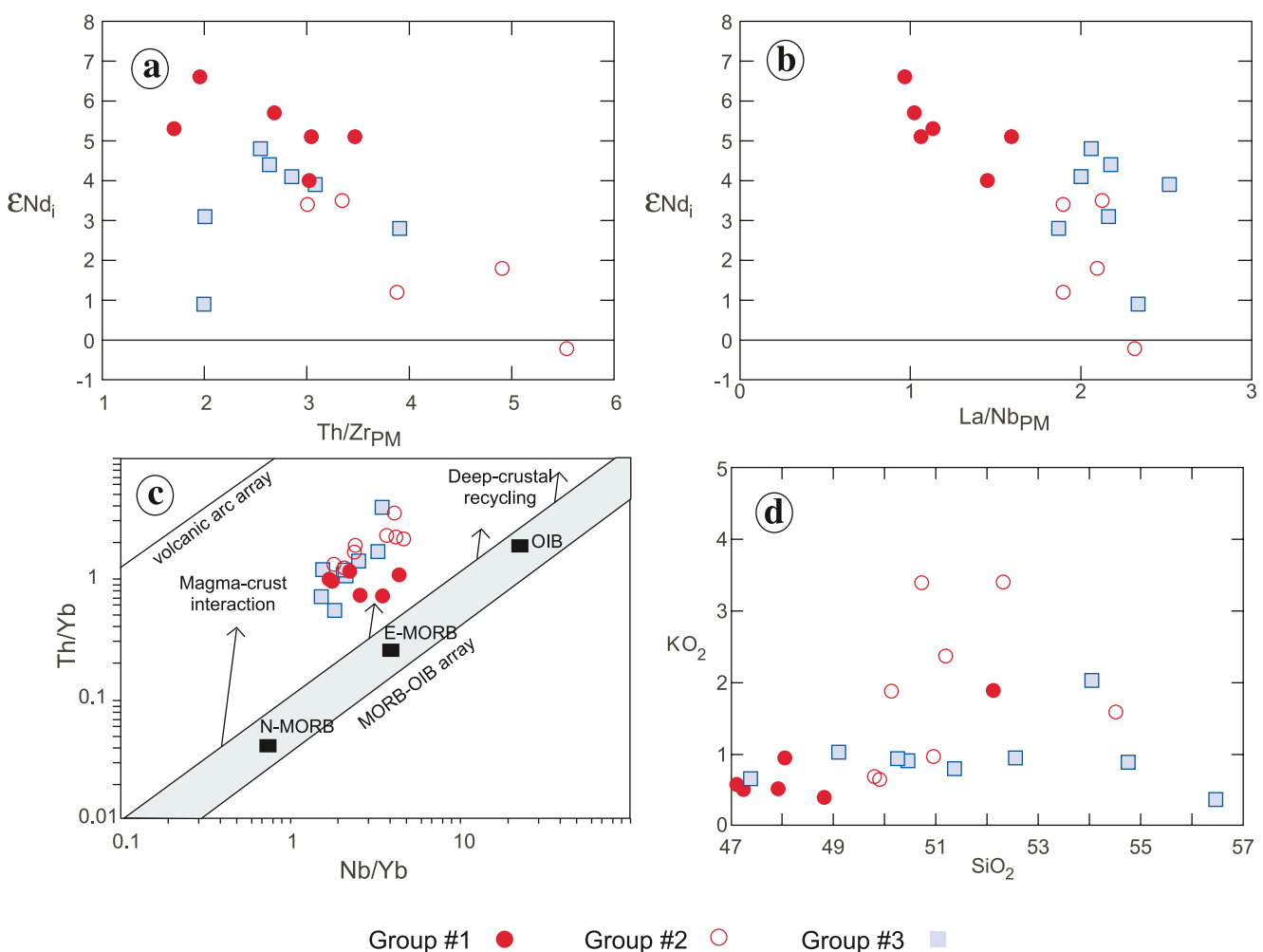
Figure 11. εNd_i variation trends with respect to (a) Th/Zr_{PM} ratio, and (b) La/Nb_{PM} ratio of the identified geochemical groups in the "basic volcanism" of the Matachel Basin; normalization values with respect to the primitive mantle (Sun & McDonough, 1989). Projection of the geochemical groups identified in the "basic volcanism" of the Matachel Basin in the (c) $Th/Yb–Nb/Yb$ diagram of "MORB–OIB array" (Pearce, 2008), and (d) $K_2O–SiO_2$ diagram.

HREE patterns and the moderate Nd radiogenic character of the "primitive" samples (εNd_i = +5.1–+6.6), likely point to a (garnet-free) lherzolitic mantle. The relatively low Nb/Nb* values of the most "primitive" tholeiitic samples (Group #1: 0.457–0.701) with respect to mantle values (<1 ppm; Taylor & McLennan, 1985) is also congruent with the presence of Ti-bearing phases both in the upper mantle (e.g., rutile, $FeTiO_3$ ilmenite, garnet, pyroxene, spinel and post-spinel phases; Matrosova et al., 2021) and underneath (Al, Ca, and Ti oxide and silicate refractory constituents of perovskite; O'Neill & Palme, 1998; Matrosova et al., 2020), and/or amphibole in the mantle source (Foley et al., 2000). Additionally, if amphibole was present in the source rocks, the E-MORB fingerprints that exhibit the studied tholeiites (Figure 8) might be explained, too.

From the perspective of the two end-member Low–Ti tholeiites types of Peate and Hawkesworth's (1996) classification, the Matachel Group #1 basalts fit the "Esmeralda-type", whereas basalts and basaltic andesites of the Group #2 are closer to the "Gramado-type." The cited authors suggested that "Gramado-type" tholeiites might result from a prime contribution of heterogeneous continental mantle lithosphere, whereas "Esmeralda-type" counterparts might result from the contamination of asthenosphere-derived melts by subcontinental lithospheric mantle/magmas. Stepanova et al. (2014) have shown that primary magmas of "Esmeralda-type" tholeiites might result from relatively high melting degrees (c. 15%) of a depleted mantle (DM-type) source in the spinel peridotite stability field. However, the debate persists so far as to whether Low-Ti continental tholeiites result from the assimilation of enriched lithosphere by proportionally larger asthenospheric melts or the most significant melt generation occurred within the lithospheric mantle (Dessureau et al., 2000).

The Variscan orogeny triggered an abrupt geochemical change in mafic magmatism in most of the central-Europe terranes (Dostal et al., 2019). In the Iberian Massif most of the Variscan mafic magmatism implied melting of lithospheric mantle sources, variably enriched due to crustal material subducted during the Late Cadomian and the Variscan orogenic cycles (Bea et al., 2021; Orejana et al., 2020; Villaseca et al., 2004). Nevertheless, the moderately high initial εNd values (from +5.4 to +5.8) and younger model ages (T_{DM} = 735–620 Ma) of the tholeiitic rocks of Central Iberian (López-Moro et al., 2007), coupled with their low Th/Yb and relatively high Nb/U (mostly from 20 to 47) values, suggests a scarce continental crustal imprint, and therefore, the lack of supra-subduction signatures and the existence of an old (pre-Neoproterozoic) heterogeneous enriched subcontinental mantle beneath Central Iberia (Villaseca et al., 2022). In the regional setting of Matachel magmatic province, provenance of the Group #1 "primitive" samples from an enriched MORB-type source beneath the Ossa-Morena Zone places additional constraints on magma source identification. The assumed source after the above discussion points to a "metasomatically" enriched lithospheric mantle source (e.g.,: Donnelly et al., 2004; Workman et al., 2004). The enriched MORB signature, on its part, is usually related to intra-oceanic subduction environments (Schilling et al., 1983). However, such a plate-convergence geodynamic setting is at odds with the intra-continental transcurrent setting currently observed (and interpreted to have persisted since the early Cambrian, well before the Mississippian). The mantle source enrichment should, thus, be inherited. Moreover, the existence in the Iberian Massif of sanukites and, therefore, the participation of metasomatized mantle sources by a subducting basaltic slab and sediments (e.g., Gómez-Frutos & Castro, 2022; Gómez-Frutos et al., 2023) reinforces the heterogeneous character of the inferred lithospheric mantle, which led to the near coeval generation of tholeiitic and sanukitoid magmas during the Variscan orogeny.

Bearing in mind the regional tectonic evolution of the region, the Cadomian subduction setting is the best candidate to explain the enriched mantle source (see Sarrionandia et al., 2020, and references therein, for further details). Although this would need to be confirmed with more robust evidence, the principal mantle source region of the Matachel Low-Ti continental tholeiites would correspond to a (rutile-) amphibole-bearing, garnet-free lherzolite of the subcontinental mantle lithosphere conformed as a supra-subduction mantle wedge beneath the northern margin of Gondwana during the late Neoproterozoic-early Cambrian.

The presence of "Esmeralda-type" Low-Ti continental tholeiites in the Matachel basin likely discloses a limited contribution of asthenospheric melts (Peate & Hawkesworth, 1996; Stepanova et al., 2014) from neighbor mantle domains underneath, which is also possible in supra-subduction inherited settings. Slight variations in the degree of melting and the heterogeneous character of the mantle sources frozen after Cadomian lithospheric stabilization would be consistent with the variations of conservative element ratios ascribed to the most "primitive" tholeiitic batches (Condie, 2005; Pearce, 2008; Pearce & Norry, 1979). Interaction of these mantle-derived melts with a metabasic continental lower and middle crust would explain the rest of the geochemical characteristics of the Matachel continental tholeiites.

The previous discussion departs from the usually assumed relationship (direct or indirect) between Low–Ti continental tholeiites and mantle-plumes (Stepanova et al., 2014, and references therein), in spite of the fact that the distinctive geochemical signature of mantle-plume sources is not evident in some Low-Ti rocks (Peate & Hawkesworth, 1996). Indeed, MORB-type tholeiites (i.e., the "Esmeralda-type") could indicate a transition from mantle-plume melting to decompression-induced melting of ambient mantle during continental breakup and ocean basin opening (Stepanova et al., 2014). Decompression and melting of a tectonically complex enriched lithospheric mantle can be achieved by alternative mechanisms, too. As discussed below in further detail (Section 7.5), generation of the Low-Ti continental tholeiites studied might have taken place in relation to wrench shear zone reworking across the lithosphere.

7.3. Origin of the Association With Calc-Alkaline Signature

The Matachel "basic volcanism" association with calc-alkaline signature (Group #3 rocks) exhibits no discernible time and/or spatial gaps with respect to the of Low-Ti continental tholeiite outpourings (Groups #1 and #2). The observed calc-alkaline basalt Al_2O_3 contents are similar to or within the range of those of tholeiitic basalts. The same stands for $Fe_{0.8}$ values calculated after Klein and Langmuir (1,987; $Fe_{0.8}$ = 5.7 in calc-alkaline basalts, $Fe_{0.8}$ = 3.8–8.7 in Group #1, $Fe_{0.8}$ = 5.4–7.3 in Group #2 rocks) for CaO/Al_2O_3 ratios (CaO/Al_2O_3 = 0.6, 0.55–0.64, and 0.34–0.55, respectively), and for the Ti/Y ratios (326–268 in the calc-alkaline basalts). The main difference observed relates to the more enriched character of the LREE content of Group #3 rocks (Figure 8).

Geochemical similarities are also observed in the moderate Nd radiogenic character of the samples with calc-alkaline signature (εNd_i = +2.8–+4.8; excluding sample MTC274B). The positive εNd_i values and the observed trends in diagrams coupling εNd_i values with conservative element ratios (Th/Zr_{PM}, Nb/Th_{PM}, La/Nb_{PM}), alike the Groups #1 and #2 tholeiites, point to an addition of a metabasic crustal component to the mantle source prior to magma diversification (DePaolo, 1988; Pearce, 2008). The higher relative abundances in Th_{PM} (34.1–102) and La_{PM} (27.0–42.4) of the calc-alkaline basalts further support a crustal component in them (Puchtel et al., 1997; Rudnick & Fountain, 1995; Rudnick & Gao, 2003; Taylor & McLennan, 1985) higher than in the tholeiites. Also remarkable in this regard are the loose or absent troughs in P, Ti and Nb in the E-MORB multielemental normalization-diagrams (Figure 8) usually observed in calc-alkaline rocks (Foley et al., 2000, and references therein). The Nb/Nb_{PM}* (0.32–0.41), Nb/Th_{PM} (0.22–0.39) and Nb/La_{PM} (0.43–0.54) ratios in the calc-alkaline basalts are only slightly smaller than those of the Group #2 tholeiites. Actually, the Group #3 samples studied overlap the "late to post-orogenic intra-continental" domain of the La/10–Y/15–Nb/8 diagram of Cabanis and Lecolle (1989; Figure 10b). As was the case for the tholeiites, a "within-plate" character of the calc-alkaline rocks is outstanding. This can be inferred also from their near clustered projection in the "within-plate basalts' field of the Zr/Y–Zr diagram (Pearce & Norry, 1979; Figure 10a). It is therefore apparent that both the calc-alkaline and tholeiitic associations might have formed contemporaneously and that the genetic relationships of their parent magmas are plausible.

Explaining the difference between calc-alkaline and tholeiitic magmatic series has been one of the central topics of Igneous Petrology, a general consensus far from being reached so far (Kelemen et al., 2007). Low-Ti tholeiitic basalts with arc-like trace-element characteristics were described in the Ferrar large igneous province (LIP; e.g., Hergt & Brauns, 2001, and references therein). According to these authors, a small proportion (~3%) of subducted terrigenous sediments contaminating a highly depleted mantle might explain geochemical features as the dealt with here. The mantle wedge (involving the asthenosphere and subcontinental lithosphere above a subduction channel) is the most likely tectonic scenario for such a mantle source (Hacker et al., 2003). Nevertheless, such enrichment would promote high Al_2O_3 and K_2O contents in primitive magmas, contrary to those observed in the less evolved samples from Group #3 (Figures 6 and 11d). An alternative hypothesis would involve contamination of MORB-type magmas by an enriched-MORB source, followed by the addition of calc-alkaline rocks/magmas extracted from a depleted mantle reservoir (Pereira et al., 2007, and references therein). Such a complex model was intended to explain specifically the origin of metabasites with convergent plate margin geochemical signatures formed during the Cadomian orogeny in the OMZ. Thus, unless it is regarded as a possible inherited scenario, the time gap with Carboniferous Low-Ti continental tholeiites makes it an insufficient explanation by itself.

Despite the low Mg# values of the Group #3 rocks with calc-alkaline signature (32.55–55.67; Table 1), their derivation from partial melting of subducted basalt without major-element equilibration with the overlying mantle might be discarded, as this process remains controversial (Kelemen et al., 2007, and references therein). The fact that the εNd_i values of Group #3 rocks with calc-alkaline signature fall within the range of those of Groups #1 and #2 tholeiitic rocks could point to a single primitive magma (e.g., Figures 9c and 9d) that later experienced two distinct evolutionary paths (i.e., tholeiitic and calc-alkaline). In this regard, interactions with a heterogeneous crust would be of prime importance. The Group #3 basalts with calc-alkaline signature bear very high TiO_2 and Fe_2O_3 contents compared with the tholeiites (Figure 6; Table 1) that support magma crustal contamination. Though to some extent speculative, further contamination of a Low-Ti tholeiitic primary magma with H_2O-rich (e.g., amphibole-rich) crustal metabasites would led to an increase of the oxygen fugacity leading to a calc-alkaline evolutionary trend (Waters et al., 2020). Alternatively, interaction with less ferriferous and titaniferous dry rocks (olivine- and, notably, pyroxene-rich metabasites) might lead to generation of the parental magmas from which evolved the Group #2 Low-Ti continental tholeiites. Whatever the case, and considering also that LOI values of most samples of the Group #3 are markedly low (see Table 1), the relative abundance of H_2O in the calc-alkaline parental magma would be below ~2 wt.%, since geochemical modeling (see Section 7.4) indicates that plagioclase saturation was reached (Kelemen et al., 1990; Müntener et al., 2001). Note that these hypotheses discard the existence of primary Carboniferous (Variscan) arc basalts.

The presence of pre-Variscan metaigneous rocks in the OMZ is well documented after decades of geological exploration (see Section 2.1 for further details). Igneous activity in the OMZ was widespread between ca. 645 Ma and ca. 534 Ma in relation with an active subduction setting (Bandrés et al., 2002; López-Guijarro et al., 2008; Pin et al., 2002; Sánchez-Lorda et al., 2014; Sarrionandia et al., 2020, and references therein). Further magmatic
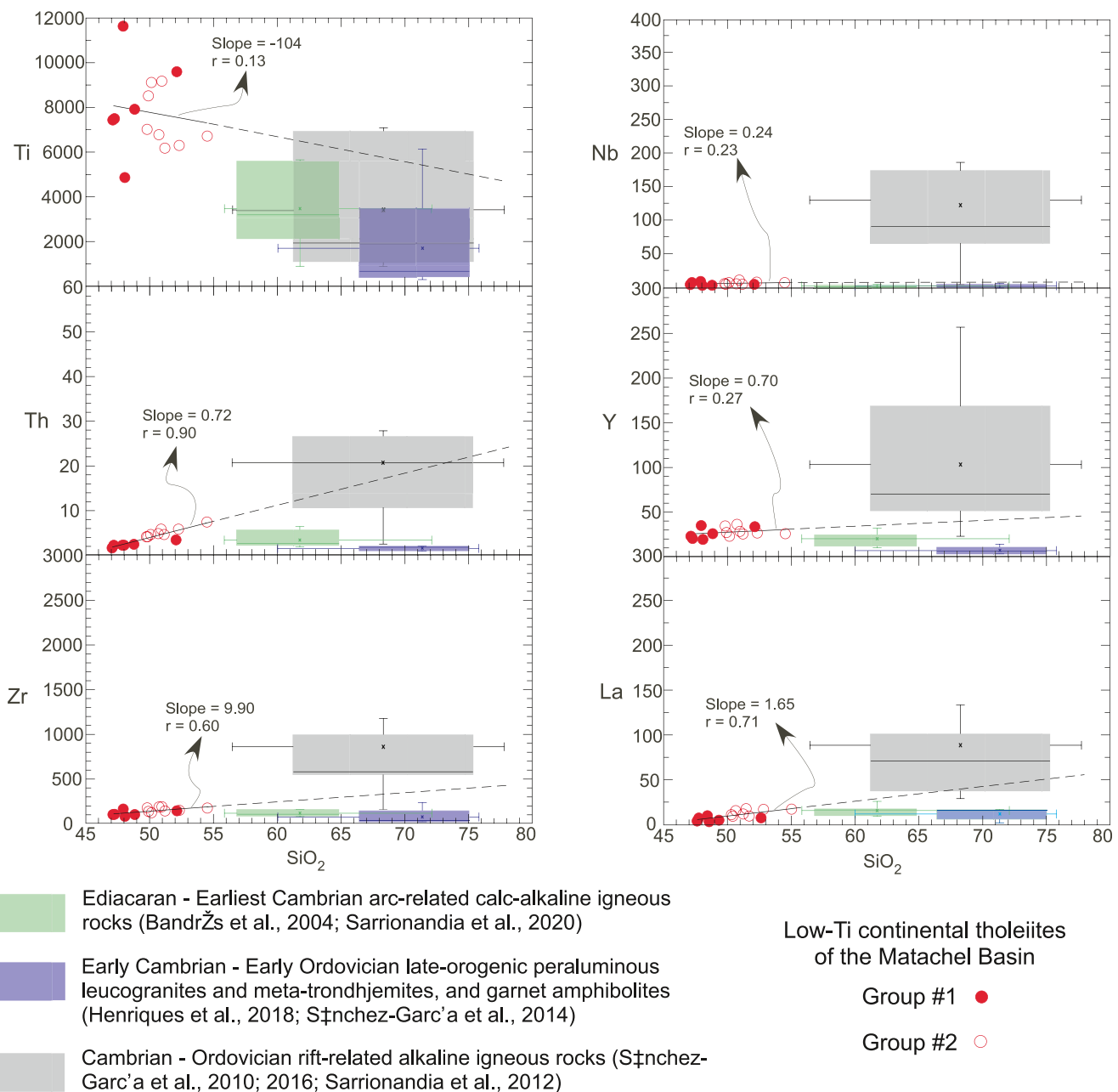
Figure 12. Box and whisker charts of the main basement rock units of the studied lithospheric segment. Both types of continental tholeiites of the "basic volcanism" of the Matachel Basin and the regression line defined by the composition of these samples are also plotted, including the slope of the line and the correlation coefficient.

activity was also significant during the Middle- to Upper Cambrian in relation to a different tectonic scenario of intra-continental rift (Chichorro et al., 2008; Sánchez-García et al., 2010; Sarrionandia et al., 2012). Both pre-Variscan tectono-magmatic events led to continental crust growth after mantle-derived magmas.

Identification of the crustal metaigneous rocks that interacted with the primitive Low-Ti tholeiitic magmas can be done by comparing available geochemical data for the pre-Variscan OMZ crustal segment in the Matachel area (Figure 12). Silica contents and εNd_i values of tholeiites vary within a relatively narrow range ($SiO_2 = 47.11$–54.51 wt.%; $\varepsilon Nd_i = -0.2$–+6.6). Consideration of pre-Variscan metaigneous samples with similar SiO_2 contents >55.0 wt.% and positive εNd_i values in Figure 12 shows an array that intersects the calculated regression line for the Low-Ti continental tholeiites (dashed line). This permits to circumscribe the crustal components that interacted with the parental tholeiitic magma. The Low-Ti "tholeiitic trend" exhibits a strong positive correlation in Th and
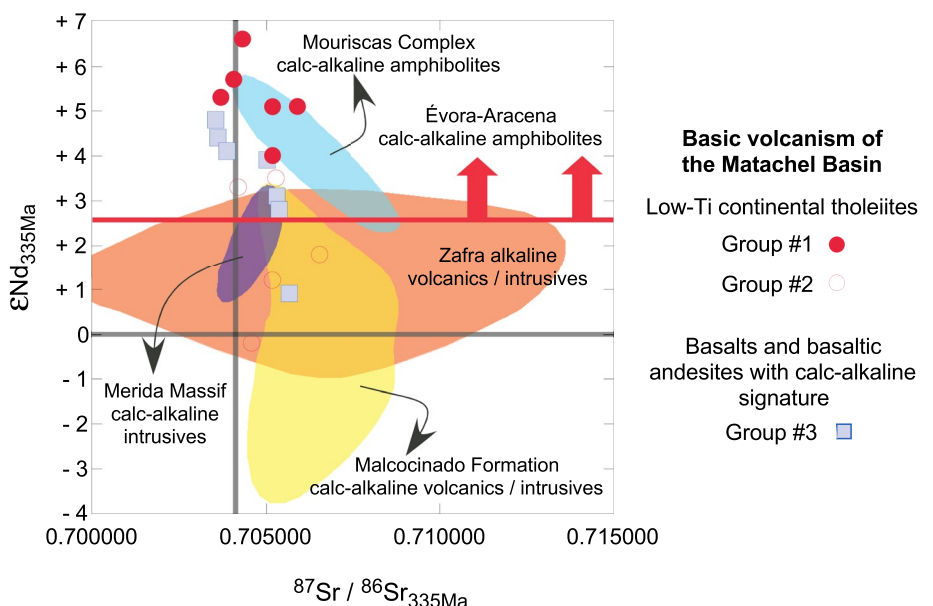
Figure 13. Projection of the geochemical groups identified in the "basic volcanism" of the Matachel Basin in the εNd_i versus $^{87}Sr/^{86}Sr_i$ diagram. Labeled fields correspond with the main basement rock units of the studied lithospheric segment (data compiled from the references indicated in Figure 12).

moderate to weak positive correlation with La and Zr that intercepts the field of Cambro-Ordovician rift-related igneous rocks (Figure 12). The "tholeiitic line" defined by Th, La and Zr deviates from the field where Cadomian arc-related and late-orogenic metaigneous rock compositions plot (Figure 12). In spite of the lack of a statistical correlation, Nb and Y trends might support a similar conclusion. By contrast, overlapping in Ti contents of the metaigneous rocks of the studied regional lithospheric segment, difficults discussion on potential crustal contributors.

The εNd_i values and the $^{87}Sr/^{86}Sr_i$ isotopic ratios of the Matachel volcanic rocks can be also compared with the published data for older metaigneous crustal rocks from the area (Figure 13) to better constrain the nature of the crustal rocks that likely interacted with the Mississippian tholeiitic magma and transformed it into the magma with calc-alkaline signature that nurtured the Group #3 rocks. The respective εNd_i and $^{87}Sr/^{86}Sr_i$ geochemical graphs (Figure 13) show with more confidence that most of the Group #3 samples with calc-alkaline signature bear isotopic characteristics close to those of OMZ Cadomian calc-alkaline amphibolites. Hence, the interaction of Low-Ti tholeiitic magmas with basement calc-alkali metaigneous rocks can be inferred.

7.4. Magma Diversification Mechanisms

The distinct tholeiitic and calc-alkaline evolutionary trends identified in the Matachel "basic volcanism" exhibit some variance with respect to the tendency expected for standard primary magmas. The Low-Ti tholeiitic associations (Groups #1 and #2) exhibit a relatively evolved character similar to that characteristic of continental tholeiites (Dupuy & Dostal, 1984; Peate & Hawkesworth, 1996; Pouclet et al., 2017; Shellnutt et al., 2014; Stepanova et al., 2014). Their differentiation trends are roughly characterized by depletion in Al_2O_3, CaO, MgO, Cr, and Ni, accompanied by progressive enrichments in K_2O, Na_2O, Ba, Rb, Sr, U, Th, Y, Zr, and REE (Table 1 and Figures 6 and 11d). This enrichment of such lithophile elements from Group #1 to Group #2 suggests that the evolution of the tholeiitic association might have resulted from the assimilation of crustal materials. The parental melts of this association would correspond to the less siliceous samples from Group #1 that show, in fact, the lowest contents of mentioned lithophile elements (Table 1). The Low-Ti "tholeiitic trend" exhibits a strong positive correlation in Th, and moderate to weak positive correlation with La and Zr that intercepts the field of Cambro-Ordovician rift-related igneous rocks in Figure 12. The "tholeiitic line" defined by Th, La and Zr deviates from the field where Cadomian arc-related and late-orogenic metaigneous rock compositions plot (Figure 12). In spite of the lack of a statistical correlation, Nb and Y trends might support a similar conclusion. The increase of K_2O as

differentiation proceeds from Group #1 to Group #2, contrary to the near horizontal trend observed for the Group #3 samples (Figure 11d), points to a feldspar-rich crustal source assimilation for the evolution of the tholeiitic association. This hypothesis is reinforced by the accompanying increase of Na_2O, Ba, Rb, and Sr in the same evolutionary trend (Table 1). Therefore, the evolution by crustal contamination of these "tholeiitic" magmas, which show a clear intra-continental geochemical affinity (Figure 10), would have occurred by the assimilation of feldspar-rich felsic Cambro-Ordovician metaigneous rocks (Figure 12). Such conditions concur with the observed negative correlation of the εNd_i values with SiO_2 and Th contents (Figures 9c and 9d).

Thus, the integration of both Low-Ti tholeiite types in a single array in the aforementioned diagrams (Figures 9c, 9d, 12, and 13) might support that progressive interaction of "Esmeralda-type" tholeiitic magmas with crustal alkali metaigneous rocks would transform them into "Gramado-type" tholeiitic magmas. Despite the similarity in εNd_i and $^{87}Sr/^{86}Sr_i$ of the involved crustal rocks on the origin of both the tholeiitic and calc-alkaline associations from Matachel (Figure 13), whole-rock elemental geochemistry has allowed the distinction of the specific crustal materials in the petrogenesis. While Cadomian-related mafic amphibolitic rocks interacted with primitive tholeiitic magmas to promote the association with calc-alkaline signature (Group #3), Cambro-Ordovician alkali felsic metaigneous rocks were involved in the geochemical evolution from Group #1 to Group #2. Isotope similarities of assimilated crustal rocks would explain the relatively homogeneity in the isotope characteristics of the identified associations in the Matachel Basin.

By contrast with the Low-Ti tholeiitic associations, the magmas of Group #3 rocks with calc-alkaline signature display fairly homogeneous εNd_i and Th values with increasing SiO_2 (Figures 9c and 9d) that rather supports a closed-system differentiation process. In this case, progressive depletion in Fe_2O_3, TiO_2, V, Y, REE and, to a lesser extent, MgO, Al_2O_3, CaO, and Zr, is accompanied by enrichment in Th (Figure 6). Variation diagrams depict horizontal Nb, Ni, and $(La/Lu)_N$ trends, the low Ni contents being outstanding as compared with the tholeiites (Table 1). Assumption of a closed-system fractionation process is also supported by the steep log(incompatible element) versus log(compatible element) trends observed (Janoušek et al., 2016). The absence of positive correlation between Ni and Mg# would argue against olivine fractionation, whereas depletion trends could be the result of crystallization of clinopyroxene and Ti-bearing oxides. In order to evaluate this hypothesis, geochemical modeling of major elements was performed based on mineral and whole-rock geochemical data (Sarrionandia et al., 2023, and this study). Mass-balance equations, least-square constraints, and compositions of fractionating minerals selected from the data set that accompanies this study (Table S4 and Figure S2 in Supporting Information S1) were used for reverse modeling of TiO_2, Al_2O_3, FeO^t, MnO, and MgO (Janoušek et al. (2016)). In the model, samples MTC-275 were considered as representative of the parent magma with calc-alkaline signature of Group #3 and sample MGA-13 as resultant of the crystallization of an evolved magma. Considering a labradorite composition (An_{60}) for the fractionating plagioclase (the less albitic composition determined for plagioclase cores; Sarrionandia et al., 2023), a Ti-rich clinopyroxene ($TiO_2 = 2.87$ wt.%; mg# = 0.77), and the compositions of analyzed ilmenite and magnetite, a satisfactory result was obtained (with a sum of squared residuals $\Sigma R^2 = 0.92$). Actually, the model would explain the observed geochemical variation by 65.2% fractional crystallization of an assemblage constituted by 48.5% of plagioclase (An_{60}) +38.3% of clinopyroxene +7.7% of magnetite +7.3% of ilmenite.

7.5. Was the Matachel "Basic Volcanism" Related to a Mantle Plume?

Generation of intraplate tholeiitic basalts after mantle plumes or as the products of different stages of plume evolution has sound foundations (Stepanova et al., 2014, and references therein). Interpretation of the occurrence of Mississippian continental tholeiites in the Matachel area might follow such hypothesis. In such a case, upwelling of a mantle plume underneath the southern Iberian Massif during the Carboniferous would be implied. The existence of plume-derived mafic intrusions during the Early Carboniferous in the OMZ was postulated by Carbonell et al. (2004), Simancas et al. (2006), and Palomeras et al. (2011) based upon the interpretation of a mid-crustal highly reflective layer from the IBERSEIS deep seismic reflection profile as a giant plume-derived sill-like mafic intrusion (the so-called "Iberian Reflective Body"; IRB). Following this hypothesis, Cambeses et al. (2019) interpreted the zircon U-Th-Pb and O isotopic characteristics of a Variscan OMZ granitoid pluton (Brovales) as the result of early Carboniferous calk-alkaline magmatism linked to a mantle-plume. The interpretation might possibly include other granitoid massifs of the OMZ bearing similar radiometric and geochemical characteristics.

In spite of the above, the high conductivity and relatively high density inferred for the suggested mafic (gabbroic) sill can be interpreted in an alternative way. The reported geophysical properties might also be shown by mid-crustal, graphite-rich, denser, metamorphosed equivalents of the Serie Negra schists (Pous et al., 2004; Puelles et al., 2014). In fact, crystal boundary graphite has been already identified as the likely cause of mid and lower crust anomalous electric conductivity (Frost et al., 1989). Also, in the case the IRB actually corresponds to a large mafic sill complex, Sarrionandia et al. (2012) postulated that it might be composed of mantle-derived Cambrian intrusions, rather than Carboniferous. This hypothesis was based upon the reported amplitude (20–30 km ascent of the asthenosphere/lithosphere thermal boundary layer) and extension (>3,000 km^2) of a likely frozen Hales transition velocity anomaly in SW Iberia (Ayarza et al., 2010; Palomeras et al., 2009, 2011), and upon the implied lithosphere lower boundary doming at a larger scale.

Plume-related Carboniferous magmatism in the OMZ, and in the SW Iberian Massif at a larger scale, is at odds with the lack of a cohort of complementary geological evidence lines observed elsewhere in such settings (Tornos et al., 2005). For example, extensive Carboniferous mantle-plume-related magmatism with emission of continental tholeiites is absent elsewhere in western Europe (Kirstein et al., 2004). There can be also highlighted the absence in SW Iberia of large ultramafic emissions and prolific volcanism during the relatively long time interval of continuous Variscan magmatism (ca. 50 Myr). Indeed, the actual volume of Matachel "basic volcanism" products was small (<1 km^3) and, thus, inconsistent with a deep fertile asthenospheric source (Figures 2 and 14). Also, it can be highlighted the absence of cartographic criteria of plume-induced crustal uplift and doming with marine regression and huge conglomerate production (Campbell, 2007; Campbell & Griffiths, 1990; Dam et al., 1998). Finally, the Carboniferous adscription of the IRB origin is contentious (Carbonell et al., 2004; Pous et al., 2004; Sarrionandia et al., 2012).

The origin of SW Iberian Mississippian basic volcanism might be explained in part by the lateral migration of a mantle plume (Elliot et al., 1999; Leat, 2008; Nielsen et al., 2002). However, the current limitations on knowledge of the precise OMZ paleogeographic location during the late Devonian–Mississippian and the lack of supporting evidence for the existence of a hotspot wandering across the Variscan orogenic front (from which basic-ultrabasic magmas could have been channeled over large distances) likewise rule out this hypothesis.

Bearing in mind all the above, so far the lack of definitive arguments for Carboniferous mantle-plume upwelling and lithospheric thinning is a major drawback, by contrast with the Cambrian rift processes recorded in the basement of the OMZ (Sánchez-García et al., 2010; Sarrionandia et al., 2012). Specifically for this case, a secondary or tertiary ""baby"" mantle plume of shallow origin and only 100–200 km in diameter (Cloetingh & Ziegler, 2009; Courtillot et al., 2003; Koptev et al., 2021; Torsvik et al., 2016) might provide a plausible scenario for the mantle source of some primitive Matachel Mississippian magmas (Figure 15). This would also be congruent with lithospheric and asthenospheric mantle provincialism that might include older (Neoproterozoic-early Cambrian) enriched mantle segments originated in a supra-subduction mantle wedge beneath the northern margin of Gondwana.

7.6. Was Lithosphere Reworking the Cause of Mississippian Magmatism?

Despite the hindering effects of crustal contamination processes on the geochemical identification of magmatic rock sources, the fingerprint of a direct contribution of the mantle lithosphere is out of discussion in the rocks studied herein. The petrogenesis inferred for the three magmatic associations identified and the small volcanic production rates permit us to infer that Mississippian basic magmatism resulted of short-lived, low melting degrees of the lithospheric mantle under volatile-present solidus conditions (Gallagher & Hawkesworth, 1992). This process likely prevented extensive decompression melting of the asthenosphere (Peate & Hawkesworth, 1996).

Low-Ti continental tholeiite magma generation along crustal-scale strike–slip faults has been ascribed elsewhere to plume mantle partial melting and subsequent contamination of asthenospheric melts during ascent across the subcontinental lithospheric mantle (Dessureau et al., 2000). In this sense, Low-Ti continental tholeiites could represent a transition from mantle-plume melting to decompression-induced melting of the ambient mantle during continental breakup (Stepanova et al., 2014). However, unlike continental tholeiite emissions fed from contrasting mantle regions (Dessureau et al., 2000; Ingle et al., 2004; Peate & Hawkesworth, 1996; Peate et al., 1992; Pouclet et al., 2017), the Matachel basic volcanism exhibits an "ephemeral" character likely disconnected of a protracted evolution after different mantle source regions. Emission of continental thoeliites fed from a single mantle reservoir would overcome the problems discussed above. Such mechanism has been invoked in
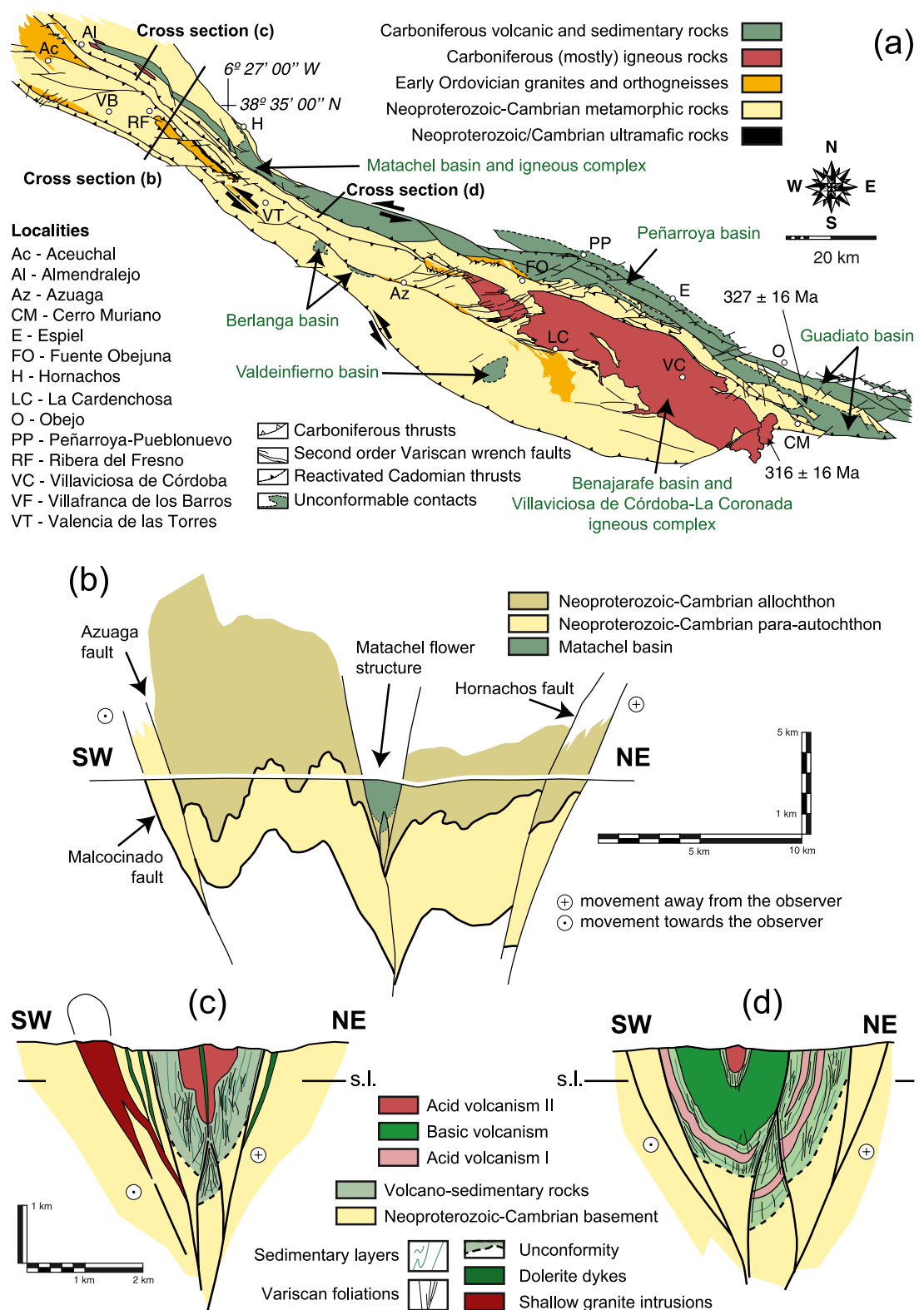
Figure 14.

certain regions (e.g., Sandeman et al., 2014; Shellnutt et al., 2014; Stepanova et al., 2014) and might be taken into consideration for the Matachel case.

Lithospheric shear zones associate significant thermal effects. Conduction into the overlying crust of the heat released during subcontinental mantle shear zones strain increments can result in variable degrees of partial melting of mantle and crustal rocks leading to plutonic/volcanic bimodal magmatism and both the emplacement of those igneous rocks at shallower crustal levels or extrusion at the Earth's surface (Fleitout & Froidevaux, 1980; Leloup et al., 1999; Nicolas et al., 1977). Thus, the alignment of igneous rocks in map view (hundreds of kilometers long and spaced tens of km) might delineate shear zones underneath separating mantle provinces subjected by thermo-mechanical instabilities (Long & Becker, 2010; Savage & Silver, 1993; Tommasi & Vauchez, 2015; Tommasi et al., 1999; Vauchez & Nicolas, 1991). By contrast, shear zones cutting only across the continental crust would not develop such important thermal effects. Notwithstanding, they can be delineated as major deformation localization bands and wrench faults likely with an important metamorphic and fabric overprint. Actually, polyorogenic reworking of anisotropic crust can give rise to complex relationships of reactivation and overprinting of crustal and lithospheric mantle shear zones (Tommasi & Vauchez, 1997, 2001).

This might have been the case for the Carboniferous bimodal magmatism of SW Iberia (Armendáriz et al., 2019; Oliveira & Quesada, 2019; Sánchez-Carretero et al., 1990). This includes, among others, the Los Pedroches-Alburquerque magmatic alignment (a 400 km long complex oriented N130°E and made of batholithic-scale granite and granodiorite plutons and a few minor volcanic and subvolcanic units) and the also N130°E-trending Villaviciosa de Córdoba bimodal magmatic complex, formed by plutonic, subvolcanic and volcanic rocks (Castro, 2019; Sánchez Carretero et al., 1989, 1990; Figure 1). The former alignment likely separates subcontinental mantle domains with different anisotropic teleseismic fabrics (Ábalos & Díaz, 1995; Banda et al., 1981; Díaz et al., 1996; Silver & Chan, 1988). The latter alignment is spatially related to fault-bounded volcano-sedimentary basins (including the Matachel basin) filled with shallow marine and continental sediments as well as with bimodal volcanic and volcanosedimentary formations (Figures 14a and 14b). These basins developed at the site of a ductile and brittle/ductile Variscan intracontinental shear zone (Burg et al., 1981) that reworked an older suture (Ábalos, 1992; Ábalos et al., 2023) and during the late Paleozoic generated a flower structure with nested strike-slip basins (Figures 14c and 14d).

8. Conclusions

The geological evidence presented in this study supports that the Matachel Low-Ti continental tholeiites were not derived of Carboniferous mantle plume upwelling, but of reactivation of a heterogeneous mantle with petrological and geochemical characteristics inherited from a Neoproterozoic mantle wedge and a mid-late Cambrian plume (Figure 15a). Surface geology evidences pervasive Mississippian continental crust/lithosphere-scale transcurrent deformation in SW Iberia. Coeval equivalents of the Matachel Low-Ti continental tholeiites to the North are the MORB-type tholeiites described by Armendáriz et al. (2008). This geochemical gradation further supports the existence of a complex, inherited mantle configuration in SW Iberia, capable of producing different magma types under shear zone reactivation, including lithospheric (Low-Ti continental tholeiites) and restricted asthenospheric magma sources (MORB-type tholeiites).

We postulate that late Devonian–Mississippian lithospheric-scale left lateral transcurrent tectonics triggered low degrees of mantle melting. Melting near the base of the lithosphere might have involved marginally the underlying asthenosphere, and both the lithosphere and asthenosphere characteristics would have inherited the imprints of older processes, including Neoproterozoic (Cadomian) plate convergence and Cambrian rifting. Carboniferous magma ascent along major shear zones through the continental crust permitted interaction with Cadomian metamafic rocks and Cambrian sills, leading to progressive increases in magma geochemical/petrological complexity.

From the detailed petrogenetic viewpoint, late Devonian-Mississippian lithospheric-scale intra-continental wrenching promoted partial melting of an enriched lithospheric mantle, probably made of (rutile-)

Figure 14. (a) Geological sketch map of the Badajoz-Córdoba ductile shear zone area showing relevant Carboniferous sedimentary basins and igneous complexes, as well as its pre-Variscan basement. Outcrops of a discontinuous Tertiary cover have been removed in order to highlight the distribution of concealed geological units. Geochronological references after Bellon et al. (1979). (b) Cross section of the Badajoz-Córdoba shear zone depicting the Variscan reworking of earlier structures (refolded Cadomian crystalline nappe) and the down-dip convergent character of major transcurrent crustal faults, with a central flower structure hosting the Matachel basin volcano-sedimentary Mississippian infill. (c, d) Representative cross sections of the NW and SE segments, respectively, of the Matachel basin showing the three volcanic episodes recorded and spatially related acid and basic coeval intrusive bodies. See text for further details.
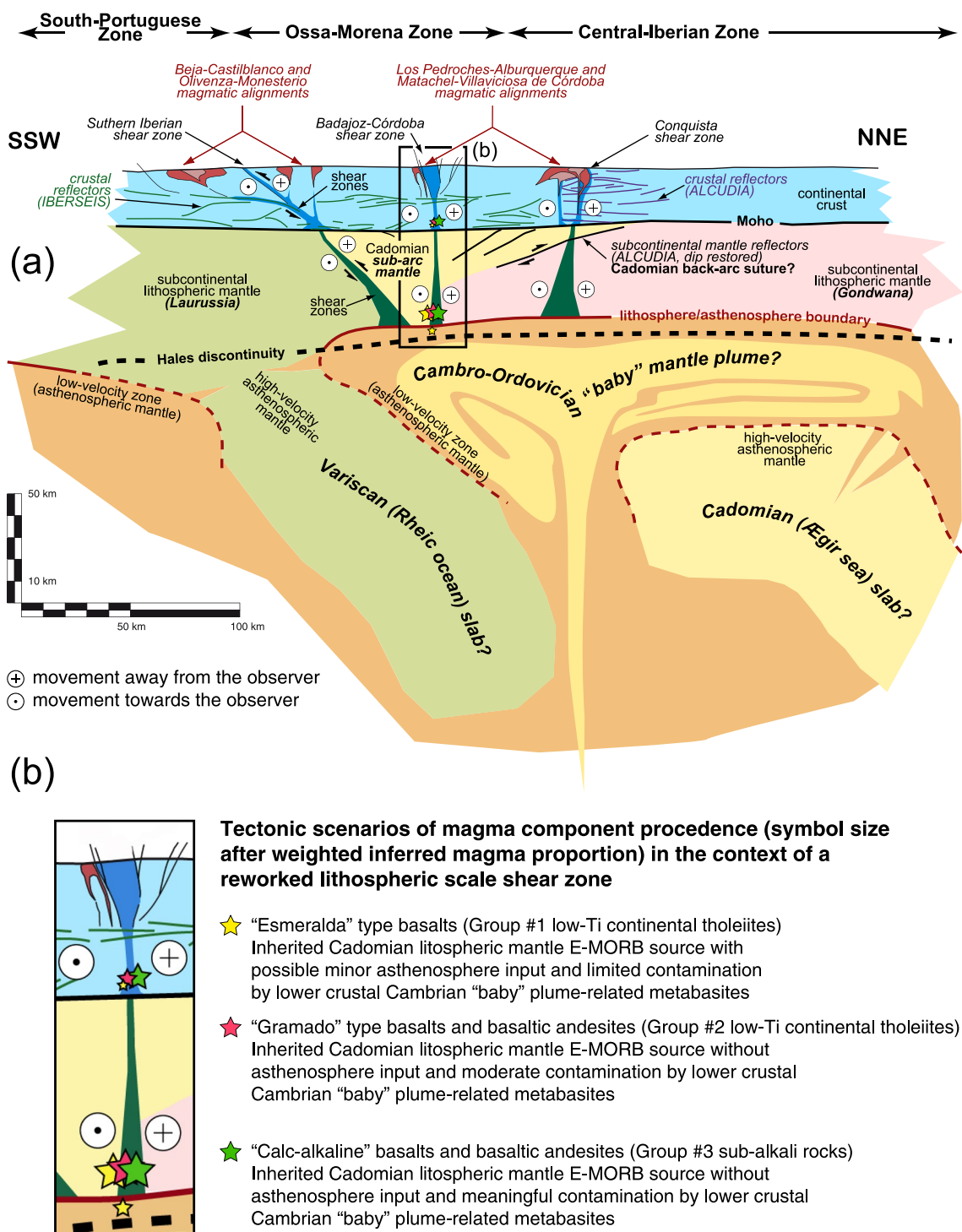
Figure 15. (a) Tectonic model of the SW Iberian lithosphere and underlying upper mantle showing its envisaged complex (inherited) structural geology. See text for further details. Drawing of crustal features, subcontinental lithospheric mantle reflectors and tectonic province arrangements were inspired in the IBERSEIS deep seismic reflection profile (SSW crustal segment; Carbonell et al., 2004), the ALCUDIA profile (NNE crustal segment; Martínez-Poyatos et al., 2012) and Ábalos and Díaz (1995). Upper mantle high/low seismic velocity zone boundaries (in cases the lithosphere/asthenosphere boundary) and Hales transition after Palomeras et al. (2011, 2017), respectively. The "baby" mantle plume and the sinking slabs are speculative interpretations proposed in this study. (b) Close view of the rectangle area in (a) with details of the magma source inherited tectonic realms and their relationship with the three rock groups studied.

amphibole-bearing, garnet-free lherzolite. This would have given rise to formation of primitive Group #1 Low-Ti tholeiitic magmas (possibly with a very limited asthenosphere melting input; Figure 15b). Progressive interaction of these magmas with crustal (likely Cambrian) alkali igneous rocks resulted in formation of the petrological evolutionary trends observed, to a larger extent in the case of Group #2 Low-Ti tholeiites. Further assimilation of amphibole-rich calc-alkaline metaigneous rocks (likely Cadomian) and subsequent plagioclase, clinopyroxene, and Ti-bearing oxide fractionation can explain the nature of parent melts of calc-alkaline basaltic rocks (seemingly "Cordilleran-type" calc-alkaline, though unrelated to plate convergence) after the Low-Ti tholeiites. Enduring mid-upper crustal processes (magma storage in mid-crustal chambers) likely shaped the latest petrologic and geochemical aspects of the Matachel Low-Ti tholeiites and related rocks with calc-alkaline signature.

Data Availability Statement

Mineral chemical data are available (Open Access) in Sarrionandia et al. (2023). Studied rock samples are available in the Faculty of Science and Technology of Campus de Lejona (fernando.sarrionandia@ehu.eus). Information about field location coordinates of the studied samples is in Supporting Information S1 of this article. Regarding the reproducibility of results, no specific fee-based software is needed; as for whole-rock data processing, the open-source software Geochemical Data Toolkit (GCDkit; Janoušek et al., 2016) was used.

References

Ábalos, B. (1992). Variscan shear-zone deformation of late Precambrian basement in SW Iberia, implications for circum-Atlantic pre-Mesozoic tectonics. *Journal of Structural Geology*, *14*(7), 807–823. https://doi.org/10.1016/0191-8141(92)90042-U

Ábalos, B., & Díaz, J. (1995). Correlation between seismic anisotropy and major geological structures in SW Iberia: A case study on continental lithosphere deformation. *Tectonics*, *14*(4), 1021–1040. https://doi.org/10.1029/95TC01204

Ábalos, B., & Eguíluz, L. (1991). Deformación transpresiva carbonífera en la Zona de Cizalla de Badajoz-Córdoba (Macizo Ibérico meridional). *Revista de la Sociedad Geologica de Espana*, *4*, 229–249.

Abalos, B., Gil Ibarguchi, J. I., & Eguiluz, L. (1991). Cadomian subduction, collision and Variscan transpression in the Badajoz-Cordoba shear belt, southwest Spain. *Tectonophysics*, *199*(1), 51–72. https://doi.org/10.1016/0040-1951(91)90118-c

Ábalos, B., Puelles, P., & Gil Ibarguchi, J. I. (2023). Polyphase tectonic reworking of serpentinites and chlorite-tremolite-talc rocks (SW Spain) from the subduction forearc to intracontinental emplacement. *Journal of Metamorphic Geology*, *41*(4), 491–523. https://doi.org/10.1111/jmg.12704

Apalategui, O., Higueras, P., & Quesada, C. (1983). *Hoja y memoria explicativa del Mapa Geológico de España a escala 1:50.000 (Map No. 855, Usagre)*. Instituto Geológico y Minero de España.

Armendáriz, M., López-Guijarro, R., Quesada, C., Pin, C., & Bellido, F. (2008). Genesis and evolution of a syn-orogenic basin in transpression: Insights from petrography, geochemistry and Sm–Nd systematics in the Variscan Pedroches basin (Mississippian, SW Iberia). *Tectonophysics*, *461*(1–4), 395–413. https://doi.org/10.1016/j.tecto.2008.02.007

Armendáriz, M., Quesada, C., Gabaldón, V., & Rosales, I. (2019). Pedroches basin and correlatives (Missisippian). In C. Quesada & J. T. Oliveira (Eds.), *The geology of Iberia: A geodynamic approach* (Vol. 2, pp. 384–390). Springer.

Arriola, A., Cachón, J., Eraso, A., Eguiluz, L., Garrote, A., Sánchez Carretero, R., et al. (1983). *Hoja y memoria explicativa del Mapa Geológico de España a E. 1:50.000 (Map No. 829, Villafranca de los Barros)*. Instituto Geológico y Minero de España.

Arthaud, F., & Matte, P. (1977). Late Paleozoic strike-slip faulting in southern Europe and northern Africa; result of a right lateral shear zone between the Appalachians and the Urals. *Geological Society of America Bulletin*, *88*(9), 1305–1320. https://doi.org/10.1130/0016-7606(1977)88<1305:lpsfis>2.0.co;2

Ayarza, P., Palomeras, I., Carbonell, R., Afonso, J. C., & Simancas, F. (2010). A wide-angle upper mantle reflector in SW Iberia: Some constraints on its nature. *Physics of the Earth and Planetary Interiors*, *181*(3–4), 88–102. https://doi.org/10.1016/j.pepi.2010.03.004

Balcaen, L., De Schrijver, I., Moens, L., & Vanhaecke, F. (2005). Determination of the $^{87}Sr/^{86}Sr$ isotope ratio in USGS silicate reference materials by multi-collector ICP-mass spectrometry. *International Journal of Mass Spectrometry*, *242*(2–3), 251–255. https://doi.org/10.1016/j.ijms.2004.10.025

Banda, E., Suriñach, E., Aparicio, A., Sierra, J., & Ruiz de la Parte, E. (1981). Crustal and upper mantle structure of the central Iberian Meseta. *Geophysical Journal of the Royal Astronomical Society*, *87*(3), 779–789. https://doi.org/10.1111/j.1365-246x.1981.tb06954.x

Bandrés, A., Eguíluz, L., Gil Ibarguchi, J. I., & Palacios, T. (2002). Geodynamic evolution of a Cadomian arc region: The northern Ossa-Morena zone, Iberian Massif. *Tectonophysics*, *352*(1–2), 105–120. https://doi.org/10.1016/S0040-1951(02)00191-9

Bandrés, A., Eguiluz, L., Pin, C., Paquette, J. L., Ordóñez, B., Le Fèbre, J., et al. (2004). The northern Ossa Morena Cadomian batholith (Iberian Massif): Magmatic arc origin and early evolution. *International Journal of Earth Sciences*, *93*(5), 860–885. https://doi.org/10.1007/s00531-004-0423-6

Barth, M. G., McDonough, W. F., & Rudnick, R. L. (2000). Tracking the budget of Nb and Ta in the continental crust. *Chemical Geology*, *165*(3–4), 197–213. https://doi.org/10.1016/s0009-2541(99)00173-4

Bea, F., Gallastegui, G., Montero, P., Molina, J. F., Scarrow, J., Cuesta, A., & González-Menéndez, L. (2021). Contrasting high-Mg, high-K rocks in central Iberia: The appinite-vaugnerite conundrum and their (non-existent) relation with arc magmatism. *Journal of Iberian Geology*, *47*(1–2), 235–261. https://doi.org/10.1007/s41513-020-00152-x

Bellieni, G., Comin-Chiaramonti, P., Marques, L. S., Melfi, A. J., Piccirillo, E. M., Nardy, A. J. R., & Roisenberg, A. (1984). High- and low-Ti flood basalts from the Paraná plateau (Brazil): Petrology and geochemical aspects bearing on their mantle origin. *Neues Jahrbuch für Mineralogie, Geologie und Palaontologie Abhandlungen*, *150*, 273–306.

Bellon, H., Blanchére, H., Crousilles, M., Deloche, C., Dixsaut, C., Hertritch, B., et al. (1979). Radiochronologie, évolution téctono-magmatique et implications métallogéniques dans les cadomo-variscides du Sud-Est Hespérique. *Bulletin de la Societe Geologique de France*, *21*(2), 113–120. https://doi.org/10.2113/gssgfbull.s7-xxi.2.113

Benek, R., Kramer, W., McCann, T., Scheck, M., Negendank, J. F. W., Korich, D., et al. (1996). Permo-Carboniferous magmatism of the northeast German basin. *Tectonophysics*, *266*(1–4), 379–404. https://doi.org/10.1016/s0040-1951(96)00199-0

Bertrand, H., Dostal, J., & Dupuy, C. (1982). Geochemistry of early Mesozoic tholeiites from Morocco. *Earth and Planetary Science Letters*, *58*(2), 225–239. https://doi.org/10.1016/0012-821x(82)90196-0

Braid, J. A., Murphy, J. B., Quesada, C., Gladney, E. R., & Dupuis, N. (2018). Progressive magmatism and evolution of the Variscan suture in southern Iberia. *International Journal of Earth Sciences*, *107*(3), 971–983. https://doi.org/10.1007/s00531-017-1540-3

Brun, J. P., & Burg, J. P. (1982). Combined wrenching and thrusting in the Ibero-Armoricain arc: A corner effect guring continental collision. *Earth and Planetary Science Letters*, *61*(2), 319–322. https://doi.org/10.1016/0012-821x(82)90063-2

Burg, J. P., Iglesias, M., Laurent, P., Matte, P., & Ribeiro, A. (1981). Variscan intracontinental deformation: The Coimbra-Cordoba shear zone (SW Iberian Peninsula). *Tectonophysics*, *78*(1–4), 15–42. https://doi.org/10.1016/0040-1951(81)90012-3

Cabanis, B., & Lecolle, M. (1989). Le diagramme La/10–Y/15–Nb/8: Un outil pour la discrimination des series volcaniques et en evidence des mélange et/ot de vontamination crustale. *Comptes Rendus de l'Académie des Sciences*, *309*, 2023–2029.

Cambeses, A., Montero, P., Molina, J. F., Hyppolito, T., & Bea, F. (2019). Constraints of mantle and crustal sources and interaction during orogenesis: A zircon SHRIMP U-Th-Pb and O isotope study of the "calc-alkaline" Brovales pluton, Ossa-Morena zone, Iberian Variscan belt. *Lithos*, *324–325*, 661–683. https://doi.org/10.1016/j.lithos.2018.11.037

Cambeses, A., Scarow, J. H., Montero, P., Molina, J. F., & Moreno, J. A. (2015). SHRIMP U-Pb zircon dating of the Valencia del Ventoso plutonic complex, Ossa-Morena zone, SW Iberia: Early carboniferous intra-orogenic extension-related "calc-alkaline" magmatism. *Gondwana Research*, *28*(2), 735–756. https://doi.org/10.1016/j.gr.2014.05.013

Campbell, I. H. (2007). Testing the plume theory. *Chemical Geology*, *241*(3–4), 153–176. https://doi.org/10.1016/j.chemgeo.2007.01.024

Campbell, I. H., & Griffiths, R. W. (1990). Implications of plume structure for the evolution of flood basalts. *Earth and Planetary Science Letters*, *99*(1–2), 79–93. https://doi.org/10.1016/0012-821x(90)90072-6

Carbonell, R., Simancas, J. F., Juhlin, C., Pous, J., Pérez-Estaún, A., González-Lodeiro, F., et al. (2004). Geophysical evidence of a mantle derived intrusion in SW Iberia. *Geophysical Research Letters*, *31*(11), L11601. https://doi.org/10.1029/2004gl019684

Castro, A. (2019). An overview on the petrogenesis of the large batholiths and the mantle-related, basic and intermediate rocks. In C. Quesada & J. T. Oliveira (Eds.), *The geology of Iberia: A geodynamic approach* (Vol. 2, pp. 384–390). Springer.

Castro, A., Fernandez, C., de la Rosa, J. D., Moreno-Ventas, I., & Rogers, G. (1996). Significance of MORB-derived amphibolites from the Aracena metamorphic belt, southwest Spain. *Journal of Petrology*, *37*(2), 235–260. https://doi.org/10.1093/petrology/37.2.235

Chichorro, M. (2006). A evolução tectónica da zona de cisalhamento de Montemor-o-Novo (Sudoeste da Zona de Ossa Morena—Área de Santiago de Escoural—Cabrela). (Doctoral dissertation). Universidade de Évora.

Chichorro, M., Pereira, M. F., Díaz-Azpiroz, M., Williams, I. S., Fernández, C., Pin, C., & Silva, J. B. (2008). Cambrian ensialic rift-related magmatism in the Ossa-Morena zone (Évora-Aracena metamorphic belt, SW Iberian Massif): Sm-Nd isotopes and SHRIMP zircon U-Th-Pb geochronology. *Tectonophysics*, *461*(1–4), 91–113. https://doi.org/10.1016/j.tecto.2008.01.008

Class, C., Goldstein, S. L., Altherr, R., & Bachelery, P. (1998). The process of plume-lithosphere interactions in the ocean basins—The case of the Grand Comore. *Journal of Petrology*, *39*(5), 881–903. https://doi.org/10.1093/petroj/39.5.881

Cloetingh, S. A. P. L., & Ziegler, P. A. (2009). TOPO-EUROPE: Coupled deep earth-surface processes in Europe. *European Review*, *17*(3–4), 517–540. https://doi.org/10.1017/S1062798709000933

Colmenero, J. R., Fernández Luis, P., Moreno, C., Bahamonde, J. R., Barba, P., Heredia, N., & González, F. (2002). Carboniferous. In W. Gibbons & T. Moreno (Eds.), *The geology of Spain* (pp. 93–116). Geological Society.

Condie, K. C. (2005). High field strength element ratios in Archean basalts: A window to evolving sources of mantle plumes? *Lithos*, *79*(3–4), 491–504. https://doi.org/10.1016/j.lithos.2004.09.014

Courtillot, V., Davaille, A., Besse, J., & Stock, J. (2003). Three distinct types of hotspots in the Earth's mantle. *Earth and Planetary Science Letters*, *205*(3–4), 295–308. https://doi.org/10.1016/S0012-821X(02)01048-8

Cox, K. G. (1980). A model for flood basalt volcanism. *Journal of Petrolology*, *21*(4), 629–650. https://doi.org/10.1093/petrology/21.4.629

Cox, K. G., & Hawkesworth, C. J. (1985). Geochemical stratigraphy of the Deccan Traps at Mahabaleshwar, Western Ghats, India, with implications for open system magmatic processes. *Journal of Petrology*, *26*(2), 355–377. https://doi.org/10.1093/petrology/26.2.355

Dam, G., Larsen, M., & Sønderholm, M. (1998). Sedimentary response to mantle plumes: Implication from Paleocene onshore successions, West and East Greenland. *Geology*, *26*(3), 207–210. https://doi.org/10.1130/0091-7613(1998)026<0207:srtmpi>2.3.co;2

Deer, W. A., Howie, R. A., & Zussman, J. (1963). Rock-forming minerals. *Framework silicates* (Vol. 4). Longman.

DePaolo, D. J. (1988). *Neodymium isotope geochemistry: An introduction*. Springer Verlag.

Dessureau, G., Piper, D. J. W., & Pe-Piper, G. (2000). Geochemical evolution of earliest Carboniferous continental tholeiitic basalts along a crustal-scale shear zone, southwestern Maritimes basin, eastern Canada. *Lithos*, *50*(1–3), 27–50. https://doi.org/10.1016/s0024-4937(99)00042-0

Díaz, J., Hirn, A., Gallart, J., & Ábalos, B. (1996). Upper mantle anisotropy in SW Iberia from long-range seismic profiles and teleseismic shear-wave data. *Physics of the Earth and Planetary Interiors*, *95*(3–4), 153–166. https://doi.org/10.1016/0031-9201(95)03127-8

Díaz Azpíroz, M., Fernández, C., Castro, A., & El-Biad, M. (2006). Tectonometamorphic evolution of the Aracena metamorphic belt (SW Spain) resulting from ridge-trench interaction during Variscan plate convergence. *Tectonics*, *25*(1), TC1001. https://doi.org/10.1029/2004TC001742

Díez-Fernández, R., Arenas, R., Pereira, M. F., Sánchez Martinez, S., Albert, R., Martin Parra, L., et al. (2016). Tectonic evolution of Variscan Iberia: Gondwana-Laurussia collision revisited. *Earth-Science Reviews*, *162*, 269–292. https://doi.org/10.1016/j.earscirev.2016.08.002

Díez Fernández, R., Fernández, C., Arenas, R., & Novo-Fernández, I. (2021). On the rootless nature of a Devonian suture in SW Iberia (Ossa-Morena complex, Variscan orogen): Geometry and kinematics of the Azuaga fault. *Tectonics*, *40*(6), e2021TC006791. https://doi.org/10.1029/2021TC006791

Donnelly, K. E., Goldstein, S. L., Langmuir, C. H., & Spiegelman, M. (2004). Origin of enriched ocean ridge basalts and implications for mantle dynamics. *Earth and Planetary Science Letters*, *226*(3–4), 347–366. https://doi.org/10.1016/j.epsl.2004.07.019

Dostal, J., & Dupuy, D. (1984). Geochemistry of the North mountain basalts (Nova Scotia, Canada). *Chemical Geology*, *45*(3–4), 245–261. https://doi.org/10.1016/0009-2541(84)90040-8

Dostal, J., Murphy, J. B., & Shellnutt, J. G. (2019). Secular isotopic variation in lithospheric mantle through the Variscan orogeny: Neoproterozoic to Cenozoic magmatism in continental Europe. *Geology*, *47*(7), 637–640. https://doi.org/10.1130/g46067.1

Droop, G. T. R. (1987). A general equation for estimating Fe^{3+} concentrations in ferromagnesian silicates and oxides from microprobe analyses, using stoichiometric criteria. *Mineralogical Magazine*, *51*(361), 431–435. https://doi.org/10.1180/minmag.1987.051.361.10

Dupuy, D., & Dostal, J. (1984). Trace element geochemistry of some continental tholeiites. *Earth and Planetary Science Letters*, *67*(1), 61–69. https://doi.org/10.1016/0012-821x(84)90038-4

Eguíluz, L., Gil Ibarguchi, J. I., Ábalos, B., & Apraiz, A. (2000). Superposed Hercynian and Cadomian orogenic cycles in the Ossa Morena zone and related areas of the Iberian Massif. *Geological Society of America Bulletin*, *112*(9), 1398–1413. https://doi.org/10.1130/0016-7606(2000)112<1398:SHACOC>2.0.CO;2

Elliot, D. H., Fleming, T. H., Kyle, P. R., & Foland, K. A. (1999). Long distance transport of magmas in the Jurassic Ferrar large igneous province, Antarctica. *Earth and Planetary Science Letters*, *167*(1–2), 89–104. https://doi.org/10.1016/s0012-821x(99)00023-0

Errandonea-Martin, J., Sarrionandia, F., Janoušek, V., Carracedo-Sánchez, M., & Gil Ibarguchi, J. I. (2019). Origin of cordierite-bearing monzogranites from the southern central Iberian zone—Inferences from the zoned Sierra Bermeja Pluton (Extremadura, Spain). *Lithos*, *342–343*, 440–462. https://doi.org/10.1016/j.lithos.2019.06.009

Fenner, C. N. (1929). The crystallization of basalts. *American Journal of Science*, *18*(105), 225–253. https://doi.org/10.2475/ajs.s5-18.105.225

Fitton, J. G., Saunders, A. D., Norry, M. J., Hardarson, B. S., & Taylor, R. N. (1997). Thermal and chemical structure of the Iceland plume. *Earth and Planetary Science Letters*, *153*(3–4), 197–208. https://doi.org/10.1016/s0012-821x(97)00170-2

Fleitout, L., & Froidevaux, C. (1980). Thermal and mechanical evolution of shear zones. *Journal of Structural Geology*, *2*(1–2), 159–164. https://doi.org/10.1016/0191-8141(80)90046-2

Foley, S. F., Barth, M. G., & Jenner, G. A. (2000). Rutile/melt partition coefficients for trace elements and an assessment of the influence of rutile on the trace element characteristics of subduction zone magmas. *Geochimica et Cosmochimica Acta*, *64*(5), 933–938. https://doi.org/10.1016/s0016-7037(99)00355-5

Frey, F. A., McNaughton, N. J., Nelson, D. R., de Laeter, J. R., & Duncan, R. A. (1996). Petrogenesis of the bunbury basalt, Western Australia: Interaction between the Kerguelen plume and Gondwana lithosphere? *Earth and Planetary Science Letters*, *144*(1–2), 163–183. https://doi.org/10.1016/0012-821x(96)00150-1

Frost, B. R., Fyfe, W. S., Tazaki, K., & Chan, T. (1989). Grain-boundary graphite in rocks and implications for high electrical conductivity in the lower crust. *Nature*, *340*(6229), 134–213. https://doi.org/10.1038/340134a0

Gabaldón, V., Garrote, A., & Quesada, C. (1985). *Geología del Carbonífero inferior del Norte de la Zona de Ossa Morena. Introducción a la excursión de la V Reunión del Grupo de Ossa Morena, Bélmez (Córdoba)* (pp. 101–137). Temas Geológicos-Mineros de España.

Gallagher, K., & Hawkesworth, C. J. (1992). Dehydration melting and the generation of continental flood basalts. *Nature (London)*, *358*(6381), 57–59. https://doi.org/10.1038/358057a0

García Casquero, J. L. (1991). El Complejo Plutónico de Burguillos del Cerro (Badajoz). Un Macizo Politípico y Polintrusivo en la Cadena Hercínica Ibérica. (Doctoral dissertation) University of Salamanca.

García de Madinabeitia, S., Sánchez Lorda, M. E., & Gil Ibarguchi, J. I. (2008). Simultaneous determination of major to ultratrace elements in geological samples by fusion-dissolution and inductively coupled plasma mass spectrometry techniques. *Analytica Chimica Acta*, *625*(2), 117–130. https://doi.org/10.1016/j.aca.2008.07.024

Goldstein, S. L., O'Nions, R. K., & Hamilton, P. J. (1984). A Sm-Nd isotopic study of atmospheric dusts and particulates from major river systems. *Earth and Planetary Science Letters*, *70*(2), 221–236. https://doi.org/10.1016/0012-821x(84)90007-4

Gómez-Frutos, D., & Castro, A. (2022). Sanukitoid crystallization relations at 1.0 and 0.3 GPa. *Lithos*, *414*, 106632. https://doi.org/10.1016/j.lithos.2022.106632

Gómez-Frutos, D., Castro, A., & Gutiérrez-Alonso, G. (2023). Post-collisional batholiths do contribute to continental growth. *Earth and Planetary Science Letters*, *603*, 117978. https://doi.org/10.1016/j.epsl.2022.117978

Green, D. H., Falloon, T. J., Eggins, S. M., & Yaxley, G. M. (2001). Primary magmas and mantle temperatures. *European Journal of Mineralogy*, *13*(3), 437–451. https://doi.org/10.1127/0935-1221/2001/0013-0437

Green, D. H., & Ringwood, A. E. (1970). Mineralogy of peridotite compositions under upper mantle conditions. *Physics of the Earth and Planetary Interiors*, *8*, 359–371. https://doi.org/10.1016/0031-9201(70)90076-2

Gutiérrez-Alonso, G., Fernández-Suárez, J., Jeffries, T. E., Johnston, S. T., Pastor-Galán, D., Murphy, J. B., et al. (2011). Diachronous post-orogenic magmatism within a developing orocline in Iberia, European Variscides. *Tectonics*, *30*(5). TC–5008. https://doi.org/10.1029/2010tc002845

Hacker, B. R., Abers, G. A., & Peacock, S. M. (2003). Subduction factory 1: Theoretical mineralogy, densities, seismic wave speeds and H_2O contents. *Journal of Geophysical Research*, *108*(B1), 2029. https://doi.org/10.1029/2001JB001127

Hawkesworth, C. J., Kelley, S., Turner, S., Le Roex, A. P., & Storey, B. C. (1999). Mantle processes during Gondwana break-up and dispersal. *Journal of African Earth Sciences*, *28*(1), 239–261. https://doi.org/10.1016/s0899-5362(99)00026-3

Hergt, J. M., & Brauns, C. M. (2001). On the origin of Tasmanian dolerites. *Australian Journal of Earth Sciences*, *48*(4), 543–549. https://doi.org/10.1046/j.1440-0952.2001.00875.x

Hofmann, A. (1971). Fractionation corrections for mixed-isotope spikes of Sr, K, and Pb. *Earth and Planetary Science Letters*, *10*(4), 397–402. https://doi.org/10.1016/0012-821X(71)90087-2

Ingle, S., Scoates, J. S., Weis, D., Brügmann, G., & Kent, R. W. (2004). Origin of Cretaceous continental tholeiites in southwestern Australia and eastern India: Insights from Hf and Os isotopes. *Chemical Geology*, *209*(1–2), 83–106. https://doi.org/10.1016/j.chemgeo.2004.04.023

Janoušek, V., Moyen, J.-F., Martin, H., Erban, V., & Farrow, C. (2016). *Geochemical modelling of igneous processes—Principles and recipes in R language*. Springer-Verlag. https://doi.org/10.1007/978-3-662-46792-3

Jesus, A. P., Munhá, J., Mateus, A., Tassinari, C., & Nutman, A. P. (2007). The Beja layered gabbroic sequence (Ossa-Morena Zone, southern Portugal): Geochronology and geodynamic implications. *Geodinamica Acta*, *20*(3), 139–157. https://doi.org/10.3166/ga.20.139-157

Julivert, M., Fonboté, J. M., Ribeiro, A., & Conde, L. A. (1972). *Mapa Tectónico de la Península Ibérica y Baleares (scale 1:1.000.000)*. Instituto Geológico y Minero de España.

Kelemen, P. B., Hanghøj, K., & Greene, A. R. (2007). One view of the geochemistry of subduction-related magmatic arcs, with an emphasis on primitive andesite and lower crust. *Treatise on geochemistry*, *3*, 1–70. https://doi.org/10.1016/B0-08-043751-6/03035-8

Kelemen, P. B., Joyce, D. B., Webster, J. D., & Holloway, J. R. (1990). Reaction between ultramafic rock and fractionating basaltic magma. II: Experimental investigation of reaction between olivine tholeiite and harzburgite at 1150–1050 1C and 5 kb. *Journal of Petrology*, *31*(1), 99–134. https://doi.org/10.1093/petrology/31.1.99

Keppie, J. D., Dostal, J., Miller, B. V., Ramos-Arias, M. A., Morales-Gámez, M., Nance, R. D., et al. (2008). Ordovician–earliest Silurian rift tholeiites in the Acatlán Complex, southern Mexico: Evidence of rifting on the southern margin of the Rheic Ocean. *Tectonophysics*, *461*(1–4), 130–156. https://doi.org/10.1016/j.tecto.2008.01.010

Kirstein, L. A., Dunai, T. J., Davies, G. R., Upton, B. G. J., & Nikogosian, I. K. (2004). Helium isotope signature of lithospheric mantle xenoliths from the Permo-Carboniferous magmatic province in Scotland—No evidence for a lower-mantle plume. *Geological Society, London, Special Publications*, *223*(1), 243–258. https://doi.org/10.1144/GSL.SP.2004.223.01.11

Koptev, A., Cloetingh, S., & Ehlers, T. A. (2021). Longevity of small-scale ("baby") plumes and their role in lithospheric break-up. *Geophysical Journal International*, *227*(1), 439–471. https://doi.org/10.1093/gji/ggab223

Kroner, U., & Romer, R. L. (2013). Two plates—Many subduction zones: The Variscan orogeny reconsidered. *Gondwana Research*, *24*(1), 298–329. https://doi.org/10.1016/j.gr.2013.03.001

LaFléche, M. R., Camiré, G., & Jenner, G. A. (1998). Geochemistry of post-Acadian, carboniferous continental intraplate basalts from the Maritimes basin, Magdalen islands, Québec, Canada. *Chemical Geology*, *148*(3–4), 115–136. https://doi.org/10.1016/s0009-2541(98)00002-3

Larrondo, E. (2014). Vulcanismo de la Cuenca Carbonífera del Matachel (Zona de Ossa-Morena): implicaciones paleogeográficas y geodinámicas. (Doctoral dissertation). University of the Basque Country UPV/EHU.

Lassiter, J. C., & DePaolo, D. J. (1997). Plume/lithosphere interaction in the generation of continental and oceanic flood basalts: Chemical and isotopic constraints. *Geophysical Monography*, *100*, 335–355.

Leake, B. E., Woolley, A. R., Arps, C. E. S., Birch, W. D., Gilbert, M. C., Grice, J. D., et al. (1997). Nomenclature of amphiboles. Report of the subcommittee on amphiboles of the international mineralogical association, commission on the new mineral names. *The Canadian Mineralogist*, *35*, 219–246.

Leat, P. T. (2008). On the long-distance transport of Ferrar magmas. *Geological Society, London, Special Publications*, *302*(1), 45–61. https://doi.org/10.1144/SP302.4

Leloup, P. H., Ricard, Y., Battaglia, J., & Lacassin, R. (1999). Shear heating in continental strike-slip shear zones: Model and field examples. *Geophysical Journal International*, *136*(1), 19–40. https://doi.org/10.1046/j.1365-246X.1999.00683.x

Liew, T. C., & Hofmann, A. W. (1988). Precambrian crustal components, plutonic associations, plate environment of the Hercynian Fold Belt of Central Europe: Indications from a Nd and Sr isotopic study. *Contributions to Mineralogy and Petrology*, *98*(2), 129–138. https://doi.org/10.1007/BF00402106

Lightfoot, P. C., Hawkesworth, C. J., Hergt, J., Naldrett, A. J., Gorbachev, N. S., Fedorenko, V. A., & Doherty, W. (1993). Remobilisation of the major-trace-element, and from picritic and tholeiitic Siberian Trap, Russia continental lithosphere by a mantle plume: Sr-Nd-and Pb-isotope evidence from picritic and tholeiitic lavas of the Noril'sk District. *Contributions to Mineralogy and Petrology*, *114*(2), 171–188. https://doi.org/10.1007/bf00307754

Lima, S. M., Corfu, F., Neiva, A. M. R., & Ramos, M. F. (2012). Dissecting complex magmatic processes: An in-depth U-Pb study of the Pavia Pluton, Ossa-Morena zone, Portugal. *Journal of Petrology*, *53*(9), 1887–1911. https://doi.org/10.1093/petrology/egs037

Long, M. D., & Becker, T. W. (2010). Mantle dynamics and seismic anisotropy. *Earth and Planetary Science Letters*, *297*(3–4), 341–354. https://doi.org/10.1016/j.epsl.2010.06.036

López-Guijarro, R., Armendáriz, M., Quesada, C., Fernández-Suárez, J., Murphy, J. B., Pin, C., & Bellido, F. (2008). Ediacaran-Palaeozoic tectonic evolution of the Ossa Morena and Central Iberian zones (SW Iberia) as revealed by Sm-Nd isotope systematics. *Tectonophysics*, *461*(1–4), 202–214. https://doi.org/10.1016/j.tecto.2008.06.006

López-Moro, J., Murciego, A., & López-Plaza, M. (2007). Silurian/ordovician asymmetrical sill-like bodies from La Codosera syncline, W Spain: A case of tholeiitic partial melts emplaced in a single magma pulse and derived from a metasomatized source. *Lithos*, *96*(3–4), 567–590. https://doi.org/10.1016/j.lithos.2006.12.006

Lotze, F. (1945). Zur Gliederung der Variszidien der Iberischen Meseta. *Geotektonische Forschungen*, *6*, 78–92.

Mantovani, M. S. M., Marques, L. S., De Sousa, M. A., Civetta, L., Atalla, L., & Innocenti, F. (1985). Trace element and strontium isotope constraints on the origin and evolution of Paraná continental flood basalts of Santa Catarina state (southern Brazil). *Journal of Petrology*, *26*(1), 187–209. https://doi.org/10.1093/petrology/26.1.187

Marsaglia, K. M., & Tazaki, K. (1992). Diagenetic trends in Leg 126 sandstones. *Proceedings of the Ocean Drilling Program, Scientific Results*, *126*, 125–138.

Martin, H., Moyen, J.-F., & Rapp, R. (2009). The sanukitoid series: Magmatism at the Archaean–Proterozoic transition. *Earth and Environmental Science Transactions of the Royal Society of Edinburgh*, *100*(1–2), 15–33. https://doi.org/10.1017/s1755691009016120

Martin, H., Smithies, R. H., Rapp, R., Moyen, J.-F., & Champion, D. (2005). An overview of adakite, tonalite-trondhjemite-granodiorite (TTG), and sanukitoid: Relationships and some implications for crustal evolution. *Lithos*, *79*(1–2), 1–24. https://doi.org/10.1016/j.lithos.2004.04.048

Martínez-Poyatos, D., Carbonell, R., Palomeras, I., Simancas, J. F., Ayarza, P., Marti, D., et al. (2012). Imaging thte crustal structure of the Central Iberian Zone (Variscan Belt): The ALCUDIA deep seismic transect. *Tectonics*, *31*, 1–21. https://doi.org/10.1029/2011TC002995

Matrosova, E. A., Bobrov, A. V., Bind, L., & Pushcharovski, D. Y. (2021). Titanium minerals and their assemblages in the Earth's mantle: A review of natural and experimental data. *Geochemistry International*, *59*(8), 725–742. https://doi.org/10.1134/S001670292108005X

Matrosova, E. A., Bobrov, A. V., Bind, L., Pushcharovski, D. Y., & Irifune, T. (2020). Titanium-rich phases in the Earth's transition zone and lower mantle: Evidence from experiments in the system $MgO-SiO_2-TiO_2$ ($\pm Al_2O_3$) at 10-24 GPa and 1600 ºC. *Lithos*, *366–367*, 105539. https://doi.org/10.1016/j-lithos2020.105539

Matte, P., & Ribeiro, A. (1975). Forme et orientation de l'éllipsoide de déformation dans la virgation hercynienne de Galice Rélations avec le plissement et hipothèses sur la génèse de l'arc Ibero-Armoricain. *Comptè Rendus de l'Académie des Sciences de la Terre Paris*, *280*, 2825–2828.

McPhie, J., Doyle, M., & Allen, R. (1993). *Volcanic textures: A guide to the interpretation of textures in volcanic rocks*. University of Tasmania.

Mitjavila, J., Martí, J., & Soriano, C. (1997). Magmatic evolution and tectonic setting of the Iberian Pyrite Belt volcanism. *Journal of Petrology*, *38*(6), 727–755. https://doi.org/10.1093/petroj/38.6.727

Miyashiro, A. (1974). Volcanic rock series in island arcs and active continental margins. *American Journal of Science*, *274*(4), 321–355. https://doi.org/10.2475/ajs.274.4.321

Moita, P., Santos, J. F., & Pereira, M. F. (2009). Layered granitoids: Interaction between continental crust recycling processes and mantle-derived magmatism. Examples from the Évora Massif (Ossa-Morena Zone, Southwest Iberia, Portugal). *Lithos*, *111*(3–4), 125–141. https://doi.org/10.1016/j.lithos.2009.02.009

Moita, P., Santos, J. F., Pereira, M. F., Costa, M. M., & Corfu, F. (2015). The quartz-dioritic Hospitais intrusion (SW Iberian Massif) and its mafic microgranular enclaves—Evidence for mineral clustering. *Lithos*, *224–225*, 78–100. https://doi.org/10.1016/j.lithos.2015.02.012

Morimoto, N., Fabries, J., Ferguson, A. K., Ginzburg, I. V., Ross, M., Seifert, F. A., et al. (1988). Nomenclature of pyroxenes. *Mineralogy and Petrology*, *39*(1), 55–76. https://doi.org/10.1180/minmag.1988.052.367.15

Munhá, J. (1983). Hercynian magmatism in the Iberian pyrite belt. *Memorias Servicio. Geologico Portugal*, *29*, 39–81.

Müntener, O., Kelemen, P. B., & Grove, T. L. (2001). The role of H_2O and composition on the genesis of igneous pyroxenites: An experimental study. *Contributions to Mineralogy and Petrology*, *141*(6), 643–658. https://doi.org/10.1007/s004100100266

Neal, C. R., Mahoney, J., & Chazey, W. (2002). Mantle sources and the highly variable role of continental lithosphere in basalt petrogenesis of the Kerguelen plateau and Broken ridge LIP: Results from ODP Leg 183. *Journal of Petrology*, *43*(7), 1177–1205. https://doi.org/10.1093/petrology/43.7.1177

Nesbitt, H. W., & Young, G. M. (1982). Early Proterozoic climates and plate motions inferred from major element chemistry of Intites. *Nature*, *299*(5885), 715–717. https://doi.org/10.1038/299715a0

Nicolas, A., Bouchez, J. L., Blaise, J., & Poirier, J. P. (1977). Geological aspects of deformation in continental shear zones. *Tectonophysics*, *42*(1), 55–73. https://doi.org/10.1016/0040-1951(77)90017-8

Nielsen, T. K., Larsen, H. C., & Hopper, J. R. (2002). Contrasting rifted margins styles south of Greenland: Implications for mantle plume dynamics. *Earth and Planetary Science Letters*, *200*(3–4), 271–286. https://doi.org/10.1016/s0012-821x(02)00616-7

Oliveira, J. T., & Quesada, C. (2019). Synorogenic basins in the southern Iberian Massif. In C. Quesada & J. T. Oliveira (Eds.), *The geology of Iberia: A geodynamic approach* (Vol. 2, pp. 361–364). Geological Society. https://doi.org/10.1007/978-3-030-10518-1

Oliveira, J. T., Rosa, C. J. P., Pereira, Z., Rosa, D. R. N., Matos, J. X., Inverno, C. M. C., & Andersen, T. (2013). Geology of the Rosário-Neves Corvo antiform, Iberian Pyrite Belt, Portugal: New insights from physical volcanology, palynostratigraphy and isotope geochronology studies. *Mineralium Deposita*, *48*(6), 749–766. https://doi.org/10.1007/s00126-012-0453-0

O'Neill, H. S. C., & Palme, H. (1998). Composition of the silicate earth: Implications for accretion and core formation. In I. Jackson (Ed.), *The Earth's mantle: Composition, structure and evolution* (pp. 3–126). Cambridge University Press.

Orejana, D., Villaseca, C., & Kristoffersen, M. (2020). Geochemistry and geochronology of mafic rocks from the Spanish Central System: Constraints on the mantle evolution beneath Central Spain. *Geoscience Frontiers*, *11*(5), 1651–1667. https://doi.org/10.1016/j.gsf.2020.01.002

Palomeras, I., Carbonell, R., Ayarza, P., Fernández, M., Simancas, J. F., Martínez-Poyatos, D. J., et al. (2011). Geophysical model of the lithosphere across the Variscan belt of SW-Iberia: Multidisciplinary assessment. *Tectonophysics*, *508*(1–4), 42–51. https://doi.org/10.1016/j.tecto.2010.07.010

Palomeras, I., Carbonell, R., Flecha, I., Simancas, J. F., Ayarza, P., Matas, J., et al. (2009). Nature of the lithosphere across the Variscan orogen of SW Iberia: Dense wide-angle seismic reflection data. *Journal of Geophysical Research*, *114*(B2), B02302. https://doi.org/10.1029/2007JB005050

Palomeras, I., Villaseñor, A., Thurner, S., Levander, A., Gallart, J., & Harnafi, M. (2017). Lithospheric structure of Iberia and Morocco using finite-frequency Rayleigh wave tomogrpahy from earthquakes and seismic ambient noise. *Geochemistry, Geophysics, Geosystems*, *18*, 1824–1840. https://doi.org/10.1002/2016GC006657

Pearce, J. A. (1996). A user's guide to basalt discrimination diagrams. In D. A. Wyman (Ed.), *Trace element geochemistry of volcanic rocks: Applications for massive sulphide exploration* (Vol. 12, pp. 79–113). Geological Association of Canada.

Pearce, J. A. (2008). Geochemical fingerprinting of oceanic basalts with applications to ophiolite classification and the research for Archean oceanic crust. *Lithos*, *100*(1–4), 14–48. https://doi.org/10.1016/j.lithos.2007.06.016

Pearce, J. A., & Norry, M. J. (1979). Petrogenetic implications of Ti, Zr, Y, and Nb variations in volcanic rocks. *Contributions to Mineralogy and Petrology*, *69*(1), 33–47. https://doi.org/10.1007/bf00375192

Pearce, J. A., & Reagan, M. K. (2019). Identification classification and interpretation of boninites from the Recent-Eoarchean geologic record using Si-Mg-Ti systematics. *Geosphere*, *15*(4), 1–30. https://doi.org/10.1130/GES01661.1

Peate, D. W. (1997). The paraná-etendeka province. In J. Mahoney & M. Coffin (Eds.), *Large igneous provinces: Continental, oceanic and planetary flood volcanism. Geophysical monograph series* (Vol. 100, pp. 217–245). American Geophysical Union.

Peate, D. W., & Hawkesworth, C. J. (1996). Lithospheric to asthenospheric transition in low-Ti flood basalts from southern Parana, Brazil. *Chemical Geology*, *127*(1–3), 1–24. https://doi.org/10.1016/0009-2541(95)00086-0

Peate, D. W., Hawkesworth, C. J., & Mantovani, M. S. M. (1992). Chemical stratigraphy of the Paraná lavas (South America): Classification of magma types and their spatial distribution. *Bulletin of Volcanology*, *55*(1–2), 119–139. https://doi.org/10.1007/bf00301125

Pereira, M. F., Chichorro, M., Johnston, S. T., Gutiérrez-Alonso, G., Silva, J. B., Linnemann, U., & Drost, K. (2012). The missing Rheic ocean magmatic arcs: Provenance analysis of late Paleozoic sedimentary clastic rocks of SW Iberia. *Gondwana Research*, *22*(3–4), 882–891. https://doi.org/10.1016/j.gr.2012.03.010

Pereira, M. F., Chichorro, M., Williams, I., Silva, J. B., Fernandez, C., Díaz-Azpíroz, M., et al. (2009). Variscan intra-orogenic extensional tectonics in the Ossa-Morena zone (Évora-Aracena-Lora del Río metamorphic belt, SW Iberian Massif): SHRIMP zircon U-Th-Pb geochronology. *Geological Society, London, Special Publications*, *327*(1), 215–237. https://doi.org/10.1144/sp327.11

Pereira, M. F., Chichorro, M. A., Silva, J. B., Ordóñez-Casado, B., Lee, J. K. W., & Williams, I. S. (2012). Early carboniferous wrenching, exhumation of high-grade metamorphic rocks and basin instability in SW Iberia. *Tectonophysics*, *558–559*, 28–44. https://doi.org/10.1016/j.tecto.2012.06.020

Pereira, M. F., Gutíerrez-Alonso, G., Murphy, J. B., Drost, K., Gama, C., & Silva, J. B. (2017). Birth and demise of the Rheic Ocean magmatic arc(s): Combined U–Pb and Hf isotope analyses in detrital zircon from SW Iberia siliciclastic strata. *Lithos*, *278*, 383–389. https://doi.org/10.1016/j.lithos.2017.02.009

Pereira, M. F., Silva, J. B., Chichorro, M., Moita, P., Santos, J. F., Apraiz, A., & Ribeiro, C. (2007). Crustal growth and deformational processes in the northern Gondwana margin: Constraints from the Évora Massif (Ossa-Morena zone, southwest Iberia, Portugal). In U. Linnemann, R. D. Nance, P. Kraft, & G. Zulauf (Eds.), *The evolution of the Rheic Ocean: From Avalonian-Cadomian active margin to Alleghenian-Variscan collision* (Vol. 423, pp. 333–358). Geological Society of America Special Paper. https://doi.org/10.1130/2007.2423(16)

Pereira, M. F., Silva, J. B., Drost, K., Chichorro, M., & Apraiz, A. (2010). Relative timing of transcurrent displacements in northern Gondwana: U–Pb laser ablation ICP-MS zircon and monazite geochronology of gneisses and sheared granites from the western Iberian Massif (Portugal). *Gondwana Research*, *17*(2–3), 461–481. https://doi.org/10.1016/j.gr.2009.08.006

Pérez-Lorente, F. (1979). Geología de la Zona de Ossa Morena al Norte de Córdoba (Pozoblanco-Belmez-Villaviciosa de Córdoba). (Doctoral dissertation). University of Granada.

Pin, C., Briot, D., Bassin, C., & Poitrasson, F. (1994). Concomitant separation of strontium and samarium-neodymium for isotopic analysis in silicate samples, based on specific extraction chromatography. *Analytica Chimica Acta*, *298*(2), 209–217. https://doi.org/10.1016/0003-2670(94)00274-6

Pin, C., Fonseca, P. E., Paquette, J.-L., Castro, A., & Matte, P. (2008). The ca. 350 Ma Beja igneous complex: A record of transcurrent slab break-off in the southern Iberia Variscan belt? *Tectonophysics*, *461*(1–4), 356–377. https://doi.org/10.1016/j.tecto.2008.06.001

Pin, C., Liñán, E., Pascual, E., Donaire, T., & Valenzuela, A. (2002). Late Neoproterozoic crustal growth in the European variscides: Nd isotope and geochemical evidence from the Sierra de Córdoba andesites (Ossa-Morena zone, southern Spain). *Tectonophysics*, *352*(1–2), 133–151. https://doi.org/10.1016/S0040-1951(02)00193-2

Pin, C., & Santos Zalduegui, J. F. (1997). Sequential separation of light rare-earth elements, thorium and uranium by miniaturized extraction chromatography: Application to isotopic analyses of silicate rocks. *Analytica Chimica Acta*, *339*(1–2), 79–89. https://doi.org/10.1016/S0003-2670(96)00499-0

Pin, C., & Waldhausrová, J. (2007). *Sm-Nd isotope and trace element study of Late Proterozoic metabasalts ("spilites") from the Central Barrandian domain (Bohemian Massif, Czech Republic)* (Vol. 423, pp. 231–247). Geological Society of America, Special Paper.

Pons, J. (1982). Un modèle d'évolution de complexes plutonics: gabbros et granitoïdes de la Sierra Morena occidentale (Espagne). (Doctoral dissertation). University of Toulouse.

Pouclet, A., Javier Álvaro, J., Bardintzeff, J.-M., Gil Imaz, A., Monceret, E., & Vizcaïno, D. (2017). Cambrian–early Ordovician volcanism across the South Armorican and Occitan domains of the Variscan belt in France: Continental breakup and rifting of the northern Gondwana margin. *Geoscience Frontiers*, *8*(1), 25–64. https://doi.org/10.1016/j.gsf.2016.03.002

Pous, J., Muñoz, G., Heise, W., Melgarejo, J. C., & Quesada, C. (2004). Electromagnetic imaging of Variscan crustal structures in SW Iberia: The role of interconnected graphite. *Earth and Planetary Science Letters*, *217*(3–4), 435–445. https://doi.org/10.1016/S0012-821X(03)00612-5

Puchtel, I., Arndt, N., Hofmann, A., Haase, K. M., Kröner, A., Kulikov, V. S., et al. (1998). Petrology of mafic lavas within the Onega plateau, central Karelia: Evidence for 2.0 Ga plume-related continental crustal growth in the Baltic Shield. *Contributions to Mineralogy and Petrology*, *130*(2), 134–153. https://doi.org/10.1007/s004100050355

Puchtel, I. S., Haase, K., Hofmann, A. W., Chauvel, C., Kulikov, V. S., Garbe-Schönberg, C.-D., & Nemchin, A. A. (1997). Petrology and geochemistry of crustally contaminated komatiitic basalts from the Vetreny Belt, southeastern Baltic Shield: Evidence for an early Proterozoic mantle plume beneath rifted Archean continental lithosphere. *Geochimica et Cosmochimica Acta*, *61*(6), 1205–1222. https://doi.org/10.1016/s0016-7037(96)00410-3

Puelles, P., Ábalos, B., & Fernández-Armas, S. (2014). Graphite and quartz petrofabrics: Examples from the Ediacaran black quartzites of the Ossa-Morena zone (SW Iberia). *Tectonophysics*, *615–616*, 53–68. https://doi.org/10.1016/j.tecto.2013.12.0018

Quesada, C. (1991). Geological constraints on the Paleozoic tectonic evolution of tectonostratigraphic terranes in the Iberian Massif. *Tectonophysics*, *185*(3–4), 225–245. https://doi.org/10.1016/0040-1951(91)90446-y

Quesada, C. (1998). A reappraisal of the structure of the Spanish segment of the Iberian Pyrite Belt. *Mineralium Deposita*, *33*(1–2), 31–34. https://doi.org/10.1007/s001260050131

Ribeiro, A. (1983). Relações entre formações do Devónico superior e o Maciço de Évora na região de Cabrela (Vendas Novas). *Comunicacoes dos Servicos Geologicos de Portugal*, *69*(2), 267–282.

Robardet, M., & Gutiérrez-Marco, J. C. (2004). The Ordovician, Silurian and Devonian sedimentary rocks of the Ossa-Morena zone (SW Iberian Peninsula, Spain). *Journal of Iberian Geology*, *20*, 73–92.

Rosa, D. R. N., Finch, A. A., Andersen, T., & Inverno, C. M. C. (2008). U–Pb geochronology of felsic volcanic rocks hosted in the Gafo formation, South Portuguese zone: Relationship with Iberian Pyrite Belt magmatism. *Mineralogical Magazine*, *72*(5), 1103–1118. https://doi.org/10.1180/minmag.2008.072.5.1103

Rudnick, R. L., & Fountain, D. M. (1995). Nature and composition of the continental crust: A lower crustal perspective. *Reviews of Geophysics*, *33*(3), 267–309. https://doi.org/10.1029/95rg01302

Rudnick, R. L., & Gao, S. (2003). Composition of the continental crust. In R. L. Rudnick (Ed.), *The crust, treatise on geochemistry* (Vol. 3, pp. 1–64). Elsevier-Pergamon.

Sánchez Carretero, R., Carracedo, M., Gil Ibarguchi, J. I., & Ortega Cuesta, L. A. (1989). Unidades y datos geoquímicos del magmatismo Hercínico de la "Alineación de Villaviciosa de Córdoba-La Coronada" (Ossa-Morena oriental). *Studia Geologica Salmanticensia spec*, *4*, 107–131.

Sánchez-Carretero, R., Eguíluz, L., Pascual, E., & Carracedo, M. (1990). Ossa-morena zone: Igneous rocks. In R. D. Dallmeyer & E. Martínez-García (Eds.), *Pre-Mesozoic geology of Iberia* (pp. 292–313). Springer-Verlag.

Sánchez Cela, V., Gabaldón, V., León, C., Leal, M. C., & Ordoñez, S. (1977). *Hoja y memoria explicativa del Mapa Geológico de España a E. 1:50.000 (Map No. 856, Maguilla)*. Instituto Geológico y Minero de España.

Sánchez-García, T., Bellido, F., Pereira, M. F., Chichorro, M., Quesada, C., Pin, C., & Silva, J. B. (2010). Rift-related volcanism predating the birth of the Rheic Ocean (Ossa-Morena zone, SW Iberia). *Gondwana Research*, *17*(2–3), 392–407. https://doi.org/10.1016/j.gr.2009.10.005

Sánchez-García, T., Pereira, M. F., Bellido, F., Chichorro, M., Silva, J. B., Valverde-Vaquero, P., et al. (2014). Early Cambrian granitoids of North Gondwana margin in the transition from a convergent setting to intra-continental rifting (Ossa-Morena Zone, SW Iberia). *International Journal of Earth Sciences*, *103*(5), 1203–1218. https://doi.org/10.1007/s00531-013-0939-8

Sánchez-Lorda, M. E., Sarrionandia, F., Ábalos, B., Carracedo, M., Eguiluz, L., & Gil Ibarguchi, J. I. (2014). Geochemistry and paleotectonic setting of Ediacaran metabasites from the Ossa-Morena zone (SW Iberia). *International Journal of Earth Sciences*, *103*(5), 1263–1286. https://doi.org/10.1007/s00531-013-0937-x

Sandeman, H. A., Ootes, L., Cousens, B., & Kilian, T. (2014). Petrogenesis of Gunbarrel magmatic rocks: Homogeneous continental tholeiites associated with extension and rifting of Neoproterozoic Laurentia. *Precambrian Research*, *252*, 166–179. https://doi.org/10.1016/j.precamres.2014.07.007

Santos, J. F., Soares de Andrade, A., & Munhá, J. M. (1990). Magmatismo orogénico Varisco no limite meridional da Zona de Ossa-Morena. *Comunicacoes dos Servicos Geologicos de Portugal*, *76*, 91–124.

Sarrionandia, F. (2006). Estudio petrológico del Complejo Plutónico de Valencia del Ventoso (Badajoz). (Doctoral dissertation). University of the Basque Country UPV/EHU.

Sarrionandia, F., Ábalos, B., Errandonea-Martin, J., Eguíluz, L., Santos-Zalduegui, J. F., García de Madinabeitia, S., et al. (2020). Ediacaran–Earliest Cambrian arc-tholeiite and adakite associations of the Malcocinado Formation (Ossa-Morena Zone, SW Spain): Juvenile continental crust and deep crustal reworking in northern Gondwana. *Lithos*, *372–373*, 105683. https://doi.org/10.1016/j.lithos.2020.105683

Sarrionandia, F., Carracedo, M., Eguíluz, L., Junguitu, J., Lobo, P., & Gil Ibarguchi, J. I. (2013). Geologic map of the Valencia del Ventoso Variscan igneous complex (SW Iberian Massif, Spain): An example of multi-stage intrusion building by contrasted magma compositions. *Journal of Maps*, *9*(4), 498–504. https://doi.org/10.1080/17445647.2013.820675

Sarrionandia, F., Carracedo-Sánchez, M., Eguiluz, L., Ábalos, B., Rodríguez, J., Pin, C., & Gil Ibarguchi, J. I. (2012). Cambrian rift-Related magmatism in the Ossa-Morena zone (Iberian Massif): Geochemical and geophysical evidence of Gondwana break-up. *Tectonophysics*, *570–571*, 135–150. https://doi.org/10.1016/j.tecto.2012.07.023

Sarrionandia, F., Errandonea-Martin, J., Larrondo, E., Carracedo-Sánchez, M., Ábalos, B., & Gil-Ibarguchi, J. I. (2023). Mineral chemistry dataset of the Tournaisian–Lower Viséan submarine basaltic volcanism of the Matachel Basin (SW Iberian Massif). *Data in Brief*, *46*, 108826. https://doi.org/10.1016/j.dib.2022.108826

Sato, H. (1977). Nickel content of basaltic magmas: Identification of primary magmas and a measure of the degree of olivine fractionation. *Lithos*, *10*(2), 113–120. https://doi.org/10.1016/0024-4937(77)90037-8

Savage, M. K., & Silver, P. G. (1993). Mantle deformation and tectonics, constraints from seismic anisotropy in the western United States. *Physics of the Earth and Planetary Interiors*, *78*(3–4), 207–227. https://doi.org/10.1016/0031-9201(93)90156-1

Schilling, J. G., Zajac, M., Evans, R., Johnston, T., White, W., Devine, J. D., & Kingsley, R. (1983). Petrologic and geochemical variations along the Mid-Atlantic ridge from 29N to 73N. *American Journal of Science*, *283*(6), 510–586. https://doi.org/10.2475/ajs.283.6.510

Schulmann, K., Edel, J. B., Martínez-Catalán, J. R., Mazur, S., Guy, A., Lardeaux, J. M., et al. (2022). Tectonic evolution and global crustal architecture of the European Variscan belt constrained by geophysical data. *Earth-Science Reviews*, *234*, 104195. https://doi.org/10.1016/j.earscirev.2022.104195

Shaw, J. E., Baker, J. A., Menzies, M. A., Thirlwall, M. F., & Ibrahim, K. M. (2003). Petrogenesis of the largest intraplate volcanic field of the Arabian plate (Jordan): A mixed lithosphere–asthenosphere source activated by lithospheric extension. *Journal of Petrology*, *44*(9), 1657–1679. https://doi.org/10.1093/petrology/egg052

Shelley, D., & Bossière, G. (2000). A new model for the Hercynian Orogen of Gondwanan France and Iberia. *Journal of Structural Geology*, *22*(6), 757–776. https://doi.org/10.1016/s0191-8141(00)00007-9

Shellnutt, J. G., Bhat, G. M., Wang, K.-L., Brookfield, M. E., Jahn, B.-M., & Dostal, J. (2014). Petrogenesis of the flood basalts from the early Permian Panjal Traps, Kashmir, India: Geochemical evidence for shallow melting of the mantle. *Lithos*, *204*, 159–171. https://doi.org/10.1016/j.lithos.2014.01.008

Shellnutt, J. G., & Jahn, B.-M. (2011). Origin of Late Permian Emeishan basaltic rocks from the Panxi region (SW China): Implications for the Ti-classification and spatial compositional distribution of the Emeishan basalts. *Journal of Volcanology and Geothermal Research*, *199*(1–2), 85–95. https://doi.org/10.1016/j.jvolgeores.2010.10.009

Silva, J. B., & Pereira, M. F. (2004). Transcurrent continental tectonics model for the Ossa-Morena zone Neoproterozoic-Paleozoic evolution, SW Iberian Massif, Portugal. *International Journal of Earth Sciences*, *93*(5), 886–896. https://doi.org/10.1007/s00531-004-0424-5

Silver, P. G., & Chan, W. W. (1988). Implications for continental structure and evolution from seismic anisotropy. *Nature*, *335*(6185), 34–39. https://doi.org/10.1038/335034a0

Simancas, J. F., Carbonell, R., González-Lodeiro, F., Pérez-Estaún, A., Juhlin, C., Ayarza, P., et al. (2006). Transpressional collision tectonics and mantle plume dynamics: The variscides of southwestern Iberia. In D. G. Gee & R. A. Stephenson (Eds.), *European lithosphere dynamics, memoirs geological society of London* (Vol. 32, pp. 345–354). Geological Society Publishing House.

Stampfli, G. M., Hochard, C., Vérard, C., Wilhem, C., & von Raumer, J. (2013). The formation of Pangea. *Tectonophysics*, *593*, 1–19. https://doi.org/10.1016/j.tecto.2013.02.037

Stepanova, A. V., Samsonov, A. V., Salnikova, E. B., Puchtel, I. S., Larionova, Y. O., Larionov, A. N., et al. (2014). Palaeoproterozoic continental MORB-type tholeiites in the Karelian Craton: Petrology, geochronology, and tectonic setting. *Journal of Petrology*, *55*(9), 1719–1751. https://doi.org/10.1093/petrology/egu039

Sun, S.-s., & McDonough, W. F. (1989). Chemical and isotopic systematics of oceanic basalts: Implications for mantle composition and processes. In A. D. Saunders & M. J. Norry (Eds.), *Magmatism in the ocean basins, geological society of London special publications* (Vol. 42, pp. 315–345). Blackwell Scientific Publications.

Taylor, S. R., & McLennan, S. M. (1985). *The continental crust: Its composition and evolution*. Blackwell Scientific Publications.

Tilley, C. E. (1960). Some new chemical data on the alkali rocks of the Vredefort Mountain Land, South Africa. *Transactions of the Geological Society of South Africa*, *63*, 65–70.

Tommasi, A., Tikoff, B., & Vauchez, A. (1999). Upper mantle tectonics: Three-dimensional deformation, olivine crystallographic fabrics and seismic properties. *Earth and Planetary Science Letters*, *168*(1–2), 173–186. https://doi.org/10.1016/s0012-821x(99)00046-1

Tommasi, A., & Vauchez, A. (1997). Continental-scale rheological heterogeneities and complex intraplate tectono-metamorphic patterns: Insights from a case-study and numerical models. *Tectonophysics*, *279*(1–4), 327–350. https://doi.org/10.1016/s0040-1951(97)00117-0

Tommasi, A., & Vauchez, A. (2001). Continental rifting parallel to ancient collisional belts: An effect of the mechanical anisotropy of the lithospheric mantle. *Earth and Planetary Science Letters*, *185*(1–2), 199–210. https://doi.org/10.1016/s0012-821x(00)00350-2

Tommasi, A., & Vauchez, A. (2015). Heterogeneity and anistotropy in the lithospheric mantle. *Tectonophysics*, *661*, 11–37. https://doi.org/10.1016/j.tecto.2015.07.026

Tornos, F., Casquet, C., & Relvas, J. M. R. S. (2005). Transpressional tectonics, lower crust decoupling and intrusion of deep mafic sills: A model for the unusual metallogenesis of SW Iberia. *Ore Geology Reviews*, *27*(1–4), 133–163. https://doi.org/10.1016/j.oregeorev.2005.07.020

Torsvik, T. H., Steinberger, B., Ashwal, L. D., Doubrovine, P. V., & Trønnes, R. G. (2016). Earth evolution and dynamics—A tribute to Kevin Burke. *Canadian Journal of Earth Sciences*, *53*(11), 1073–1087. https://doi.org/10.1139/cjes-2015-0228

Vauchez, A., & Nicolas, A. (1991). Mountain building: Strike-parallel motion and mantle anisotropy. *Tectonophysics*, *185*(3–4), 183–201. https://doi.org/10.1016/0040-1951(91)90443-v

Villaseca, C., Orejana, D., Higueras, P., Pérez-Soba, C., García Serrano, J., & Lorenzo, S. (2022). The evolution of the subcontinental mantle beneath the Central Iberian Zone: Geochemical tracking of its mafic magmatism from the Neoproterozoic to the Cenozoic. *Earth-Science Reviews*, *228*, 103997. https://doi.org/10.1016/j.earscirev.2022.103997

Villaseca, C., Orejana, D., Pin, C., López-García, J. A., & Andonaegui, P. (2004). Le magmatisme basique hercynien et post-hercynien du Système Central Espagnol: Essai de caractérisation des sources mantelliques. *Comptes Rendus Geoscience*, *336*(10), 877–888. https://doi.org/10.1016/j.crte.2004.02.008

Waters, L. E., Cottrell, E., Coombs, M. L., & Kelley, K. A. (2020). Generation of calc-alkaline magmas during crystallization at high oxygen fugacity: An experimental and petrologic study of tephras from Buldir Volcano, Western Aleutian Arc, Alaska, USA. *Journal of Petrology*, *62*(3), 1–36. https://doi.org/10.1093/petrology/egaa104

Weaver, B. L. (1991). The origin of ocean island basalt end-member compositions: Trace element and isotopic constraints. *Earth and Planetary Science Letters*, *104*(2–4), 381–397. https://doi.org/10.1016/0012-821x(91)90217-6

White, R., & McKenzie, D. (1989). Magmatism at rift zones: The generation of volcanic continental margins and flood basalts. *Journal of Geophysical Research*, *94*(B6), 7685–7729. https://doi.org/10.1029/jb094ib06p07685

Workman, R. K., Hart, S. R., Jackson, M., Regelous, M., Farley, K. A., Blusztajn, J., et al. (2004). Recycled metasomatized lithosphere as the origin of the Enriched Mantle II (EM2) end-member: Evidence from the Samoan Volcanic Chain. *Geochemistry, Geophysics, Geosystems*, *5*(4), 1–44. https://doi.org/10.1029/2003GC000623

Yoder, H. S., & Tilley, C. E. (1962). Origin of basalt magmas: An experimental study of natural and synthetic rock systems. *Journal of Petrology*, *3*, 342–532. https://doi.org/10.1093/petrology/3.3.342